Research Square

Preprints are preliminary reports that have not undergone peer review.
They should not be considered conclusive, used to inform clinical practice,
or referenced by the media as validated information.

A Small Molecule Drug, Formoterol Fumarate, Potently Reverses Anemia

Laurie Glimcher

Laurie_Glimcher@dfci.harvard.edu

Dana-Farber Cancer Institute https://orcid.org/0000-0002-4971-0404

Shrestha Ghosh

Dana-Farber Cancer Institute https://orcid.org/0000-0003-1861-8581

Shengze Xu

Dana Farber Cancer Institute, Boston https://orcid.org/0009-0005-7581-8012

Merve Akyol

Dana Farber Cancer Institute, Boston https://orcid.org/0000-0001-8803-0965

Shaokun An

Brigham and Women's Hospital

Ha Eun Choi

Korea Advanced Institute of Science and Technology, South Korea

Mileena Nguyen

Yale School of Medicine, Yale University, New Haven https://orcid.org/0009-0002-8087-1879

Jae-Won Cho

hanyang university https://orcid.org/0000-0003-2930-4836

Edward Doherty

Attivare Therapeutics Inc. https://orcid.org/0009-0006-8944-2236

Gregory Petsko

Brigham and Women's Hospital, Harvard Medical School, Boston, Department of Medicine, Harvard Medical School, Boston, MA 02215 https://orcid.org/0000-0003-3668-3694

Martin Hemberg

The Gene Lay Institute of Immunology and Inflammation at Harvard Medical School and Brigham and Women's Hospital https://orcid.org/0000-0001-8895-5239

Article

Keywords:

Posted Date: October 30th, 2026

DOI: https://doi.org/10.21203/rs.3.rs-7020627/v1

License: This work is licensed under a Creative Commons Attribution 4.0 International License.
Read Full License

Additional Declarations: Yes there is potential Competing Interest. S.G. and L.H.G. are co-founders of a new company, Antero Biosciences, that is developing drugs for prevention and management of anemia, based on this work. L.H.G. is a former Director of Bristol-Myers Squibb, GlaxoSmithKline Pharmaceuticals and the Waters Corporation and recently stepped down on the Board of Directors of Analog Devices, Inc. L.H.G. is a consultant for JP Morgan healthcare and she has recently joined the Board of Directors of ReAlta, Inc. E.D. is a co-founder and the Chief Technology Officer of a biotech company, Attivare Therapeutics Inc., that is developing Immunotherapies to treat oncology and infectious diseases. G.A.P. is on the Scientific Advisory Boards of Amicus Therapeutics, MeiraGTx, Annovis Bio, Retromer Therapeutics, and Proclara Biosciences and holds equity or stock options in Denali Therapeutics, MeiraGTx, Annovis Bio, Retromer Therapeutics and Proclara Biosciences, companies that are developing therapies for neurodegenerative diseases. All other authors declare no relevant competing interests. S.G. and L.H.G. have 2 patents filed with Dana-Farber Cancer Institute, Boston based on this work.

Title: A Small Molecule Drug, Formoterol Fumarate, Potently Reverses Anemia

Authors: Shrestha Ghosh[1,2*], Shengze Xu[1#], Merve Akyol[1,2#], Shaokun An[3], Ha Eun Choi[4], Mileena T. Nguyen[5], Jae-Won Cho[3§], Edward Doherty[6], Gregory A. Petsko[7], Martin Hemberg[3], and Laurie H. Glimcher[1,2,8*]

Affiliations:

[1]Department of Cancer Immunology and Virology, Dana-Farber Cancer Institute, Harvard Medical School; Boston, MA 02215, USA.

[2]Department of Immunology, Harvard Medical School; Boston, MA, 02215, USA.

[3]Gene Lay Institute of Immunology and Inflammation, Brigham and Women's Hospital, Massachusetts General Hospital and Harvard Medical School, Boston, MA, USA

[4]Korea Advanced Institute of Science and Technology, South Korea.

[5]Yale School of Medicine, Yale University, New Haven, USA.

[6]Attivare Therapeutics Inc, Natick, MA 01760, USA.

[7]Department of Neurology, Ann Romney Center for Neurologic Diseases, Brigham and Women's Hospital, Harvard Medical School; Boston, MA 02215, USA.

[8]Department of Medicine, Harvard Medical School; Boston, MA 02215, USA.

§Present address: Hanyang Institute of Bioscience & Biotechnology, Hanyang University, Seoul 04763, Republic of Korea.

[#]These authors contributed equally.

*These authors jointly supervised this work: Shrestha Ghosh, Laurie H. Glimcher.

Email: Shrestha_Ghosh@dfci.harvard.edu, Laurie_Glimcher@dfci.harvard.edu

ABSTRACT

Anemia is a major societal health risk that greatly lowers quality of life in roughly a quarter of the world population[1]. However, current treatments are effective in only a subset of patients with hematological malignancies and disorders[2,3]. We have identified dynamic surface expression of β2-adrenoceptors in erythroid progenitors at various stages of differentiation. Here, we report that formoterol fumarate (FF), a highly selective β2-adrenoceptor agonist, promotes erythroid differentiation in the bone marrow and spleen to enhance hemoglobin and hematocrit levels in peripheral blood, thereby reversing anemia. FF treatment at very low doses via multiple routes of administration confers striking survival benefits in lethal hemolytic anemia. FF also boosts red blood cells in mouse models of myelodysplastic syndrome (MDS)/acute myeloid leukemia, chronic kidney disease (CKD), hemolytic stress-induced anemia, and in naïve mice at steady state. Furthermore, FF augments erythropoiesis in human stem cells derived from bone marrow aspirates of MDS patients. Mechanistically, FF promotes erythropoiesis partly via *HIF-1α* and associated hypoxia-responsive genes along with induction of mitochondrial biogenesis, thereby suggesting that the therapeutic relevance of FF may reflect its specific ability to induce coordinated *HIF-1α* and mitochondrial programs in addition to general β_2 activation. Importantly, we have developed a unique capsule formulation of FF that markedly reverses anemia when dosed orally in mice. Our study uncovers FF-driven stimulation of β2-adrenenoceptors as a new therapeutic strategy for treatment of anemia associated with MDS, CKD and hemolytic stress.

INTRODUCTION

Anemia, characterized by loss of red blood cells (RBCs), is the most prevalent blood disorder worldwide[4]. Patients with hematological malignancies, such as myelodysplastic syndrome (MDS) and acute myeloid leukemia (AML), often present with anemia as their predominant comorbidity[5,6]. A vast majority of cancer patients undergoing chemotherapy also develop anemia. Patients suffering from chronic kidney disease (CKD) frequently present with anemia as a significant health risk[3]. Hemolytic anemia is a serious complication in patients suffering from infectious diseases and autoimmune disorders[7]. Although iron-deficiency anemia can be managed with proper nutrition and iron supplementation[8,9], treatment of anemia arising from ineffective hematopoiesis in the bone marrow (BM) is more challenging. Recently, imetelstat[10], luspatercept[11] and lenalidomide[12] received US Food and Drug administration (FDA) approvals for anemia management in specific subsets of MDS patients. Also, vadadustat received FDA-approval to treat anemia in CKD patients[13]. However, inadvertent toxicities and progressive unresponsiveness to FDA-approved medications often compel patients to discontinue such treatment[14-17]. A significant fraction of CKD patients do not respond to FDA-approved erythropoiesis-stimulating agents (ESAs), such as epoetin-α or darbepoietin-α[18]. Furthermore, MDS patients are reported to develop serious side-effects such as neutropenia, thrombocytopenia, and hepatic adverse events in response to the available FDA-approved drugs[10,19]. Consequently, anemia continues to lower quality of life of a staggering ~23% of the world population[20], which emphasizes the urgent need to identify novel and improved therapeutic approaches.

β2-adrenoceptors (β2-AR) are G-protein coupled receptors for adrenaline that mediate smooth muscle relaxation and vasodilation[21,22]. Although β2-AR has been previously implicated in hematopoiesis[23,24], the direct impact of these receptors on erythroid progenitors (EP) in the bone marrow (BM) and peripheral blood (PB) components remains elusive. Here, we report that formoterol fumarate (FF), a highly selective β2-adrenergic receptor agonist, stimulates erythroid differentiation in human and murine BM stem cells, and dramatically reverses anemia in

multiple pre-clinical mouse models of MDS and CKD. FF is FDA-approved as an inhalant for the treatment of chronic obstructive pulmonary disorder (COPD) and asthma patients and is well-tolerated[25,26]. We demonstrate the previously unappreciated dynamic surface expression patterns of β2-AR on EP cells. Consequently, FF directly stimulates early and late-stage EPs in the BM to promote erythropoiesis, thereby enhancing hemoglobin (Hb) and hematocrit (HCT%) levels in PB to rescue anemia. We have developed an oral capsule formulation of FF that strikingly reverses anemia in mice. Our findings present an innovative approach to treat anemia associated with hemolytic stress, CKD and ineffective erythropoiesis, such as MDS, by repurposing FF (FDA-approved inhalant) as an orally administered drug, and provides the mechanistic basis of β2-AR-driven stimulation of erythropoiesis.

RESULTS

Formoterol fumarate (FF) promotes erythropoiesis *in vitro* and in patient *ex vivo* settings

Since a vast majority (>80%) of MDS patients present with anemia[5,6], we first sought to identify genes that may be linked to MDS-associated dyserythropoiesis. We focused on the del(5q) subtype of MDS, as these patients harbor a commonly deleted region (CDR) 5q31-5q33 in their genome[27,28]. Interestingly, we noted that the gene *ADRB2* (encoding β2-AR) is located at human chromosome 5q32, which falls within the CDR of del(5q) MDS patients[29] (Extended Data Fig. 1a). Our independent assessment of a publicly available dataset[30] revealed decreased *ADRB2* transcripts in the bone marrow (BM) $CD34^+$ cells of del(5q) MDS patients as compared to non del(5q) MDS patients and healthy controls (Extended Data Fig. 1b). To define the functional involvement of *ADRB2* in erythropoiesis, we depleted it in $CD34^+$ primary human hematopoietic stem and progenitor cells (HSPCs) isolated from healthy donors. Loss of *ADRB2* dampened erythroid lineage-specific cell surface marker CD235a, while minimally affecting myelopoiesis and megakaryopoiesis markers CD11b and CD41/61, respectively (Extended Data Fig. 1c-g). Erythroid lineage-specific genes were also downregulated upon loss of *ADRB2* (Extended Data Fig. 1h). In-depth analysis of distinct stages in human $CD34^+$ erythroid differentiation *in*

vitro (Extended Data Fig. 1i)[31] uncovered that loss of ADRB2 significantly dampened progression of erythroid progenitors towards later stages (late basophilic (LB), polychromatic (Poly) and orthochromatic (Ortho) erythroblasts), while retaining blasts in the early developmental stages (early progenitors 1,2 (EP1,2), early basophilic (EB) erythroblasts) (Extended Data Fig. 1j-l, 2a). This led us to hypothesize whether stimulation of β2-AR augments erythropoiesis. Hence, we studied the impact of formoterol fumarate (FF), a highly selective and potent β2-AR agonist[32], in erythroid differentiation. In accordance with prior studies[23,33], we observed appreciable surface expression of ADRB2 on primary human HSPCs, that dampened after ADRB2 knockdown via CRISPR-Cas9 (Extended Data Fig. 2b,c). Indeed, FF significantly promoted cell surface expression of CD235a in HSPCs in a dose-dependent manner, without affecting viability, expansion, myelopoiesis or megakaryopoiesis (Fig. 1a,b and Extended Data Fig. 2d-m). Comprehensive analysis of distinct stages in erythroid differentiation revealed that FF enhanced various progenitor stages at multiple time points, with a consistent increase in the final stage of orthochromatic erythroblasts (ortho) (Fig. 1c and Extended Data Fig. 3a,b). Consequently, proportion of reticulocytes and enucleation% improved with FF administration (Extended Data Fig. 3c,d). However, cellular or nuclear morphology in these distinct stages of erythroblasts were not affected by FF (Extended Data Fig. 3e). Additionally, FF treatment augmented the cell surface expression of CD71 and CD235a in the late erythroid progenitor stages (Extended Data Fig. 4a-e). Our structural model of the FF-β2AR complex predicted that FF makes more interactions with the receptor than adrenaline (Fig. 1d). This is consistent with existing studies[21,32] reporting stronger binding of FF than adrenaline and FF's enhanced potency to stimulate β2-AR. FF-driven erythropoiesis was ablated upon *ADRB2* deficiency, confirming prior studies stating FF's specificity towards ADRB2[34] (Extended Data Fig. 4f,g). We examined the effect of FF in a semi-solid methylcellulose colony-forming assay for healthy donor-derived $CD34^+$ HSPCs. Consistently, FF enhanced burst-forming unit-erythroid (BFU-e) and colony-forming unit-erythroid (CFU-e) cells, but not colony forming unit-granulocyte macrophage (CFU-GM) cells (Fig. 1e-g). Next, we tested our predictions in a patient *ex vivo* setting. $CD34^+$ stem cells were isolated from BM aspirates of MDS patients and cultured in methylcellulose media (Fig. 1h). FF treatment significantly promoted erythroid differentiation in MDS patient-derived BM cells, as evidenced

by increased BFU-e and CFU-e cells (Fig. 1i,j). By contrast, CFU-GM cells were unaffected (Fig. 1k,l). Similarly, FF enhanced erythropoiesis, but did not affect myelopoiesis or megakaryopoiesis, in MDS patient-derived BM cells in an orthogonal liquid differentiation culture (Extended Data Fig. 4h-j). These findings indicate that FF may be repurposed to overcome impaired erythropoiesis in MDS patients.

FF increases hemoglobin and reverses hemolytic stress-induced anemia *in vivo*

Next, we evaluated FF's potency in a self-resolving mouse model of hemolytic stress-induced anemia upon sub-lethal doses of phenylhydrazine (Phz), a treatment that readily lyses RBCs in peripheral blood (PB)[35] (Fig. 2a). FF administered at a very low dose of 0.3 mg/kg intraperitoneally (IP) significantly revived Hb and HCT% in PB, as compared to vehicle (Veh)-treated counterparts (Fig. 2b). FF treatment for only 2 weeks increased absolute Hb content by ~1.7 g/dL (Extended Data Fig. 5a). Consistent with our *in vitro* and *ex vivo* studies (Fig. 1), FF enriched EPs at various maturation stages in the BM: RI-RII-RIII-RIV (Fig. 2c,d, Extended Data Fig. 5b) while minimally affecting WBCs and platelets in PB, and granulocyte-macrophage progenitors (GMPs) in the BM (Extended Data Fig. 5c,d). However, MEPs (megakaryocyte-erythroid progenitors) were boosted by FF treatment (Extended Data Fig. 5e), suggesting FF's selective activation of the erythroid lineage since platelets were unaltered in PB (Extended Data Fig. 5c). Consistent with Phz-induced hemolysis that causes stress erythropoiesis in the spleen[36,37], we noted increased spleen size after Phz treatment that normalized in 2 weeks (Extended Data Fig. 5f,g). FF treatment led to significant increase in spleen size, weight and also enriched erythroid progenitors in the spleen (Extended Data Fig. 5f-j). We also noted the long-term effect of FF in boosting splenic erythroid progenitors on day 15 post Phz treatment when the spleen size and weights were comparable between vehicle and FF-treated groups (Extended Data Fig. 5f-j). Additionally, FF enhanced erythropoiesis in both Phz-treated and non-treated mice (Extended Data Fig. 5k). Besides stress erythropoiesis, FF induced Hb levels in naïve mice dose-dependently but did not induce WBCs or platelets (Fig. 2e,f and Extended Data Fig. 5l-n). FF also increased EPs and MEPs in the BM of naïve mice, but not GMPs (Fig. 2g and Extended Data Fig. 5o,p). However, dose-

dependent upregulation of EPs was not observed, suggesting qualitative changes in these progenitors leading to enhanced Hb levels with increasing doses of FF. Most importantly, in a lethal hemolytic anemia model induced by high dose of Phz (Extended Data Fig. 6a), FF treatment at 0.3 mg/kg IP for only 7 days conferred striking survival benefits (Fig. 2h). FF-treated mice (7/10) displayed complete revival and were euthanized after 365 days, whereas all vehicle-treated mice (10/10) succumbed to lethal hemolytic anemia by day 3 (Fig. 2h).

Since revival of anemia may not solely stem from stimulation of EPs in the BM, we analyzed other pathways that contribute to RBC production. Erythropoietin (EPO) and hepcidin are two key proteins that induce and modulate erythropoiesis, respectively[38,39]. However, FF showed no discernible impact on serum EPO or hepcidin levels (Extended Data Fig. 6b,c), strongly suggesting that FF stimulates erythroid differentiation in the BM to increase RBCs in PB. Concomitant with sustained erythropoietic drive that leads to low ferritin and free iron levels in PB[40-42], we noted reduction in ferritin, free iron and transferrin saturation levels in the serum isolated from FF-treated mice as compared to vehicle-treated controls (Extended Data Fig. 6d). Since FF is an FDA-approved smooth muscle relaxant[43,44], we studied the effect on cardiologic functions *in vivo*. FF treatment at 0.3 mg/kg daily IP for a month neither affected systolic or diastolic blood pressure in mice nor produced detrimental impact on heart rates, which could be a potential risk factor for tachycardia (Extended Data Fig. 6e,f). These findings highlight the potency of low dose FF treatment in mitigating anemic burden without undue cardiovascular toxicities.

We further tested FF's efficacy via an alternate route of drug administration: oral gavage (OG) (Fig. 2i). Consistently, FF administered via OG enhanced Hb and HCT% in response to sub-lethal Phz doses that generate hemolytic anemia (Fig. 2j and Extended Data Fig. 6g). Also, naïve mice treated with FF via OG showed increased HCT% and Hb levels at steady state (Extended Data Fig. 6h-j). FF via OG led to increased EPs and MEPs in the BM, but not GMPs (Fig. 2k, Extended Data Fig. 6k-m). Again, FF administration via OG led to a dramatic increase in survival benefits upon lethal hemolytic anemia (Fig. 2l). We also examined cytotoxic responses due to systemic FF administration but did not observe signs of organ toxicities in response to prolonged FF treatment for a month (Extended Data Fig. 6n). These findings demonstrate the safety and efficacy of low dose FF treatment,

via multiple routes of systemic administration, in stimulating erythropoiesis and reversing hemolytic anemia *in vivo*.

FF rescues anemia in a variety of pre-clinical mouse models of MDS and CKD

Since Phz treatment results in a chemically induced mouse model of hemolytic anemia, we next evaluated the efficacy of FF in pre-clinical mouse models of anemia with ineffective erythropoiesis. We employed a transgenic MDS model where translocation of *HOXD13* to the *NUP98* locus in the hematopoietic compartment recapitulates characteristic features of MDS patients, such as development of anemia at an older age of ~6-8 months, BM dysplasia and progression to AML[45]. Notably, FF IP treatment at 0.3 mg/kg 5 times weekly was sufficient to stabilize RBC parameters (HCT% and Hb) and rescue anemia in these MDS mice (Fig. 3a,b, Extended Data Fig. 7a). This was reflected in the paw redness of FF-treated MDS mice displaying a near-complete rescue as compared to the littermate controls treated with vehicle (Control+ Veh) (Fig. 3c, Extended Data Fig. 7b). FF significantly enriched EPs in the BM and spleen of MDS mice (Fig. 3d and Extended Data Fig. 7c), thus explaining the reversal of anemia. Again, FF's impact was restricted to the erythroid lineage since GMPs and MkPs (megakaryocytic progenitors) were unaffected by FF treatment (Fig. 3e,f). Blast cell percentages in the BM and spleen of MDS mice were not significantly affected upon FF treatment, thus indicating that leukemic progression is not impacted by FF treatment (Extended Data Fig. 7e). Next, we created a model of anemia secondary to chronic kidney disease (CKD) in response to low-dose chemotherapy treatment (Fig. 3g). In accordance with previous studies[46,47], low dose cisplatin treatment led to CKD and resultant anemia in mice (Fig. 3g-i, Extended Data Fig. 57f,g). Indeed, FF IP treatment at 0.3 mg/kg 3 times weekly for only 2 weeks markedly rescued anemia in CKD mice (Fig. 3i, Extended Data Fig. 7h,i). Similarly, EPs, but not GMPs or MkPs, were increased in CKD mice upon FF treatment (Fig. 3j, k, Extended Data Fig. 7j,k). On the other hand, haploinsufficiency of *APC* (Adenomatous Polyposis Coli) leads to aggressive anemia in mice at ~3 months and makes them susceptible to spontaneous formation of multiple intestinal neoplasia (min)[48]. *APC* targeted (Apc^{min}) mice are a useful model of MDS[48]. Notably, FF 0.3 mg/kg 3

times weekly IP treatment significantly stabilized HCT% and Hb in *Apc*^{min} mice, which was also reflected in the revival of their paw redness (Fig. 3l, m, Extended Data Fig. 7l,m).

Management of anemia is a primary goal of current intervention strategies in MDS and CKD patients[17,49]. Daprodustat (Dap) had received FDA-approval for treating anemia in CKD patients[50,51] but has been withdrawn in the USA. Nevertheless, we compared low dose FF (0.3 mg/kg) with the highest recommended dose of Daprodustat (~0.3 mg/kg) administered via oral gavage in a mouse model of CKD that is induced by prolonged treatments with aristolochic acid (AA), a nephrotoxic agent[52,53]. FF efficaciously revived HCT% and Hb in PB, as compared to Daprodustat or vehicle treatments in this CKD mouse model (Extended Data Fig. 7n-q). On the other hand, ESAs such as epoetin α and darbepoetin α, are frequently prescribed to MDS patients for treating anemia[54]. However, a significant fraction of these patients become unresponsive or refractory to these ESAs[55]. Recently, Reblozyl (Luspatercept: SMAD2/3 signaling inhibitor) was FDA-approved for a small fraction of low-risk MDS patients[56]. Although Reblozyl was administered at 10mg/kg or higher doses in murine models to achieve efficacy in rescuing anemia[57,58], the FDA-approved dose for MDS patients is set at 1-1.7 mg once every 3 weeks owing to toxicities, such as hypertension, peripheral edema, diarrhea, and dyspnea[59,60]. In contrast, FF is administrated as an inhalant at daily doses of ~9-40 µg to COPD and asthma patients[61,62]. Hence, to stringently test FF's efficacy against FDA-approved drugs for treating anemia in MDS patients, we compared very low dose FF treatment (0.3 mg/kg: ~6 µg; 5x weekly) vs high doses of epoetin α (EPO: 100 IU/kg 3x weekly) or Reblozyl (REB: 10 mg/kg 2x weekly) in the *Hoxd13-Nup98* transgenic MDS mouse model. Low-dose FF treatment was as efficacious as high doses of epoetin α (EPO) and Reblozyl (REB) in stabilizing Hb levels in MDS mice (Fig 3n,o and Extended Data Fig. 8a). Also, FF administration as a single agent showed comparable potency with combination therapies in the revival of MDS-associated anemia (Extended Data Fig. 8b,c). Combination treatment of FF and EPO displayed mild improvement in splenomegaly- a complication in several MDS patients[63,64] (Extended Data Fig. 8d,e). However, combination treatment of FF with Reblozyl seemed to exacerbate splenomegaly in MDS mice (Extended Data Fig. 8d,e), likely due to unfavorable drug-drug

interactions. Taken together, our study underscores the potency of low dose FF treatment in alleviating anemia associated with a variety of hematological malignancies and disorders, such as MDS, CKD and hemolytic stress.

ADRB2 is expressed on the surface of erythroid progenitors

Given the striking effects of FF in boosting EPs, we investigated whether FF directly impacts erythropoiesis in the BM. To this end, we first investigated the dynamics of ADRB2 cell surface expression at each stage of human erythroid differentiation *in vitro*. Indeed, cell surface staining via 2 different antibodies of ADRB2 revealed that the later erythroid progenitor stages exhibit increased extracellular surface expression of ADRB2 (Extended Data Fig. f,g). Next, we evaluated surface expression patterns of ADRB2 on murine EPs across various stages of differentiation in the BM[65] (Fig. 4a). In congruence with prior studies[23,33], we observed surface expression of ADRB2 on stem and progenitor cells, also known as multipotent progenitors (Fig. 4b, Extended Data Fig. 8h). However, hematopoietic stem cells , the earliest progenitors in the BM, showed negligible surface expression of ADRB2. Consistent with human EPs, murine EPs also displayed dynamic surface expression of ADRB2 across various stages of erythroid differentiation (Fig. 4b, extended data fig. 8h). The presence of ADRB2 on early (CFU-E, RI) as well as late (RII-RIII-RIV) EPs strongly indicates that FF not only promotes progression of the erythroid lineage from multi-potent progenitors but also stimulates maturation of erythroid progenitors towards the terminal stages. By contrast, GMPs and MkPs in the BM did not show detectable surface expression of ADRB2, thus explaining the specificity of FF in selectively augmenting erythroid differentiation, but not myelopoiesis or megakaryopoiesis (Fig. 4c). Consistently, EPs in the spleen also exhibited surface expression of ADRB2 (Extended Data Fig. 8i).

Although β2-AR is reported to be involved in hematopoietic development and $CD34^+$ HSPC proliferation[23,24,33], its direct roles in erythropoiesis remain poorly understood thus far. While some studies suggest that ADRB2 may be linked to promoting erythropoiesis via enhancement of EPO production[66,67], others implicated antagonism of β2-AR in the stimulation of erythropoiesis[68,69]. Also, constitutive deletion of *Adrb2* in mice does not affect

erythropoiesis at steady state[70]. Hence, to directly investigate the relevance of β2-AR in response to hemolytic stress-driven anemia, we generated mice with selective deletion of *Adrb2* in the hematopoietic compartment by crossing *Adrb2* floxed (*Adrb2$^{fl/fl}$*) mice with the *Vav^{cre}* strain. Mice with complete deletion of *Adrb2* (*Adrb2$^{fl/fl}$Vav^{cre}*) were not born at mendelian frequency (5 out of 126 littermates over 2 years), hence we further characterized *Adrb2*-haploinsufficient mice (*Adrb2$^{Wt/fl}$Vav^{cre}*) (Fig. 4d). Consistent with previous reports, depletion of *Adrb2* in hematopoietic cells did not alter basal RBC parameters of mice (Extended Data Fig. 9a,b). However, *Adrb2$^{Wt/fl}$Vav^{cre}* mice exhibited delayed revival from anemia in response to Phz-driven hemolytic stress as compared to their wild-type counterparts (*Adrb2$^{Wt/Wt}$Vav^{cre}*), whereas platelets and WBCs were not impacted significantly (Fig. 4e, Extended Data Fig. 9c,d). Administration of FF did not improve HCT% in *Adrb2*-deficient mice (Fig. 4f), thus confirming FF's specificity to Adrb2 in promoting erythropoiesis. Furthermore, to validate *Adrb2*'s roles in the EPs, we generated conditional deletion of *Adrb2* in the erythroid lineage by crossing *Adrb2* floxed (*Adrb2$^{fl/fl}$*) mice with *EpoR^{cre}* strain (Fig. 4g, Extended Data Fig. 9e, f). Complete deletion of *Adrb2* could not be achieved in erythroid cells likely due to incomplete penetrance of this *Cre*-strain, as previously reported[71] (Extended Data Fig. 9e, f). Again, basal Hb and HCT% were unaltered in *Adrb2$^{Wt/fl}$EpoR^{cre}* and *Adrb2$^{fl/fl}$EpoR^{cre}* mice (Extended Data Fig. 9g). Notably, *Adrb2* depletion in the erythroid lineage markedly dampened revival from Phz-induced hemolytic anemia (Fig. 4h, Extended Data Fig. 9h,i), thus highlighting the key roles of Adrb2 in promoting erythropoiesis and overcoming anemia upon hemolytic stress. Deficiency of *Adrb2* in EPs also rendered FF ineffective in augmenting erythropoiesis (Fig. 4i). These findings further verify our observation that FF boosts RBC production by directly stimulating β2-AR present on the surface of EPs.

Oral capsule formulation of FF potently reverses hemolytic anemia

Since FF is FDA-approved as an inhalant[25,26], we synthesized a novel capsule formulation of FF for oral dosing in mice to simulate capsule dosing in humans. To improve the absorption of low dose FF into the bloodstream, we coated inert microbeads with United States Pharmacopeia (USP)-grade FF and applied a lipophilic excipient

layer on the surface to slow the release of FF, thus protecting it from enteric degradation (Fig. 5a, b). FF-coated beads containing a modified release layer substantially extended the dissolution of FF in comparison to beads that contained no release modification layer, and allowed immediate release of FF, as captured by liquid chromatography (Fig. 5c). Next, we filled FF-modified release beads in gelatin capsules that allow dosing in mice via oral gavage (Fig. 5d, Supplementary Video 1). The release profile of gelatin-encapsulated FF beads aligned well with gastrointestinal transit time in mice (Fig. 5e), where stomach emptying takes place in ~0.5-1 hr and passage through the small intestine ranges from ~1-2 hrs for maximal absorption of nutrients/drugs into the bloodstream[72]. Furthermore, aligning with the total gastrointestinal transit time of ~6-8 hrs in mice, the dissolution of FF from capsules reached completion by 6-8 hrs (Fig. 5e). Next, we tested these FF capsules in Phz-driven hemolytic anemia model (Fig. 5f). Consistent with FF treatment via IP and oral gavage in mice (Fig. 2), daily administration of FF capsules at ~0.25 mg/kg dose significantly improved recovery from hemolytic anemia and enhanced both RBCs and Hb as compared to placebo controls (Fig. 5g, h). FF capsules markedly increased the redness of paws in mice undergoing hemolytic stress, further confirming reversal of anemia (Fig. 5i, j). Also, FF capsules substantially enriched terminal erythroid progenitors in the BM and spleen (Fig. 5k, l). These findings demonstrate the efficacy of low dose FF capsules in reversing anemia, thus representing a promising approach for synthesizing FF capsules to administer in anemic patients.

FF stimulates erythropoiesis partly via *HIF-1α/EPAS1* pathway

To gain an unbiased overview of FF-driven impact on EPs and other BM progenitor populations, we performed single-cell RNA-sequencing (scRNA-seq) analysis of BM cells isolated from naïve mice treated with FF (0.3 mg/kg IP 5x weekly) or vehicle (Veh) for a month. Following batch-correction and unsupervised clustering, cell clusters were annotated based on expression patterns of canonical marker genes, which enabled identification of distinct BM progenitors, including EPs[73-75] (Fig. 6a, Extended Data Fig. 9j,k). Corroborating our *in vivo* analyses (Fig. 2,3), EPs showed the most substantial enrichment with FF administration (highest odds ratio of 1.85)

amongst all other BM progenitors (Fig. 6b). Moreover, FF significantly increased the absolute cell counts of EPs (p=2.93e-05, Fig. 6c,d), orthogonally verifying that FF enriches precursors of the erythroid lineage in the BM for improved anemia outcomes. We further investigated molecular signatures in FF-treated EPs to gain deeper mechanistic insights. FF is reported to induce mitochondrial biogenesis *in vitro* and *in vivo* murine models of spinal cord and traumatic brain injury[34,76-78]. Consistently, mitochondrial biogenesis was upregulated in FF-treated EPs, suggesting increased metabolic fitness of EPs that likely supports their expansion (Fig. 6e, Extended Data Fig. 10a). To further validate this pathway, we compared the impact of FF with Clenbuterol, an ADRB2 agonist that does not lead to mitochondrial biogenesis[79,80]. Clenbuterol displayed a mild impact on erythropoiesis as compared to FF in primary human HSPCs (Extended Data Fig. 10b). Since Clenbuterol is reported to be less potent than FF[79,84,85], this may have also contributed to Clenbuterol's insufficiency in augmenting mitochondrial biogenesis and promoting erythroid differentiation. We also found marked enrichment of the cell proliferation pathway in FF-treated EPs, congruent with our observation that FF promotes expansion of EPs in the BM (Fig. 6f, Extended Data Fig. 10a). Intriguingly, gene signatures associated with the hypoxia pathway were also significantly enriched in FF-treated EPs (Fig. 6g), indicating that FF triggers alternate pathways in EPs to boost erythropoiesis.

We noted that FF IP treatment at 0.3 mg/kg thrice weekly for a month substantially increased HCT% and Hb in PB of naïve mice (Extended Data Fig. 10c). To validate our findings from scRNA-seq analyses and investigate the mechanistic underpinnings of FF-driven erythropoiesis, we performed bulk RNA sequencing (RNA-seq) of EPs isolated from the BM of naïve mice treated with vehicle or FF at 0.3 mg/kg thrice weekly IP for a month. Consistently, our gene-ontology analysis revealed a hypoxia-inducible factor-driven gene expression signature as the top upregulated pathway in FF-treated EPs (Fig. 6h). Of note, transcript levels of hypoxia-inducible transcription factors *HIF-1α* and *EPAS1* (encoding HIF-2α) were significantly upregulated in EPs upon FF treatment (Fig. 6i and Extended Data Fig. 10d). This *HIF-1α* gene signature was consistently upregulated in human erythroid progenitors upon FF treatment (Extended Data Fig. 10e). Although protein levels of HIF-1α and HIF-2α were upregulated upon FF administration in human HSPCs (Extended Data Fig. 10f,g), post-translational

protein stabilization of HIF-1α was not observed via analysis of its prolyl hydroxylation status (Extended Data Fig. 10h). This indicates that transcriptional upregulation of *HIF-1α*/ *EPAS1* upon FF treatment leads to enhancement of its protein levels. To directly test *HIF-1α*'s involvement in FF-driven erythropoiesis, we silenced it in primary human HSPCs (Fig. 6j,k), followed by differentiation towards erythroid lineage in the presence and absence of FF. Deficiency of *HIF-1α* substantially blunted FF-induced erythroid differentiation in HSPCs, as compared to control cells treated with FF (Fig. 6l,m and Extended Data Fig. 10i). Similarly, depletion of *EPAS1* also abrogated FF-driven upregulation of erythroid differentiation in HSPCs (Extended Data Fig. 10j-m). These findings reveal that the transcription factors *HIF-1α* and *EPAS1* (encoding HIF-2A) contribute to FF-driven stimulation of erythropoiesis and reversal of anemia. Thus, our data uncover an alternate mechanistic pathway employed by FF in EPs that can overcome anemia.

DISCUSSION

β2 adrenergic receptors (β2-AR) have been extensively studied in smooth muscle relaxation. Although β2-AR's function in $CD34^+$ HSPC mobilization and proliferation are reported[23,33], its direct roles in erythroid differentiation are poorly defined. Some studies reported that administration of serum from salbutamol (a short-acting β2-AR agonist)-treated hypoxic rabbits to polycythemic mice increased CFU-E colonies from murine BM cells *in vitro*, implicating salbutamol-driven induction of EPO in promoting erythropoiesis[66,67]. However, inherent limitations of this experimental strategy confound further interpretation. For example, serum from salbutamol-treated rabbits may have causal proteins/cytokines other than EPO that might have driven erythropoiesis. Also, the cells used for *in vitro* colony forming assays in these studies were not purified $CD34^+$ HSPCs but a mixture of all viable murine BM cells. Conversely, selective β2-AR inhibitors were reported to stimulate erythropoiesis in mouse models of burn injury[68,69]. Thus, our study addresses this long-standing conundrum and establishes direct roles of β2-AR agonism in promoting erythropoiesis and reversing anemia. This is consistent with a prior study where administration of albuterol, a selective short-acting β2-AR agonist, induced erythropoiesis in

busulfan-treated mice[81]. Our findings demonstrate that FF directly stimulates ADRB2 expressed on the surface of HSPCs and EPs to drive erythropoiesis, without discernible impact on serum EPO levels in murine models. We have also provided direct evidence to show that FF treatment at low doses via multiple routes of administration markedly increases HCT% and Hb levels to reverse anemia in various pre-clinical murine models of MDS, CKD and hemolytic stress. Since it is reported that defective erythroid differentiation in MDS can occur at any of the different stages of erythropoiesis[82], our *in vitro*, patient *ex vivo* and *in vivo* analyses identify FF as a beneficial therapy in reversing MDS-associated anemia. There are significant site-specific differences between human and murine erythropoiesis- BM is the primary site for erythroid differentiation in humans whereas stress erythropoiesis largely occurs in the spleen of mice[36,37]. Our findings in murine models reveal that FF not only triggers erythroid differentiation in the BM but also promotes splenic erythropoiesis in response to hemolytic stress. However, FF is not expected to yield beneficial effects in sickle cell disease or β-thalassemia since FF will not correct the sickling of RBCs in sickle cell anemia or fix globin mutations in β-thalassemia to mitigate the imbalance of hemoglobin subunit production. Nevertheless, we have shown that FF stimulates erythropoiesis in BM stem cells derived from both adult healthy donors and MDS patients, thus offering a promising therapeutic strategy to reverse anemia associated with these disorders.

Although β2-AR agonism is classically known to upregulate the cyclic adenosine monophosphate (cAMP) pathway for smooth muscle relaxation and vasodilation[83], we did not observe enrichment of gene signatures associated with this pathway in FF-treated EPs. This suggests that FF upregulates alternate pathways in EPs to promote erythropoiesis, such as *HIF-1α*/*EPAS1* and mitochondrial biogenesis. In our studies, Clenbuterol, an ADRB2 agonist that does not lead to mitochondrial biogenesis, displayed only a mild impact on improving erythropoiesis as compared to FF. However, FF is reported to be a more potent β_2 adrenoceptor agonist than Clenbuterol[79,84,85] which may have contributed to Clenbuterol's insufficiency in activating ADRB2, inducing mitochondrial biogenesis and in its inability to improve anemia. Taken together, the therapeutic efficacy of FF may be attributable to its potency to coordinately induce *HIF-1α* and mitochondrial programs that extend beyond canonical β_2-adrenergic receptor signaling. While some studies have shown that β2-AR agonism increases HIF-

1α protein levels[86,87], we have demonstrated that FF stimulates transcription of *HIF-1α*/*EPAS1* in EPs under normoxia and that deficiency of *HIF-1α* or *EPAS1* diminishes FF-mediated induction of erythropoiesis, thus identifying an alternative pathway employed by FF to drive erythroid differentiation. Although cAMP-PKA-CREB pathway is known to transcriptionally regulate *HIF-1α*[88], this signaling cascade was not identified in our RNA sequencing analyses from vehicle vs. FF-treated erythroid progenitors. On the other hand, NF-κB is reported to directly promote *HIF-1α* transcription[89,90] and we have observed that NF-κB signaling is one of the top upregulated pathways in FF-treated murine erythroid progenitors (Main Fig. 6h). Future investigation will characterize the molecular mechanisms underlying FF-driven transcriptional regulation of *HIF-1α*/*EPAS1* in EPs.

Since FF is FDA-approved as an inhalant for COPD and asthma patients[25,26], we have developed a unique capsule formulation of FF for oral dosing in mice that shows marked potency in alleviating hemolytic stress-driven anemia. This provides a strong foundation for designing a humanized version of FF capsules to treat anemia in patients. Our goal is to synthesize oral capsule formulations of FF for human dosing that could be administered to anemic patients in phase I clinical trials. Taken together, our identification of FF as a potential medication for boosting RBCs may shift paradigms in the treatment of anemia associated with MDS, CKD and hemolytic stress.

METHODS

Primary human stem cell culture

$CD34^+$ primary human hematopoietic stem and progenitor cells (HSPCs) were obtained from Fred-Hutchinson Cancer Research center, Seattle, USA (commercially available). $CD34^+$ cells were isolated by magnetic sorting from peripheral blood of adult healthy donors upon G-CSF-mobilization and were cryopreserved until further usage. The cells were thawed and washed with 1x PBS containing 1% human AB serum, and revived in expansion medium constituting StemSpan SFEM II medium supplemented with 1X CC100 (STEMCELL Technologies), 1% penicillin-streptomycin (P/S), 1% Glutamine and 10ng/ml TPO. After 3-5 days of proliferation/gene editing in the expansion phase, the cells were placed in differentiation medium comprising of IMDM reconstituted with

3% human AB serum, 2% human AB plasma, 1% P/S, 0.06% heparin solution (STEMCELL Technologies), 1 ng/ml IL-3 (Peprotech, Inc.), 10 ng/ml SCF (Peprotech, Inc.), 200 ug/ml holo-transferrin (Sigma-Aldrich) and 3U/ml erythropoietin (DFCI pharmacy). Cells were cultured at a density of 0.1-0.2 x 10^6 cells/ml and incubated at 37°C with 5% CO_2. Media were changed every alternate day, as required. These protocols have been previously described[91].

Frozen bone marrow (BM) aspirates from de-identified and coded MDS patients were obtained from the Ted and Eileen Pasquarello Tissue Bank in Hematologic Malignancies at Dana-Farber Cancer Institute, Boston under Institutional Review Board (IRB)-approved protocol 21-632. Informed consent was obtained from all recipients by the tissue bank. The BM cells were thawed, washed with 1×PBS, and allowed to revive in StemSpan SFEM II medium containing 1× CC100 (STEMCELL Technologies) and 1% penicillin–streptomycin (P/S). This was followed by surface staining and flow sorting viable $CD34^+$ stem cells, that were counted and placed in methylcellulose (semi-solid) colony forming assay or differentiation media as described above. Cells were incubated at 37°C with 5% CO_2. Media in liquid culture were changed every alternate day, as required.

Methylcellulose colony forming assay

After CRISPR-based gene editing, primary human HSPCs were washed twice with 1x PBS and mixed with semi-solid methylcellulose medium (H4034, StemCell Technologies) along with indicated drugs/vehicle by brief vortex. Cells were plated at a density of 1000 per well in a 6-well plate followed by incubation in a humidified chamber at 37°C for 14 days. For MDS patient-derived samples, 500-1000 $CD34^+$ stem cells isolated from each patient were mixed with either FF (1 μM) or vehicle, placed in separate wells of a 6-well plate, and incubated in a humidified chamber at 37°C for 14 days. Imaging of the colonies was performed using EVOS M5000 Imaging system (ThermoFisher Scientific). The colony-forming cells were then collected by triturating the wells using staining buffer and multi-color flow cytometry was performed, as previously described[91,92].

Quantitative RT-PCR

RNA was isolated from cells using the RNeasy Plus Micro kit (Qiagen) using manufacturer's protocols. Genomic DNA (gDNA) was removed using gDNA eliminator spin columns and total RNA was isolated using phenol-free

RNeasy MinElute spin columns. Reverse transcription was performed using qScript cDNA Synthesis kit (QuantaBio). Quantitative real-time polymerase chain reaction (RT-PCR) was performed using Quantstudio6 RT-PCR system (Applied Biosciences) and PerfeCTa SYBR Green FastMix Reaction Mixes (QuantaBio). Comparative C_T method has been used for all quantifications using corresponding *ACTB* mRNA levels for normalization. The primers used for qRT-PCR are listed in Supplementary Table 1.

Western blotting

For collection of whole cell lysates, cells were washed twice with ice cold 1x PBS after removal of medium, then resuspended in RIPA lysis buffer (Life Technologies) supplemented with 1x complete protease inhibitor cocktail and 1x phosphatase inhibitor cocktail (Thermo Scientific). Lysis was carried out on ice for 15-30 minutes followed by removal of cellular debris by centrifugation at 13,000 rpm for 20 minutes. The supernatant was collected in a fresh tube, mixed with Laemmli buffer and incubated at 95°C for 10 minutes. Equal amounts of proteins were resolved by SDS-PAGE method using Novex Tris-Glycine minigels submerged in Tris-Glycine-SDS buffer in a mini gel tank (Life Technologies). The proteins were then transferred onto PVDF membranes (Thermo Fisher Scientific) using Tris-Glycine buffer followed by blocking in 5% skimmed milk solution/5% BSA in 1x TBST buffer at RT for 1 hour. The membranes were then probed with the required primary antibodies diluted in fresh blocking buffer at 4°C for overnight (O/N): beta-Actin rabbit polyclonal antibody at 1:1000 (3967S, Cell Signaling Technology), ADRB2 (BS-0947R, Life Technologies), HIF-1α rabbit monoclonal antibody at 1:1000 (14179T, 36169T- Cell Signaling Technology), HIF-2α rabbit monoclonal antibody at 1:1000 (7096T- Cell Signaling Technology), Hydroxy-HIF-1α (Pro564) rabbit monoclonal antibody at 1:1000 (3434T- Cell Signaling Technology). After O/N incubation, membranes were washed four times with 1x TBST buffer for 5 minutes each on a rocker at RT, followed by incubation with HRP-linked anti-rabbit IgG (7076S, Cell Signaling Technology) at 1:3000 dilution in fresh blocking buffer for 1 hour at RT. After incubation with secondary antibodies, membranes were washed four times with 1x TBST buffer for 5 minutes each on a rocker at RT, followed by incubation with Pierce Western blotting substrates (Thermo Scientific, Supersignal) mixed at 1:1 ratio for 2-5 mins at RT. The protein bands were then visualized using the ChemiDoc Touch Imaging system (Bio-Rad).

CRISPR/Cas9 gene editing

Primary human HSPCs were electroporated using Lonza-Amaxa 4D nucleofector unit as per the manufacturer's instructions. For ribonucleoprotein (RNP) formation, tracer RNAs (IDT) and crRNAs (IDT) were incubated at 95°C for 5 mins at equimolar ratios, brought to room temperature (RT) and mixed with equal molar concentration of Cas9 peptide (IDT Technologies). This mixture was incubated at 37°C for 15 minutes and the RNP mix was kept at 4°C until use within the next 2 hours. Cells were mixed with the RNP mix at a density of 0.1-0.2 $x10^6$ cells per well of a 16-well electroporation-strip and subsequently electroporated using 4D-Nucleofector core unit (Lonza). Immediately after electroporation, fresh medium was added to the cells and incubated at RT for 10 mins before transferring the cells to 37°C. Genome editing efficiency was analyzed 48-72 hours post electroporation by nucleotide sequencing, and quantitative RT-PCR. The following crRNAs were used for knockdown (KD) of *ADRB2*: GCGATAACATTGATTCACAAGGG and CAAGACGTTAGGCATCATCATGG; HIF1α: TATCCAGGCTGTGTCGACTGAGG and GGTTTCTTATACCCACACTGAGG; *EPAS1*: CGGATGCTCGCAAAGCATGGGGG and TGTTCTCGGAGTCTAGCGCATGG. For non-targeting controls, Alt-R™ Cas9 Negative Control crRNA #1 and crRNA #2 from IDT were used.

TIDE Analysis

Cells were lysed in Buffer RLT (Qiagen, 79216), vortexed, and stored in -80°C. Genomic DNA was isolated from cell lysates using Quick-DNA Microprep Kit (Zymo Research, ZD3020) and quantified using Nanodrop. PCR reactions were performed in 15 µL volumes containing ~4 ng of gDNA, Azura 2x Taq Red Mix (Azura Genomics, AZ-1325), 0.5 µM of each primer, and nuclease-free water. PCR products were resolved on 1% agarose gel (Sigma-Aldrich, A6013-500G) at a constant voltage of 180 V for 1 hour containing SYBR Safe DNA Gel Stain (Invitrogen, S33102), along with PureView 100 bp DNA Ladder (Azura Genomics, AZ-1135). For gel extraction, DNA bands were visualized using a blue-light LED transilluminator, and gel slices were excised with clean scalpels, followed by extraction and purification using the QIAquick Gel Extraction Kit (Qiagen, 28704). Purified PCR products (quantified via Nanodrop) were premixed with corresponding primer and submitted for Sanger

sequencing (GENEWIZ). The results were analyzed online using TIDE software (tide.nki.nl). The primers sequences are listed in Supplementary Table 1.

Mice

C57BL/6J (JAX 000664), C57BL/6J-*Apc*^{Min}/J (JAX 002020), *Vav*^{Cre} (B6.Cg-*Commd10*$^{Tg(Vav1\text{-}icre)A2Kio}$/J, JAX 008610), and *EpoR*^{Cre} (B6.C-*Epor*$^{tm1.1(EGFP/icre)Uk}$/MdfJ, Jax 035702) mice were purchased from Jackson laboratories. Breeding pairs of transgenic mice to model MDS (C57BL/6-Tg(*Vav1-NUP98/HOXD13)G2Apla/J*) were a kind gift from Dr. Peter D. Aplan at National Cancer Institute and were later purchased from Jackson laboratories (JAX 010505) to maintain colonies. MDS mice were generated by breeding (C57BL/6-Tg(*Vav1-NUP98/HOXD13)G2Apla/J*) with C57BL/6J mice. *Adrb2*$^{fl/fl}$ mice on C57BL/6J background were a gift from Dr. Gerard Karsenty at Columbia University. *Adrb2*$^{fl/WT}$*Vav*^{cre} mice were generated by crossing *Adrb2*$^{fl/fl}$ mice to *Vav*^{Cre} mice at Dana-Farber Cancer Institute, Boston. *Adrb2*$^{fl/WT}$*EpoR*^{cre} and *Adrb2*$^{fl/fl}$*EpoR*^{cre} mice were generated by crossing *Adrb2*$^{fl/fl}$ mice to *EpoR*^{Cre} mice at the mouse vivarium of Dana-Farber Cancer Institute, Boston. Both male and female mice aging 6-12 weeks were used in experiments unless specified otherwise. MDS male and female mice aging 6-8 months were used in experiments when they showed signs of anemia. *Apc*^{min} mice aging 3-4 months were used in experiments when they showed signs of anemia. Age and sex-matched mice were randomly assigned in all experimental set ups. The procedures on mice required prior knowledge of experimental conditions by the operators to ensure correct dosing was administered. Sample sizes were not pre-determined by statistical methods. All mice were housed in the animal research facility of Dana-Farber Cancer Institute under pathogen-free conditions with a cycle of 6:00−18:00 light and 18:00–6:00 dark, ambient room temperature and humidity. All animal studies were approved and performed in accordance with guidelines and regulations implemented by the Institutional Animal Care and Use Committee (IACUC) at Dana-Farber Cancer Institute, Boston.

Genotyping

Mice were ear-tagged and tail snips were collected using aseptic methods. Next, tissue samples were lysed at 56°C overnight in DirectPCR Lysis Reagent Tail buffer (Viagen Biotech, 102-T) supplemented with Proteinase K solution (Viagen Biotech, 501-PK), followed by enzyme inactivation at 85 °C for 2 hours. PCR reactions were performed in 15 µL volumes containing 2 µL of tail lysate, Azura 2x Taq Red Mix (Azura Genomics, AZ-1325), 0.5 µM of each primer, and nuclease-free water. Primer sequences are listed in the Supplementary Table 1. PCR products were resolved on 3% agarose gels to analyze *Adrb2*-floxed status, and 2% gels for all other targets, containing SYBR Safe Gel Stain. Electrophoresis was performed at a constant voltage of 180 V for 30-60 mins and gels were imaged using the ChemiDoc MP Imaging System (Bio-Rad).

Drug treatments in mice

Formoterol fumarate (FF) was purchased from Selleckchem (S2020) and Sigma Aldrich (F9552) and were dosed as indicated in the respective figures and their legends. For vehicle control, ~0.3% DMSO in 1x PBS/saline was administered in mice. For oral gavage treatments, only 1x PBS was administered to control groups, since FF was dissolved in sterile H_2O at 0.4 mg/ml followed by dilution in 1x PBS before dosing in mice. Phenylhydrazine (Phz) was purchased from Sigma Aldrich (P26252) and was administered intraperitoneally (IP) on days 0 and 1 at 30 mg/kg for sub-lethal model of hemolytic stress-induced anemia. For modeling lethal hemolytic anemia in mice, Phz was administered once at 120 mg/kg dose. Cisplatin was purchased from Selleckchem (S1166) and dosed once weekly for 2-3 weeks at 5 mg/kg. Aristolochic acid was purchased from Sigma Aldrich (A5512) and was dosed once weekly for 5 months at 5mg/kg.

Hemavet for complete blood count (CBC) analyses

For collection of blood, mice were bled from their cheeks by puncturing their facial submandibular vein with a sterile lancet (size 4 mm) to drain ~50-100 µl blood each time into BD-Microtainer EDTA-coated tubes (BD-365974) during serial bleeding procedure. The bleeding was then stopped by applying a sterile gauge pad on the poked facial area followed by application of triple antibiotic to prevent infection. The freshly collected blood

samples were placed on a rocker at RT for ~10-15 minutes before analyzing their complete blood counts using the Hemavet CBC analyzer (Drew Scientific-950FS).

Blood pressure measurement

Systolic and diastolic blood pressure along with heart rates of mice were measured from their tail vein using the BP-2000 Blood Pressure Analysis System from Visitech Systems according to the manufacturer's instructions. Briefly, mice were placed inside a sterile holder and their tails were taped to restrict vigorous movements. Transmission photoplethysmography was used by the instrument whereby variations in the amount of light transmitted through the tail vein is analyzed to determine the blood pressure and pulse rates of mice.

Enzyme-linked immunosorbent assay (ELISA)

Erythropoietin was measured from mouse serum using mouse erythropoietin ELISA kit from Abcam (ab270893), according to the manufacturer's instructions. Similarly, Hepcidin was measured from mouse serum using Intrinsic Life Sciences Hepcidin murine complete assay kit from Fisher Scientific (NC0807369). Ferritin was measured from mouse serum using mouse ferritin ELISA kit from Fisher Scientific (89028656), according to the manufacturer's instructions. Transferrin saturation and free iron levels in mouse serum were measured using Total Iron-Binding Capacity (TIBC) and serum Iron assay kit from Cayman chemicals (702230), as per manufacturer's instructions. Mouse blood was collected into BD-Microtainer tubes with clot-activator (365978), allowed to clot for 1-2 hours at RT, and centrifuged at 2000 g for 15 minutes at 4°C. The serum was immediately collected into fresh Eppendorf tubes and stored at -80°C until further use. Absorbance was captured using BioTek Epoch Microplate Spectrophotometer from Agilent.

Colorimetric assay

Blood Urea Nitrogen (BUN) levels from mouse serum were measured using colorimetric detection kit from Life Technologies (EIABUN), as per manufacturer's instructions. Creatinine levels in mouse serum were measured

using mouse creatinine assay kit from Fisher Scientific (501947694), as per manufacturer's protocols. Absorbance was measured using BioTek Epoch Microplate Spectrophotometer from Agilent.

Murine organ histology

Organs dissected from euthanized mice were washed twice with ice-cold 1×PBS and incubated overnight in 4% paraformaldehyde solution in 1×PBS on rocker for fixation. The organs were removed from the fixative the following day, washed twice with 1×PBS at RT, and placed in 70% ethanol solution until paraffin sectioning and subsequent Hematoxylin & Eosin (H&E) staining was performed to visualize histological analyses. The sectioning and staining of fixed murine organ paraffin blocks were performed by the Rodent Histopathology core at Dana-Farber/Harvard Cancer Center. Images of the H&E stained tissue sections were captured using Olympus fluorescence microscope under bright field imaging using 10-40X magnification with the built-in Cell Sens software.

Tissue preparation and Fluorescence-Activated Cell sorting (FACS) analysis

Human: For analysis of cell surface marker expressions via flow cytometry in $CD34^+$ primary human HSPCs, *in vitro* cultured cells were washed twice with FACS buffer (1x PBS + 2% FBS (Atlanta Biologicals) + 0.02% EDTA (GIBCO)) and labelled with required fluorochrome-conjugated antibodies diluted in FACS staining buffer for 30 minutes at 4°C in dark: FITC-CD34 (343604, BioLegend), BV421-CD38 (356617, BioLegend)/ PE-Cy7-CD38 (356608, BioLegend), APC-CD71 (OKT9, eBioscience), PE-Cy7-CD235a (306620, BioLegend), PE-CD41/CD61 (359806, BioLegend), PerCP-Cy5.5-CD11b (301328, 101228, 393106, BioLegend), AF700-CD42b (303928, BioLegend), APC-CD135 (313307, BioLegend), BV510-Human Lineage (348807, BioLegend), PE-CD68 (333807, BioLegend), BV421-CD45RA (304129, BioLegend), BV421-CD45 (304031, 368521, BioLegend), BV785-CD45 (368527, BioLegend), PerCP-Cy5.5-CD123 (306015, BioLegend), AF700-CD117 (313245, Biolegend), PE-CD36 (336205, BioLegend), BV421-CD105 (323219, BioLegend), AF700-CD45RA (304120, BioLegend), APC/Fire750-CD123 (306041, BioLegend), BV605-CD117 (313217, BioLegend), BV510-CD34 (343527, BioLegend), PerCP-Cy5.5-CD41 (303719, BioLegend), Syto16 RNASelect Green

fluorescent stain. The stained cells were washed once with FACS buffer and then resuspended in FACS buffer containing DAPI. For analyzing surface expression of ADRB2, $CD34^+$ primary human HSPCs/mouse bone marrow (BM) progenitors were stained with unconjugated primary antibody for ADRB2 (BS-0947R, Life Technologies or AAR-016, Life Technologies) for 30 mins at 4°C in dark, washed once with FACS buffer, stained with PE-conjugated anti-rabbit IgG antibody (406421, BioLegend) for 30 mins at 4°C in dark, washed twice with FACS buffer, and resuspended in DAPI containing FACS buffer for further analysis by flow cytometry.

Murine: To harvest bone marrow, mice were euthanized (CO_2 exposure), their femur and tibia were dissected out and scrapped to remove muscle tissues, followed by crushing them using mortar and pestle in FACS staining buffer. The BM cells were resuspended in FACS buffer, passed through a 70µm cell strainer, and RBC lysis was performed by adding 1x BD PharmLyse (Biosciences) for 90 secs, followed by neutralization with 9-10X volume of FACS buffer. The BM cells were spun down, filtered through 70µm cell strainer again, and reconstituted in ice-cold FACS buffer. Spleen cells were collected by mushing the spleen on a 70µm cell strainer, and RBC lysis was performed as mentioned above. For analysis of cell surface marker expression via flow cytometry, the same protocol was applied as described above. The following antibodies were used: APC-CD71 (113820, BioLegend), FITC-Ter119 (116206, BioLegend)/ BV-510-Ter119 (116237, BioLegend), AF700-Lineage cocktail (133313, BioLegend), BV605-Sca1 (108133, BioLegend), PerCP/Cy5.5-CD41 (133918, BioLegend), PE-Cy7-CD117 (105805, BioLegend), BV510-CD150 (115929, BioLegend), Pacific Blue-CD105 (120412, BioLegend), PE-CD34 (128609, BioLegend), APC/Cy7- FcγRIV (149537, 101328, BioLegend), ADRB2 (BS-0947R or AAR-016, Life Technologies).

All FACS analyses were performed using CytoFLEX Flow Cytometer (Beckman Coulter). Data were analyzed using FlowJo 10.0.7 and plotted using GraphPad Prism.

May Grünwald Giemsa staining

Cytospins were prepared using a Thermo Shandon Cytospin 3 with FACS-sorted cells from day 7/14 of erythroid differentiation culture and resuspended in 100 µL PBS and centrifuged onto glass slides for 5 mins at 300 rpm. Slides were air dried and stained with May Grünwald modified solution (MilliporeSigma, M1014240500) for 3

mins, followed by staining with 1:20 diluted Giemsa modified solution (MilliporeSigma, 32884-250ML) for 12 mins. Slides were rinsed twice for 1 min each in buffer solution (Weise pH 6.8) and air dried at room temperature. Images were acquired using an Olympus microscope with a 60× objective. Image processing was performed using ImageJ.

Assessment of paw redness in mice

Hind paw images were captured using a smartphone digital camera under consistent, bright lighting conditions inside a biosafety cabinet. The camera was set to ~2× magnification to focus on the plantar surface of the hind paws, and each image was saved in JPEG format at the device's full resolution (3072 × 4080 pixels, ~12.5 MP) with no compression or down sampling. Image processing and redness quantification were performed using Fiji (ImageJ) software (version 2.16.0), as previously reported[93]. For each paw image, a defined workflow was applied to quantify the redness based on CIELAB color space a* values, as follows:

ROI selection: Using the polygon selection tool in Fiji, the plantar area of each hind paw was manually outlined as a region of interest (ROI), while excluding non-relevant areas such as dark fur near the ankle and the toenails (which do not reflect paw erythema). Both the left and right hind paw regions were outlined separately on each image.

Color space conversion and measurement: The RGB color photograph was converted to the CIELAB color space using Fiji's built-in function (*Image → Color → RGB to CIELAB*). This conversion produced three 32-bit images corresponding to the L*, a*, and b* channels. All subsequent analysis was carried out on the a* channel image, which represents the green–red axis of color (with higher and more positive a* values indicating stronger red coloration). Variations in brightness were controlled separately by the L* channel, rendering the a* measurements largely independent of lighting differences. The mean a* pixel value within each ROI was measured using the Analyze → Measure command in Fiji. The mean a* value provides a quantitative index of redness for that paw region[93]. The surface area of respective paws were used to normalize the values. Each mouse yielded two hind paw a* measurements (with surface area normalized), that were averaged to produce a single representative a* value per mouse.

Generation of FF-coated beads for oral capsule dosing in mice

Multi-particulate dosage form of formoterol fumarate (FF) was synthesized by BendbioScience, Inc. Excipients suitable for use in multi-particulate dosage form were identified by compatibility assessment. Compatibility study samples were prepared as binary blends of drug substance (FF) and excipient at a 1:1 ratio. Assessment of compatibility between the drug substance and excipients was performed by differential scanning calorimetry (DSC) and modulated DSC (MDSC). Development batches to generate immediate-release and modified-release forms of FF beads were produced by a fluid bed Wurster coating process in which the drug was coated onto an inert bead core using Fluid Bed Processor (ACG, 00609). Suglets® (Colorcon) were used as the inert bead particle core (composed of sucrose and starch), that is included in FDA's approved Inactive Ingredient Database (IID) (https://www.accessdata.fda.gov/scripts/cder/iig/index.cfm). Opadry 20A polymer was applied as seal layer along with the drug to ensure efficient and uniform coating onto beads. The immediate release form of FF contained no additional seal coats. The modified release form of FF contained a release modification polymer layer of Eudragit RS 30D, that has a low composition of hydrophilic substituents making it less permeable in an aqueous environment. Triethyl citrate and Kolliwax glycerol monostearate (GMS) II were used as plasticizer and anti-tacking agents respectively, for efficient particulate coating. Size M gelatin capsules (appropriate dimensions for dosing to mice) were used to encapsulate multi-particulate beads using custom capsule delivery tools for *in vivo* dosing in mice (Torpac). Dissolution evaluation of the microparticulate beads and encapsulated drug product was performed using liquid chromatography (LC). Small volume 150mL vessels were used with 100mL of USP-grade 4.5pH acetate buffer and paddles running at 50rpm were utilized for constant mixing. The placebo contained all the excipients described above along with the inert microbeads encapsulated within size M gelatin capsules, without the drug substance FF. Each FF-capsule contained a dose of ~6 µg FF for *in vivo* evaluation in mice.

Single cell RNA sequencing (scRNA-seq) and analysis

Bone marrow was harvested from Vehicle (0.3% DMSO in 1x PBS) and FF-treated (0.3 mg/kg 5xweekly IP for 4 weeks) mice (n=4 in each group) and their single-cell suspensions were freshly cryopreserved in fetal bovine serum (FBS) with 10% DMSO in a cryotube and stored at -80°C until further processing. The following

procedures of scRNA-seq was performed at the Center for Cancer Genomics (CCG) at Dana-Farber Cancer Institute. The cryopreserved samples were thawed at 37°C and immediately diluted with 6 mL of DMEM cell culture medium containing 10% FBS, followed by centrifugation at 300g for 10 minutes at room temperature (RT). Cell pellets were washed with 4 mL of ice-cold resuspension buffer (1X PBS + 0.4% BSA), centrifuged at 300g for 5 minutes at 4°C, and then resuspended in 100 µL of resuspension buffer. Subsequently, viable cells were further processed. Droplet-based microfluidic Chromium X (10X Genomics, Inc.) was used for generating single-cell Gel Beads-in-emulsions (GEMs) as per the Chromium Next GEM Single-Cell 5' HT v2 - CG000425 protocol (10X Genomics demonstrated protocol) and high throughput 10X genomics workflow was followed for all downstream steps to produce sequencing-ready libraries.

Pre-analysis processing: Pooled samples were demultiplexed using 10x *Cellranger* mkfastq (cellRanger count 7.1.0). Read pairs were aligned to the mm10 reference sequence using 10x *Cellranger* count which utilizes *STAR*[94].

Quality-control for sequencing: *Cellbender* remove-background[95] was run on aligned, barcoded reads to distinguish cell-containing droplets from empty ones and retrieve background-free gene expression profiles. The *Cellbender* algorithm was run for 150 epochs per sample.

Downstream analysis: We analyzed scRNA-seq data with the standard pipeline in Scanpy (v1.10.3)[73], starting with raw count matrices from Cell Ranger. The quality control workflow first implemented Scrublet[74] to identify and remove cell doublets from each sample independently. Cells with fewer than 200 detected genes were filtered out and cells were further removed that showed high content of mitochondrial, ribosomal, and hemoglobin genes, that indicate poor-quality or dying cells. To prevent outlier bias, cells with unusually high gene counts and total UMI counts were also excluded. For gene selection, only those genes were retained that were detected in at least 3 cells across the dataset. Following quality control, the integrated data of all samples was log-normalized with a scaling factor of 10,000 counts per cell, that allowed identification of the top 2,000 highly variable genes for downstream analysis. After this, Principal Component Analysis was performed and batch effects were corrected across all samples using Harmony[75] on the top 50 principal components. Leiden algorithm was applied to the

batch-corrected embeddings for cell clustering. Next, cell types were assigned to each cluster based on expression patterns of canonical marker genes, which enabled identification of distinct hematopoietic populations and erythroid lineage cells (Extended Data Fig. 7a).

To quantify differences in cell type distribution between FF-treated and vehicle control groups, two-sided Fisher's exact tests were conducted for each cell type. Two-sided Wilcoxon rank sum tests were employed to identify significantly upregulated pathways in the FF-treated vs vehicle control groups. Phenotypic signatures across conditions were further investigated by examining pathway activities in three key areas: hypoxia, mitochondrial biogenesis, and cell proliferation. Enrichment scores for each pathway were calculated in individual cells using established marker gene sets (hypoxia: *Hif1a, Ddit4, Cirbp, Rora, Otub1, Ptpmt1, Aph1a, Hlf*; mitochondrial biogenesis: *Maip1, Ndufa13, Ndufs6, Atp5d*; cell proliferation: *Brpf3, Otub1, Mis18a*).

Bulk RNA-sequencing

Mouse BM cells were harvested as described above, and erythroid progenitors were FACS-sorted from Vehicle and FF-treated (0.3 mg/kg 3x weekly IP for 4 weeks) animals (n=5 in each group). ~0.1-0.2X10^6 cells from each sample were processed to isolate their mRNA (following gDNA exclusion) using the RNeasy Plus Micro kit (Qiagen), as per the manufacturer's instructions. RNA library preparations, sequencing reactions and initial bioinformatic analysis were conducted at GENEWIZ, LLC. (South Plainfield, NJ, USA) as follows:

Library Preparation with polyA selection and HiSeq Sequencing: RNA samples were quantified using Qubit 2.0 Fluorometer (Life Technologies, Carlsbad, CA, USA) and RNA integrity was checked using Agilent TapeStation 4200 (Agilent Technologies, Palo Alto, CA, USA). RNA sequencing libraries were prepared using the NEBNext Ultra RNA Library Prep Kit for Illumina following manufacturer's instructions (NEB, Ipswich, MA, USA). Briefly, mRNAs were first enriched with Oligo(dT) beads. Enriched mRNAs were fragmented for 15 minutes at 94 °C. First strand and second strand cDNAs were subsequently synthesized. cDNA fragments were end repaired and adenylated at 3'ends, and universal adapters were ligated to cDNA fragments, followed by index addition and library enrichment by limited-cycle PCR. The sequencing libraries were validated on the Agilent TapeStation (Agilent Technologies, Palo Alto, CA, USA), and quantified by using Qubit 2.0

Fluorometer (Invitrogen, Carlsbad, CA) as well as by quantitative PCR (KAPA Biosystems, Wilmington, MA, USA). The sequencing libraries were clustered on 1 lane of a flowcell. After clustering, the flowcell was loaded on the Illumina HiSeq instrument (4000 or equivalent) according to manufacturer's instructions. The samples were sequenced using a 2x150bp Paired End (PE) configuration. Image analysis and base calling were conducted by the HiSeq Control Software (HCS). Raw sequence data (.bcl files) generated from Illumina HiSeq was converted into fastq files and de-multiplexed using Illumina's bcl2fastq 2.17 software. One mismatch was allowed for index sequence identification.

Data Analysis: After investigating the quality of the raw data, sequence reads were trimmed to remove possible adapter sequences and nucleotides with poor quality using Trimmomatic v.0.36. The trimmed reads were mapped to the Homo sapiens reference genome available on ENSEMBL 109 using the STAR aligner v.2.5.2b. Unique gene hit counts were calculated by using feature Counts from the Subread package v.1.5.2. Only unique reads that fell within exon regions were counted.

Gene sets were derived by accounting for the differentially regulated genes that passed the cut off of adjusted p value <0.05 in control vs FF vs Vehicle-treated samples. Additionally, canonical pathways such as KEGG, REACTOME and BIOCARTA were consulted. EnrichR was used to identify differentially regulated pathways in FF vs Vehicle-treated groups.

Structural modelling of the formoterol fumarate and β2-adrenergic receptor complex

Because multiple structures of the β2-adrenergic receptor with bound ligands, including adrenaline and formoterol, from different organisms, solved by various methods at different resolutions exist in the Protein Data Bank (e.g., 4LDO, 6IBL and 7ZB2), we employed AlphaFold 3 to construct state-of-the-art models for the human protein with FF and adrenaline bound using all available structures to form a template family[96]. The resulting models for the adrenaline and FF complexes had excellent quality scores and were virtually identical to structures 4LDO[97] and 7ZB2[98], respectively. The alignment feature in PYMOL[99] was used to superimpose the two models to examine the predicted interactions between the agonists and the protein.

Statistical tests

Data are presented as mean ± SEM. Unpaired two-tailed *t*-test or two-tailed non-parametric Wilcoxon matched-pairs signed rank test was used for comparing two groups. One-way Analysis of variance (ANOVA) with Dunnett's multiple comparisons test/Tukey's multiple comparisons test, or non-parametric Kruskal-Wallis test with Dunn's multiple comparisons test or two-way ANOVA (Mixed model) with Dunnett's multiple comparison's test were used for comparisons amongst multiple groups, wherever applicable as per requirements of data and quantification. GraphPad Prism v9.0/10.0 (GraphPad Software Inc., San Diego, CA) was used to perform statistical analyses. Sample size was not predetermined.

DATA AVAILABILITY

Raw data generated from bulk RNA-sequencing and single cell RNA-sequencing analyses are deposited in the Gene Expression Omnibus (GEO) database and the accession numbers are GSE299098 and GSE299301 respectively. The *ADRB2* mRNA levels in MDS patients have been analyzed using publicly available GEO dataset under accession code GSE19429. The source data for all figures (Main and Extended) are provided.

CODE AVAILABILITY

This study did not generate new unique codes or software.

RESOURCE AVAILABILITY

Further information and requests for resources and reagents should be directed to and will be fulfilled by Laurie H. Glimcher (Laurie_Glimcher@dfci.harvard.edu) with appropriate material transfer agreements (MTA).

MATERIALS AVAILABILITY

Requests for any materials should be directed to and will be fulfilled by Laurie H. Glimcher (Laurie_Glimcher@dfci.harvard.edu).

REFERENCES

1 Chaparro, C. M. & Suchdev, P. S. Anemia epidemiology, pathophysiology, and etiology in low- and middle-income countries. *Ann N Y Acad Sci* **1450**, 15-31, doi:10.1111/nyas.14092 (2019).

2 Schwartz, R. N. Anemia in patients with cancer: incidence, causes, impact, management, and use of treatment guidelines and protocols. *Am J Health Syst Pharm* **64**, S5-13; quiz S28-30, doi:10.2146/ajhp060601 (2007).

3 Hanna, R. M., Streja, E. & Kalantar-Zadeh, K. Burden of Anemia in Chronic Kidney Disease: Beyond Erythropoietin. *Adv Ther* **38**, 52-75, doi:10.1007/s12325-020-01524-6 (2021).

4 Marton, I., Agocs, S. & Babik, B. [Epidemiology of anemia]. *Orv Hetil* **161**, 1569-1573, doi:10.1556/650.2020.31916 (2020).

5 Castelli, R., Schiavon, R., Rossi, V. & Deliliers, G. L. Management of anemia in low-risk myelodysplastic syndromes treated with erythropoiesis-stimulating agents newer and older agents. *Med Oncol* **35**, 76, doi:10.1007/s12032-018-1135-2 (2018).

6 Steensma, D. P. Myelodysplastic syndromes current treatment algorithm 2018. *Blood Cancer J* **8**, 47, doi:10.1038/s41408-018-0085-4 (2018).

7 Dhaliwal, G., Cornett, P. A. & Tierney, L. M., Jr. Hemolytic anemia. *Am Fam Physician* **69**, 2599-2606 (2004).

8 Cappellini, M. D., Musallam, K. M. & Taher, A. T. Iron deficiency anaemia revisited. *J Intern Med* **287**, 153-170, doi:10.1111/joim.13004 (2020).

9 Leung, A. K. C., Lam, J. M., Wong, A. H. C., Hon, K. L. & Li, X. Iron Deficiency Anemia: An Updated Review. *Curr Pediatr Rev* **20**, 339-356, doi:10.2174/1573396320666230727102042 (2024).

10 Platzbecker, U. *et al.* Imetelstat in patients with lower-risk myelodysplastic syndromes who have relapsed or are refractory to erythropoiesis-stimulating agents (IMerge): a multinational, randomised, double-blind, placebo-controlled, phase 3 trial. *Lancet* **403**, 249-260, doi:10.1016/S0140-6736(23)01724-5 (2024).

11 Fenaux, P. *et al.* Luspatercept in Patients with Lower-Risk Myelodysplastic Syndromes. *N Engl J Med* **382**, 140-151, doi:10.1056/NEJMoa1908892 (2020).

12 Kronke, J. *et al.* Lenalidomide induces ubiquitination and degradation of CK1alpha in del(5q) MDS. *Nature* **523**, 183-188, doi:10.1038/nature14610 (2015).

13 Chertow, G. M. *et al.* Vadadustat in Patients with Anemia and Non-Dialysis-Dependent CKD. *N Engl J Med* **384**, 1589-1600, doi:10.1056/NEJMoa2035938 (2021).

14 Eckardt, K. U. *et al.* Safety and Efficacy of Vadadustat for Anemia in Patients Undergoing Dialysis. *N Engl J Med* **384**, 1601-1612, doi:10.1056/NEJMoa2025956 (2021).

15 Kunacheewa, C., Thongthang, P., Ungprasert, P., Utchariyaprasit, E. & Owattanapanich, W. A systematic review and meta-analysis of the efficacy and adverse events of azacitidine-plus-lenalidomide treatment for patients with acute myeloid leukemia, myelodysplastic syndromes and chronic myelomonocytic leukemia (1). *Hematology* **24**, 498-506, doi:10.1080/16078454.2019.1631425 (2019).

16 Weir, M. R. Managing Anemia across the Stages of Kidney Disease in Those Hyporesponsive to Erythropoiesis-Stimulating Agents. *Am J Nephrol* **52**, 450-466, doi:10.1159/000516901 (2021).

17 Lucero, J., Al-Harbi, S. & Yee, K. W. L. Management of Patients with Lower-Risk Myelodysplastic Neoplasms (MDS). *Curr Oncol* **30**, 6177-6196, doi:10.3390/curroncol30070459 (2023).

18 Fishbane, S. *et al.* Roxadustat Versus Epoetin Alfa for Treating Anemia in Patients with Chronic Kidney Disease on Dialysis: Results from the Randomized Phase 3 ROCKIES Study. *J Am Soc Nephrol* **33**, 850-866, doi:10.1681/ASN.2020111638 (2022).

19 Della Porta, M. G. *et al.* Luspatercept versus epoetin alfa in erythropoiesis-stimulating agent-naive, transfusion-dependent, lower-risk myelodysplastic syndromes (COMMANDS): primary analysis of a phase 3, open-label, randomised, controlled trial. *Lancet Haematol* **11**, e646-e658, doi:10.1016/S2352-3026(24)00203-5 (2024).

20 Kassebaum, N. J. *et al.* A systematic analysis of global anemia burden from 1990 to 2010. *Blood* **123**, 615-624, doi:10.1182/blood-2013-06-508325 (2014).

21 Rasmussen, S. G. *et al.* Crystal structure of the beta2 adrenergic receptor-Gs protein complex. *Nature* **477**, 549-555, doi:10.1038/nature10361 (2011).

22 Liggett, S. B. beta(2)-adrenergic receptor pharmacogenetics. *Am J Respir Crit Care Med* **161**, S197-201, doi:10.1164/ajrccm.161.supplement_2.a1q4-10 (2000).

23 Spiegel, A. *et al.* Catecholaminergic neurotransmitters regulate migration and repopulation of immature human CD34+ cells through Wnt signaling. *Nat Immunol* **8**, 1123-1131, doi:10.1038/ni1509 (2007).

24 Maestroni, G. J. M. Adrenergic Modulation of Hematopoiesis. *J Neuroimmune Pharmacol* **15**, 82-92, doi:10.1007/s11481-019-09840-7 (2020).

25 Antoniu, S. A. Formoterol as a rescue medication for asthma. *Expert Opin Pharmacother* **7**, 2439-2441, doi:10.1517/14656566.7.17.2439 (2006).

26 Hanania, N. A. *et al.* Long-term safety and efficacy of formoterol fumarate inhalation solution in patients with moderate-to-severe COPD. *Int J Chron Obstruct Pulmon Dis* **14**, 117-127, doi:10.2147/COPD.S173595 (2019).

27 Jaju, R. J. *et al.* Molecular cytogenetic delineation of the critical deleted region in the 5q- syndrome. *Genes Chromosomes Cancer* **22**, 251-256, doi:10.1002/(sici)1098-2264(199807)22:3<251::aid-gcc11>3.0.co;2-r (1998).

28 Pellagatti, A. & Boultwood, J. The molecular pathogenesis of the myelodysplastic syndromes. *Eur J Haematol* **95**, 3-15, doi:10.1111/ejh.12515 (2015).

29 Venugopal, S., Mascarenhas, J. & Steensma, D. P. Loss of 5q in myeloid malignancies - A gain in understanding of biological and clinical consequences. *Blood Rev*, 100735, doi:10.1016/j.blre.2020.100735 (2020).

30 Pellagatti, A. *et al.* Deregulated gene expression pathways in myelodysplastic syndrome hematopoietic stem cells. *Leukemia* **24**, 756-764, doi:10.1038/leu.2010.31 (2010).

31 Yan, H. *et al.* Comprehensive phenotyping of erythropoiesis in human bone marrow: Evaluation of normal and ineffective erythropoiesis. *Am J Hematol* **96**, 1064-1076, doi:10.1002/ajh.26247 (2021).

32 Isogaya, M. *et al.* Binding pockets of the beta(1)- and beta(2)-adrenergic receptors for subtype-selective agonists. *Mol Pharmacol* **56**, 875-885, doi:10.1124/mol.56.5.875 (1999).

33 Muthu, K. *et al.* Murine hematopoietic stem cells and progenitors express adrenergic receptors. *J Neuroimmunol* **186**, 27-36, doi:10.1016/j.jneuroim.2007.02.007 (2007).

34 Scholpa, N. E., Simmons, E. C., Tilley, D. G. & Schnellmann, R. G. beta2-adrenergic receptor-mediated mitochondrial biogenesis improves skeletal muscle recovery following spinal cord injury. *Exp Neurol* **322**, 113064, doi:10.1016/j.expneurol.2019.113064 (2019).

35 Shetlar, M. D. & Hill, H. A. Reactions of hemoglobin with phenylhydrazine: a review of selected aspects. *Environ Health Perspect* **64**, 265-281, doi:10.1289/ehp.8564265 (1985).

36 Myneni, V. D., Szalayova, I. & Mezey, E. Differences in Steady-State Erythropoiesis in Different Mouse Bones and Postnatal Spleen. *Front Cell Dev Biol* **9**, 646646, doi:10.3389/fcell.2021.646646 (2021).

37 An, X., Schulz, V. P., Mohandas, N. & Gallagher, P. G. Human and murine erythropoiesis. *Curr Opin Hematol* **22**, 206-211, doi:10.1097/MOH.0000000000000134 (2015).

38 Tsiftsoglou, A. S. Erythropoietin (EPO) as a Key Regulator of Erythropoiesis, Bone Remodeling and Endothelial Transdifferentiation of Multipotent Mesenchymal Stem Cells (MSCs): Implications in Regenerative Medicine. *Cells* **10**, doi:10.3390/cells10082140 (2021).

39 Agarwal, A. K. & Yee, J. Hepcidin. *Adv Chronic Kidney Dis* **26**, 298-305, doi:10.1053/j.ackd.2019.04.005 (2019).

40 Kautz, L. *et al.* Author Correction: Identification of erythroferrone as an erythroid regulator of iron metabolism. *Nat Genet* **52**, 463, doi:10.1038/s41588-019-0548-y (2020).

41 Ashby, D. R. *et al.* Erythropoietin administration in humans causes a marked and prolonged reduction in circulating hepcidin. *Haematologica* **95**, 505-508, doi:10.3324/haematol.2009.013136 (2010).

42 Camaschella, C., Nai, A. & Silvestri, L. Iron metabolism and iron disorders revisited in the hepcidin era. *Haematologica* **105**, 260-272, doi:10.3324/haematol.2019.232124 (2020).

43 Nials, A. T. *et al.* Formoterol on airway smooth muscle and human lung mast cells: a comparison with salbutamol and salmeterol. *Eur J Pharmacol* **251**, 127-135, doi:10.1016/0014-2999(94)90392-1 (1994).

44 Anderson, G. P. Pharmacology of formoterol: an innovative bronchodilator. *Agents Actions Suppl* **34**, 97-115 (1991).

45 Lin, Y. W., Slape, C., Zhang, Z. & Aplan, P. D. NUP98-HOXD13 transgenic mice develop a highly penetrant, severe myelodysplastic syndrome that progresses to acute leukemia. *Blood* **106**, 287-295, doi:10.1182/blood-2004-12-4794 (2005).

46 Fu, Y. *et al.* Chronic effects of repeated low-dose cisplatin treatment in mouse kidneys and renal tubular cells. *Am J Physiol Renal Physiol* **317**, F1582-F1592, doi:10.1152/ajprenal.00385.2019 (2019).

47 Shi, M. *et al.* Cisplatin nephrotoxicity as a model of chronic kidney disease. *Lab Invest* **98**, 1105-1121, doi:10.1038/s41374-018-0063-2 (2018).

48 Lane, S. W. *et al.* The Apc(min) mouse has altered hematopoietic stem cell function and provides a model for MPD/MDS. *Blood* **115**, 3489-3497, doi:10.1182/blood-2009-11-251728 (2010).

49 Reardon, G. *et al.* The prevalence and recognition of chronic kidney disease and anemia in long-term care residents. *Consult Pharm* **27**, 627-640, doi:10.4140/TCP.n.2012.627 (2012).

50 Singh, A. K. *et al.* Daprodustat for the Treatment of Anemia in Patients Undergoing Dialysis. *N Engl J Med* **385**, 2325-2335, doi:10.1056/NEJMoa2113379 (2021).

51 Meadowcroft, A. M. *et al.* Daprodustat for anemia: a 24-week, open-label, randomized controlled trial in participants on hemodialysis. *Clin Kidney J* **12**, 139-148, doi:10.1093/ckj/sfy014 (2019).

52 Baudoux, T. *et al.* Experimental Aristolochic Acid Nephropathy: A Relevant Model to Study AKI-to-CKD Transition. *Front Med (Lausanne)* **9**, 822870, doi:10.3389/fmed.2022.822870 (2022).

53 Zhang, L. *et al.* HDAC3 aberration-incurred GPX4 suppression drives renal ferroptosis and AKI-CKD progression. *Redox Biol* **68**, 102939, doi:10.1016/j.redox.2023.102939 (2023).

54 Santini, V. Clinical use of erythropoietic stimulating agents in myelodysplastic syndromes. *Oncologist* **16 Suppl 3**, 35-42, doi:10.1634/theoncologist.2011-S3-35 (2011).

55 Ikenoue, T., Furumatsu, Y. & Kitamura, T. Transfusion-dependent anaemia treatment using continuous erythropoietin receptor activator (epoetin beta pegol) and roxadustat after darbepoetin treatment failure in low-risk myelodysplastic syndrome: a case report. *Oxf Med Case Reports* **2021**, omab026, doi:10.1093/omcr/omab026 (2021).

56 Molica, M. & Rossi, M. Luspatercept in low-risk myelodysplastic syndromes: a paradigm shift in treatment strategies. *Expert Opin Biol Ther* **24**, 233-241, doi:10.1080/14712598.2024.2336086 (2024).

57 Mathieu, M. *et al.* Luspatercept (RAP-536) modulates oxidative stress without affecting mutation burden in myelodysplastic syndromes. *Ann Hematol* **101**, 2633-2643, doi:10.1007/s00277-022-04993-7 (2022).

58 Tanzi, E. *et al.* Bone marrow Tfr2 deletion improves the therapeutic efficacy of the activin-receptor ligand trap RAP-536 in beta-thalassemic mice. *Am J Hematol* **99**, 1313-1325, doi:10.1002/ajh.27336 (2024).

59 Platzbecker, U. *et al.* Efficacy and safety of luspatercept versus epoetin alfa in erythropoiesis-stimulating agent-naive, transfusion-dependent, lower-risk myelodysplastic syndromes (COMMANDS): interim analysis of a phase 3, open-label, randomised controlled trial. *Lancet* **402**, 373-385, doi:10.1016/S0140-6736(23)00874-7 (2023).

60 Komrokji, R. S. *et al.* Luspatercept for myelodysplastic syndromes/myeloproliferative neoplasm with ring sideroblasts and thrombocytosis. *Leukemia* **36**, 1432-1435, doi:10.1038/s41375-022-01521-4 (2022).

61 Singh, D. *et al.* Single inhaler triple therapy versus inhaled corticosteroid plus long-acting beta2-agonist therapy for chronic obstructive pulmonary disease (TRILOGY): a double-blind, parallel group, randomised controlled trial. *Lancet* **388**, 963-973, doi:10.1016/S0140-6736(16)31354-X (2016).

62 Muiser, S. *et al.* Budesonide/formoterol maintenance and reliever therapy versus fluticasone/salmeterol fixed-dose treatment in patients with COPD. *Thorax* **78**, 451-458, doi:10.1136/thorax-2022-219620 (2023).

63 Huh, Y. *et al.* Association of ASXL1 and RUNX1 Variants with Splenomegaly in Myelodysplastic Syndromes Based on Next-generation Sequencing and Computed Tomography Data: A Retrospective Study. *Ann Lab Med* **46**, 104-109, doi:10.3343/alm.2025.0033 (2026).

64 Toghill, P. J. & Green, S. The influence of spleen size on the distribution of red cells and plasma. *J Clin Pathol* **25**, 570-573, doi:10.1136/jcp.25.7.570 (1972).

65 Schneider, R. K. *et al.* Rps14 haploinsufficiency causes a block in erythroid differentiation mediated by S100A8 and S100A9. *Nat Med* **22**, 288-297, doi:10.1038/nm.4047 (2016).

66 Fink, G. D., Paulo, L. G. & Fisher, J. W. Effects of beta adrenergic blocking agents on erythropoietin production in rabbits exposed to hypoxia. *J Pharmacol Exp Ther* **193**, 176-181 (1975).

67 Fink, G. D. & Fisher, J. W. Erythropoietin production after renal denervation or beta-adrenergic blockade. *Am J Physiol* **230**, 508-513, doi:10.1152/ajplegacy.1976.230.2.508 (1976).

68 Beckman, B., Mirand, E. & Fisher, J. W. Effects of beta adrenergic agents and prostaglandin E1 on erythroid colony (CFU-E) growth and cyclic AMP formation in Friend erythroleukemic cells. *J Cell Physiol* **105**, 355-361, doi:10.1002/jcp.1041050218 (1980).

69 Hasan, S., Mosier, M. J., Szilagyi, A., Gamelli, R. L. & Muthumalaiappan, K. Discrete beta-adrenergic mechanisms regulate early and late erythropoiesis in erythropoietin-resistant anemia. *Surgery* **162**, 901-916, doi:10.1016/j.surg.2017.06.001 (2017).

70 Pierroz, D. D. *et al.* Deletion of beta-adrenergic receptor 1, 2, or both leads to different bone phenotypes and response to mechanical stimulation. *J Bone Miner Res* **27**, 1252-1262, doi:10.1002/jbmr.1594 (2012).

71 Shmukler, B. E. *et al.* Erythroid-specific inactivation of Slc12a6/Kcc3 by EpoR promoter-driven Cre expression reduces K-Cl cotransport activity in mouse erythrocytes. *Physiol Rep* **10**, e15186, doi:10.14814/phy2.15186 (2022).

72 Dahlgren, D. & Lennernas, H. Intestinal Permeability and Drug Absorption: Predictive Experimental, Computational and In Vivo Approaches. *Pharmaceutics* **11**, doi:10.3390/pharmaceutics11080411 (2019).

73 Wolf, F. A., Angerer, P. & Theis, F. J. SCANPY: large-scale single-cell gene expression data analysis. *Genome Biol* **19**, 15, doi:10.1186/s13059-017-1382-0 (2018).

74 Wolock, S. L., Lopez, R. & Klein, A. M. Scrublet: Computational Identification of Cell Doublets in Single-Cell Transcriptomic Data. *Cell Syst* **8**, 281-291 e289, doi:10.1016/j.cels.2018.11.005 (2019).

75 Korsunsky, I. *et al.* Fast, sensitive and accurate integration of single-cell data with Harmony. *Nat Methods* **16**, 1289-1296, doi:10.1038/s41592-019-0619-0 (2019).

76 Vekaria, H. J. *et al.* Formoterol, a beta2-adrenoreceptor agonist, induces mitochondrial biogenesis and promotes cognitive recovery after traumatic brain injury. *Neurobiol Dis* **140**, 104866, doi:10.1016/j.nbd.2020.104866 (2020).

77 Wills, L. P. *et al.* The beta2-adrenoceptor agonist formoterol stimulates mitochondrial biogenesis. *J Pharmacol Exp Ther* **342**, 106-118, doi:10.1124/jpet.112.191528 (2012).

78 Peterson, Y. K. *et al.* beta2-Adrenoceptor agonists in the regulation of mitochondrial biogenesis. *Bioorg Med Chem Lett* **23**, 5376-5381, doi:10.1016/j.bmcl.2013.07.052 (2013).

79 Cameron, R. B., Peterson, Y. K., Beeson, C. C. & Schnellmann, R. G. Structural and pharmacological basis for the induction of mitochondrial biogenesis by formoterol but not clenbuterol. *Sci Rep* **7**, 10578, doi:10.1038/s41598-017-11030-5 (2017).

80 Kitaoka, Y. *et al.* Effects of clenbuterol administration on mitochondrial morphology and its regulatory proteins in rat skeletal muscle. *Physiol Rep* **7**, e14266, doi:10.14814/phy2.14266 (2019).

81 Jelkmann, W. & Bauer, C. beta 2-Adrenergic stimulation of erythropoiesis in busulfan treated mice. *Exp Hematol* **8**, 742-748 (1980).

82 Ali, A. M. *et al.* Severely impaired terminal erythroid differentiation as an independent prognostic marker in myelodysplastic syndromes. *Blood Adv* **2**, 1393-1402, doi:10.1182/bloodadvances.2018018440 (2018).

83 Lima, A. T. *et al.* beta(1)- and beta(1)/beta(2)-adrenergic receptor antagonists block 6-nitrodopamine-induced contractions of the rat isolated epididymal vas deferens. *Naunyn Schmiedebergs Arch Pharmacol* **395**, 1257-1268, doi:10.1007/s00210-022-02268-6 (2022).

84 Cameron, R. B., Peterson, Y. K., Beeson, C. C. & Schnellmann, R. G. Author Correction: Structural and pharmacological basis for the induction of mitochondrial biogenesis by formoterol but not clenbuterol. *Sci Rep* **9**, 6790, doi:10.1038/s41598-019-42463-9 (2019).

85 Baker, J. G. The selectivity of beta-adrenoceptor agonists at human beta1-, beta2- and beta3-adrenoceptors. *Br J Pharmacol* **160**, 1048-1061, doi:10.1111/j.1476-5381.2010.00754.x (2010).

86 Hu, H. T. *et al.* HIF-1alpha links beta-adrenoceptor agonists and pancreatic cancer cells under normoxic condition. *Acta Pharmacol Sin* **31**, 102-110, doi:10.1038/aps.2009.181 (2010).

87 Ma, J. *et al.* Resveratrol inhibits the growth of tumor cells under chronic stress via the ADRB-2-HIF-1alpha axis. *Oncol Rep* **41**, 1051-1058, doi:10.3892/or.2018.6894 (2019).

88 Busca, R. *et al.* Hypoxia-inducible factor 1alpha is a new target of microphthalmia-associated transcription factor (MITF) in melanoma cells. *J Cell Biol* **170**, 49-59, doi:10.1083/jcb.200501067 (2005).

89 van Uden, P., Kenneth, N. S. & Rocha, S. Regulation of hypoxia-inducible factor-1alpha by NF-kappaB. *Biochem J* **412**, 477-484, doi:10.1042/BJ20080476 (2008).

90 Kumar, S. & Mehta, K. Tissue transglutaminase constitutively activates HIF-1alpha promoter and nuclear factor-kappaB via a non-canonical pathway. *PLoS One* **7**, e49321, doi:10.1371/journal.pone.0049321 (2012).

91 Ghosh, S. *et al.* Identification of RIOK2 as a master regulator of human blood cell development. *Nat Immunol* **23**, 109-121, doi:10.1038/s41590-021-01079-w (2022).

92 Li, J. *et al.* Isolation and transcriptome analyses of human erythroid progenitors: BFU-E and CFU-E. *Blood* **124**, 3636-3645, doi:10.1182/blood-2014-07-588806 (2014).

93 Logger, J. G. M., de Jong, E., Driessen, R. J. B. & van Erp, P. E. J. Evaluation of a simple image-based tool to quantify facial erythema in rosacea during treatment. *Skin Res Technol* **26**, 804-812, doi:10.1111/srt.12878 (2020).

94 Dobin, A. *et al.* STAR: ultrafast universal RNA-seq aligner. *Bioinformatics* **29**, 15-21, doi:10.1093/bioinformatics/bts635 (2013).

95 Fleming, S. J. *et al.* Unsupervised removal of systematic background noise from droplet-based single-cell experiments using CellBender. *Nat Methods* **20**, 1323-1335, doi:10.1038/s41592-023-01943-7 (2023).

96 Jumper, J. *et al.* Highly accurate protein structure prediction with AlphaFold. *Nature* **596**, 583-589, doi:10.1038/s41586-021-03819-2 (2021).

97 Ring, A. M. *et al.* Adrenaline-activated structure of beta2-adrenoceptor stabilized by an engineered nanobody. *Nature* **502**, 575-579, doi:10.1038/nature12572 (2013).

98 Zhang, Y. *et al.* Single-particle cryo-EM structural studies of the beta(2)AR-Gs complex bound with a full agonist formoterol. *Cell Discov* **6**, 45, doi:10.1038/s41421-020-0176-9 (2020).

99 Rigsby, R. E. & Parker, A. B. Using the PyMOL application to reinforce visual understanding of protein structure. *Biochem Mol Biol Educ* **44**, 433-437, doi:10.1002/bmb.20966 (2016).

ACKNOWLEDGEMENTS

We thank Dr. Jerome Ritz, Dr. Jacqueline S. Garcia (Dana-Farber Cancer Institute) and the Ted and Eileen Pasquarello Tissue Bank in Hematologic Malignancies for kind assistance in procuring primary MDS patient samples. We thank Bendbioscience Inc. for synthesizing the oral capsule formulation of FF for dosing in mice and the Center for Cancer Genomics (CCG) at Dana-Farber Cancer Institute for performing single cell RNA sequencing. We also thank Dr. Alexander J Loscalzo (Brigham and Women's Hospital) for assistance in blood pressure measurement in mice. We appreciate Dr. Kai W. Wucherpfennig (Dana-Farber Cancer Institute) for his guidance. We thank Dr. William G. Kaelin (Dana-Farber Cancer Institute) and Dr. Stuart Orkin (Boston Children's Hospital) for their valuable insights. We also thank Antero Biosciences for funding to synthesize oral FF capsules for dosing in mice. All illustrations are created with BioRender.com released under a Creative Commons Attribution-NonCommercial-NoDerivs 4.0 International license https://creativecommons.org/licenses/by-nc-nd/4.0/deed.en.

Funding

Institutional funding, Dana-Farber Cancer Institute (L.H.G.)

The Helen Gurley Brown Presidential Initiative (S.G.)

Friends of Dana-Farber Research Funding (S.G.)

The Claudia Adams Barr award (S.G.)

National Institutes of Health (S.A., M.H.)

Antero Biosciences

AUTHOR CONTRIBUTIONS

Conceptualization: S.G.; Designing: S.G. and L.H.G.; Methodology: S.G., S.X., M.A., H.E.C., M.T.N.; Sample Acquisition: S.G., S.X., M.A., H.E.C., M.T.N.; Data Analysis: S.G., S.X., S.A., M.H., E.D., G.A.P., and L.H.G.; Funding acquisition: S.G. and L.H.G.; Writing – original draft: S.G. and L.H.G.; Editing: S.G., L.H.G. and G.A.P. Supervision: S.G. and L.H.G.

COMPETING INTERESTS

S.G. and L.H.G. are co-founders of a new company, Antero Biosciences, that is developing drugs for prevention and management of anemia, based on this work.

L.H.G. is a former Director of Bristol-Myers Squibb, GlaxoSmithKline Pharmaceuticals and the Waters Corporation and recently stepped down on the Board of Directors of Analog Devices, Inc. L.H.G. is a consultant for JP Morgan healthcare and she has recently joined the Board of Directors of ReAlta, Inc.

E.D. is a co-founder and the Chief Technology Officer of a biotech company, Attivare Therapeutics Inc., that is developing Immunotherapies to treat oncology and infectious diseases.

G.A.P. is on the Scientific Advisory Boards of Amicus Therapeutics, MeiraGTx, Annovis Bio, Retromer Therapeutics, and Proclara Biosciences and holds equity or stock options in Denali Therapeutics, MeiraGTx, Annovis Bio, Retromer Therapeutics and Proclara Biosciences, companies that are developing therapies for neurodegenerative diseases.

All other authors declare no relevant competing interests.

S.G. and L.H.G. have 2 patents filed with Dana-Farber Cancer Institute, Boston based on this work.

INCLUSION AND ETHICS

We support inclusion and integrity in conduct of research.

FIGURE TITLES AND LEGENDS

Fig 1. Formoterol Fumarate (FF) enhances erythropoiesis *in vitro* and patient *ex vivo* settings. a, Median fluorescence intensity (MFI) plot and adjoining quantification of surface expression levels of CD235a on primary human HSPCs with increasing doses of FF (from Selleckchem) (day 5 of differentiation). MFI plot of a representative donor from n=4 donors. **b**, mRNA levels of erythroid lineage-specific genes (*HBB*, *HBA1*, *TFRC*) in primary human HSPCs with increasing doses of FF (normalized with *ACTB* mRNA levels). **c**, Representative flow plots showing 9 stages of erythroid differentiation in primary human HSPCs in response to FF (5 μM) or vehicle (Veh- DMSO) treatment (day 7 of differentiation). **d**, Structural modeling of FF (gray) bound to β2-adrenergic receptors (β2-AR) and magnified view of FF (blue) and adrenaline (cyan) bound to β2-AR. **e**, Representative images of burst-forming unit-erythroid (BFU-E) cells post 14 days of treating $CD34^+$ HSPCs with FF (1 μM) or vehicle (Veh) in semi-solid methylcellulose culture media (n=7 donors). **f**, Quantification of BFU-E and colony-forming unit-erythroid (CFU-E) cells after 14 days of HSPC treatment with FF (1 μM) or Veh (n=7 donors). **g**, Representative images and quantification of colony forming unit-granulocyte macrophage (CFU-GM) cells after 14 days of HSPC treatment with FF (1 μM) or Veh (n=7 donors). **h**, Schematic of $CD34^+$ cell isolation from the bone marrow (BM) aspirates of MDS patients and culturing in semi-solid methylcellulose differentiation media. **i**, Representative images of BFU-E cells post 14 days of treating non-del(5q) MDS patient-derived $CD34^+$ BM cells with FF (1 μM) or Veh (n=23 MDS patients). **j**, Quantification of BFU-E and CFU-E cells after 14 days of treating non-del(5q) MDS patient-derived $CD34^+$ BM cells with FF (1 μM) or Veh (n=23 MDS patients). **k**, **l**, Representative images and quantification of CFU-GM cells after 14 days of treating non-del(5q) MDS patient-derived $CD34^+$ BM cells with FF (1 μM) or Veh (n=23 non-del(5q) MDS patients). Data represented as mean ±

SEM. One-way analysis of variance (ANOVA) with Dunnett's multiple comparisons test performed in **a** and **b**. Two-tailed non-parametric Wilcoxon matched-pairs signed rank test performed in **f, g, j,** and **l**.

Fig 2. FF increases Hb at steady state and rescues anemia during hemolytic stress *in vivo*. **a**, Schematic of phenylhydrazine (Phz)-driven hemolytic stress and anemia in wild-type mice (C57BL/6J) followed by daily IP administrations of FF at a low dose of 0.3 mg/kg. **b**, Hemoglobin (Hb) in peripheral blood (PB) analyzed at indicated time points in vehicle (Veh) vs FF-treated mice upon Phz administration (n=9). **c**, Proportions of RI, RII, RIII, RIV erythroid progenitors in the BM of Veh vs FF-treated mice. **d**, Total erythroid progenitors (EPs-RI+RII+RIII+RIV) per $1\text{^}10^6$ viable BM cells isolated from Veh vs FF-treated mice (n=9). **e**, Schematic of daily IP administrations of FF at varying doses (0.1-0.3-0.5 mg/kg) in wild-type mice at steady state. **f**, Hb in PB analyzed at indicated time points in Veh vs FF-treated mice at steady state (n=5). **g**, Total EPs per $1\text{^}10^6$ viable BM cells isolated from Veh vs FF-treated mice at steady state after 30 days of daily drug administrations via IP. **h**, Survival of mice treated with a lethal dose of Phz (120 mg/kg) followed by daily IP administration of Veh or FF (0.3 mg/kg) for 7 days (n=10). **i**, Schematic of FF administration via oral gavage. **j**, Hb and hematocrit (HCT) in PB analyzed at indicated time points in Veh vs FF-treated mice (0.5 mg/kg) via oral gavage (OG) upon Phz administration (n=5). **k**, Proportions of RI, RII, RIII, RIV erythroid progenitors in the BM of Veh vs FF-treated mice via OG. **l**, Survival of mice treated with a lethal dose of phenylhydrazine (120 mg/kg) followed by daily OG of Veh or FF (0.3/0.5 mg/kg) for 7 days (n=5-10). Data represented as mean ± SEM. Two-way ANOVA (mixed model) in **b, f** (Dunnett's multiple comparisons test), **j**. Student's unpaired t-test performed in **d**. One-way analysis of variance (ANOVA) with Dunnett's multiple comparisons test performed in **g**. Kaplan-Meier survival analysis with Log-rank (Mantel-Cox) test performed in **h** and **l**.

Fig. 3. FF dramatically reverses anemia in pre-clinical mouse models of MDS and CKD. **a**, Schematic of experimental plan and treatment regimen in MDS transgenic mice; FF dosed at 0.3 mg/kg 5x weekly IP after

anemia developed in MDS mice aging 6-8 months. **b**, Hematocrit (HCT) and hemoglobin (Hb) in peripheral blood (PB) of MDS mice treated with vehicle (Veh) or FF; Control: littermate controls; (n=5). **c**, Representative images of paw redness in MDS mice treated with Veh or FF vs control mice treated with Veh (n=4). **d**, Proportions of RI, RII, RIII, RIV erythroid progenitors (EP) and adjoining quantification of total EPs per $1\text{^}10^6$ viable BM cells isolated from MDS/Control mice treated with Veh or FF. **e**,**f**, Granulocyte-macrophage progenitors (GMP) and megakaryocyte progenitors (MkP) per $1\text{^}10^6$ viable BM cells isolated from MDS mice treated with Veh or FF. **g**, Schematic of anemia development post Cisplatin (Cis; chemotherapy)-induced chronic kidney disease (CKD), followed by 3x weekly IP administration of FF (0.3 mg/kg) or Veh. **h**, Kidney histology (H&E staining) images showing signs of CKD (glomerular and tubular atrophy) upon Cisplatin (Cis) treatment; Control: No Cis treatment. **i**, Hb in PB analyzed at indicated time points in Cis-driven CKD mice treated with Veh or FF (n=4). **j, k**. Proportions of RI, RII, RIII, RIV EPs and their quantification in the BM of Cis-treated CKD mice given Veh or FF. **l**, Representative images showing paw redness in Apc^{min} mice treated with Veh or FF 3x weekly IP and control mice treated with Veh (n=5-6). **m**, Hb levels in Apc^{min} mice treated with Veh or FF and littermate controls (control) treated with Veh (n=5-6). **n**, Schematic of MDS mice treated with low dose of FF (0.3 mg/kg-5x weekly) vs high doses of epoetin α (EPO: 100 IU/kg- 3x weekly) and Reblozyl (REB: 10 mg/kg- 2x weekly). **o**, Hb levels in MDS mice treated with low dose of FF vs high doses of EPO or Reb for 3 weeks (n=4-5). Data represented as mean ± SEM. Two-way ANOVA (mixed model) with Dunnett's multiple comparisons test in **i, o** and Tukey's multiple comparisons test in **b, m**. One-way ANOVA with Tukey's multiple comparisons test in **d, e, f,** and **k**. Scale bar 100 μm in **h**.

Fig. 4. Adrb2 is expressed on the surface of early and late erythroid progenitors. a, Diagrammatic illustration of various stages of erythroid differentiation in mouse bone marrow (BM). **b**, Surface expression level of Adrb2 on murine hematopoietic stem cells (HSC), multipotent progenitors (MPP) and erythroid progenitors at different stages of differentiation (CFU-E, RI-E, RII-E, RIII-E, RIV-E) in the BM. **c**, Surface expression of Adrb2 on murine granulocyte-macrophage progenitors (GMP) and megakaryocyte progenitors (MkP) in the BM. **d**,

Schematic of phenylhydrazine (Phz)-induced hemolytic anemia in mice with *Adrb2*-haploinsufficiency in the hematopoietic compartment (*Adrb2*$^{Wt/fl}$*Vav*^{cre}) vs littermate controls (*Adrb2*$^{Wt/Wt}$*Vav*^{cre}). **e**, Peripheral blood hemoglobin (Hb) and hematocrit (HCT) levels in Phz-treated *Adrb2*$^{Wt/fl}$*Vav*^{cre} *and Adrb2*$^{Wt/Wt}$*Vav*^{cre} mice (n=5-8). **f**, HCT levels in *Adrb2*$^{Wt/fl}$*Vav*^{cre} mice administered with Phz and then treated with vehicle (Veh) or FF at 0.3 mg/kg daily IP (n=7-8). **g**, Schematic of Phz-induced hemolytic anemia in mice with *Adrb2*-haploinsufficiency in erythroid compartment (*Adrb2*$^{WT/fl;fl/fl}$*EpoR*^{cre}) vs littermate controls (*Adrb2*$^{Wt/Wt}$*EpoR*^{cre}). **h**, Hb and HCT levels in Phz-treated *Adrb2*$^{WT/fl;fl/fl}$*EpoR*^{cre} and littermate control *Adrb2*$^{Wt/Wt}$*EpoR*^{cre} mice (n=4-5). **i**, HCT levels in *Adrb2*$^{WT/fl}$*EpoR*^{cre} *and Adrb2*$^{fl/fl}$*EpoR*^{cre} mice administered with Phz and then treated with Veh or FF at 0.3 mg/kg daily IP (n=4-6). Data represented as mean ± SEM. Two-way ANOVA (mixed model) with Dunnett's multiple comparisons test in **h, i**, and Sidak's multiple comparisons test in **e, f**.

Fig. 5. Oral capsule formulation of FF reverses hemolytic anemia. a, Schematic illustration of the structure of FF-coated inert microbeads containing a modified release layer and FF-coated microbeads without any layer allowing immediate release of FF. **b**, Image showing synthesized FF-immediate release beads and FF-modified release beads. **c**, Release profiles of FF from modified-release beads and immediate-release beads, as measured by liquid chromatography. **d**, Image of gelatin capsules containing FF-modified release beads for dosing in mice. **e**, Release profile of FF from gelatin encapsulated modified release beads (FF-Cap) measured by liquid chromatography. **f**, Schematic of phenylhydrazine (Phz)-driven hemolytic anemia in wild-type mice followed by daily administrations of FF capsules (FF-Cap) at a low dose of ~0.25 mg/kg via oral cavity. **g, h**, RBCs and Hemoglobin (Hb) analyzed at indicated time points in placebo vs FF-Cap treated mice upon Phz administration (n=4-5). Placebo capsules contain microbeads and excipients without FF coating. **i**, **j**, Representative images and adjoining quantification of paw redness in Phz-treated mice administered with placebo vs FF-Cap (n=4-5). **k**, Terminal erythroid progenitors (EPs) per $1\text{^}10^6$ viable BM cells isolated from placebo vs FF-Cap treated mice (n=4-5). **l**, Terminal EPs per $1\text{^}10^6$ viable spleen cells isolated from placebo vs FF-Cap treated mice (n=4-5). Data

represented as mean ± SEM. Two-way ANOVA (mixed model) in **g** and **h**. Student's unpaired t-test performed in **j, k,** and **l**.

Fig. 6. FF triggers erythropoiesis partly via the *HIF-1α/EPAS1* pathway. **a**, UMAP showing unsupervised clustering of bone marrow (BM) progenitors isolated from naïve mice treated 5x weekly with vehicle (Veh) or FF at 0.3 mg/kg IP for 4 weeks. **b**, Proportions of various BM progenitors via single cell RNA sequencing (scRNA-seq) analysis; FF administration increases erythroid progenitors most significantly (p=2.93e-5) amongst other BM progenitors (highest odds ratio 1.85); "-" in bar plot denotes non-significant result. pDC: plasmacytoid dendritic cells, BMCPs: Basophils and Mast cell progenitors, HSCs: Hematopoietic stem cells. **c**, Magnified UMAP clustering of erythroid progenitors in the BM of Veh and FF-treated mice (overlaid). **d**, Enrichment of erythroid progenitors in the BM upon FF treatment at single cell resolution. **e, f, g**, Enrichment of gene signatures associated with mitochondrial biogenesis, cell proliferation and hypoxia pathways in the erythroid progenitors of Veh vs FF-treated mice: scRNA-seq analysis. **h**, Gene ontology analysis of significantly upregulated and downregulated pathways in erythroid progenitors of Veh vs FF-treated naïve mice via bulk RNA sequencing. **i**, Volcano plot showing differentially regulated genes from bulk RNA sequencing of Veh vs FF-treated erythroid progenitors. **j**, **k**, mRNA and protein levels (via immunoblotting) showing knockdown efficiency of HIF-1α in primary human HSPCs via CRISPR-Cas9 gene editing using 2 different guide RNAs (KD#1, KD#2: *ACTB* normalized) (TIDE analysis indel frequencies 54.6% and 86.4% in KD#1 and KD#2 cells, respectively); protein levels are β-Actin normalized. **l**, Cell surface expression of CD235a in control (Ctrl) vs *HIF-1α*-deficient (KD#1, KD#2) primary human HSPCs after treatment with Veh or FF (2 μM). **m**, Flow plots showing erythroblasts at distinct stages of erythroid differentiation in control (Ctrl) vs HIF-1α-deficient (KD#1, KD#2) primary human HSPCs upon treatment with vehicle (Veh) vs FF (5 μM). Data represented as mean ± SEM. One-way analysis of variance (ANOVA) with Dunnett's multiple comparisons test in **j** and Tukey's multiple comparisons test in **l**. Detailed statistical analyses of scRNA-seq and bulk RNA seq datasets are included in the Methods section. For uncropped Western blot data, see Supplementary Figure 1.

Extended Data Figures

Extended Data Fig. 1. Loss of *ADRB2* dampens erythroid differentiation. a, Genomic location of *ADRB2* at 5q32- a commonly deleted region (CDR) in del(5q) subtype of MDS patients. **b**, mRNA levels of *ADRB2* in $CD34^+$ cells isolated from bone marrow (BM) aspirates of healthy individuals, del(5q) and non del(5q) MDS patients. **c**, **d**, mRNA and protein levels (via western blotting) show depletion of *ADRB2* using 2 different guide RNAs (KD#1, KD#2) via CRISPR-Cas9 gene editing in primary human $CD34^+$ hematopoietic stem and progenitor cells (HSPCs) (TIDE analysis indel frequencies 68.8% and 37.7% in KD#1 and KD#2 cells, respectively); protein levels are β-Actin normalized. **e**. Median fluorescence intensity (MFI), adjoining quantification of CD235a surface expression and $CD235a^+$ populations in primary human HSPCs upon *ADRB2* deficiency at day 5 of erythroid differentiation. **f**, Myelopoiesis ($CD11b^+$ populations and surface expression of CD11b) upon loss of *ADRB2* in primary human HSPCs at day 5 of erythroid differentiation. **g**, Megakaryopoiesis ($CD41/61^+$ populations and surface expression of CD41/61) upon loss of *ADRB2* in primary human HSPCs at day 5 of erythroid differentiation. **h**, mRNA levels of genes associated with erythroid differentiation (*HBB, HBA1, FECH, TFRC*: *ACTB* normalized) in *ADRB2*-proficient (control) and deficient (*ADRB2* KD) primary human HSPCs. **i**, Representative flow plot showing 9 stages of erythroid differentiation in primary human $CD34^+$ HSPCs *in vitro* on day 7 of culture. **j**, **k**, Representative flow plots showing 9 stages of erythroid differentiation (EP1-Orthochromatic erythroblasts) in control and ADRB2 KD primary human HSPCs at days 7 and 12 of differentiation, respectively. **l**, Quantification of various stages of erythroid differentiation in control and ADRB2 KD primary human HSPCs at days 7 and 12 of differentiation. Data represented as mean ± SEM. Non-parametric Kruskal-Wallis test with Dunn's multiple comparisons test in **b**. One-way analysis of variance (ANOVA) with Dunnett's multiple comparisons test in **c, e, f** and **g**. Two-tailed unpaired t test in **h** and **l**. Quantifications presented in **c, e, f, g, h** from a representative donor, analyses performed in n=3 primary donors. EP1, 2, 3, 4: Erythroid Progenitors 1, 2, 3, 4; Pro: Proerythroblasts; EB, LB: Early and Late Basophilic erythroblasts; Poly:

Polychromatic erythroblasts; Ortho: Orthochromatic erythroblasts. For uncropped Western blot data, see Supplementary Figure 1.

Extended Data Fig. 2. Formoterol fumarate (FF) promotes erythropoiesis, but not myelopoiesis or megakaryopoiesis. a, Growth curves of 9 distinct stages of erythroid differentiation in ADRB2-knockdown (KD) and control human HSPCs. **b**, Surface expression of ADRB2 on primary human $CD34^+$ hematopoietic stem and progenitor cells (HSPCs); n=4 donors. **c**, ADRB2 surface expression in control and ADRB2-deficient (ADRB2 KD) primary human HSPCs, shown using BS-0947R antibody. **d**, **e**, CD235a surface expression and $CD235a^+$ populations (denoting erythropoiesis) in primary human $CD34^+$ HSPCs in response to increasing doses of FF (from Sigma and Selleckchem, respectively) on day 5 of differentiation. **f**, Viability at varying doses of FF treatment in primary human HSPCs. **g**, Expansion of human HSPCs while placed in erythroid differentiation media in the presence and absence of FF. **h-j,** Myelopoiesis (CD11b cell surface expression out of $CD11b^+$ cells and $CD11b^+$ populations) at varying doses of FF treatment in primary human HSPCs on day 5 of differentiation. **k-m**, Megakaryopoiesis (CD41/61 cell surface expression out of $CD41/61^+$ cells and $CD41/61^+$ populations) at varying doses of FF treatment in primary human HSPCs on day 5 of differentiation. Data represented as mean ± SEM. One-way analysis of variance (ANOVA) with Dunnett's multiple comparisons test performed in **d, e, f, i, j, l, m**. Two-way ANOVA (mixed model) with Dunnett's multiple comparison's test in **g**. Data shown from day 5 of erythroid differentiation in **d-f, h-m**. Quantifications presented from a representative donor, analyses performed in n=4 donors in **d, e** and n=3 donors in **f, i, j, l, m**.

Extended Data Fig. 3. FF augments erythropoiesis at various stages of differentiation. a, **b**, Representative flow plots and adjoining quantifications showing 9 stages of erythroid differentiation in primary human HSPCs in response to FF (5 μM) or vehicle (Veh- DMSO) treatments at various time-points. **c**, **d**, Reticulocytes and enucleation% during erythroid differentiation *in vitro* in response to FF (5 μM) or vehicle (Veh- DMSO)

treatments. **e**, Representative cytospin images (60x magnification) of May-Grünwald-Giemsa (MGG)-stained sorted erythroblasts at distinct stages from days 7-14 of erythroid differentiation of primary human $CD34^+$ HSPCs (Veh vs FF 5 μM). EP1, 2, 3, 4: Erythroid Progenitors 1, 2, 3, 4; Pro: Proerythroblasts; EB, LB: Early and Late Basophilic erythroblasts; Poly: Polychromatic erythroblasts; Ortho: Orthochromatic erythroblasts. Data represented as mean ± SEM. Two-tailed unpaired t test in **b-d**. Scale bar 20 μm in **e.**

Extended Data Fig. 4. FF promotes cell surface expression of CD71, CD235a across various stages of erythroid differentiation. a, Histogram showing cell surface expression patterns of CD71 across distinct stages of human erythroid differentiation *in vitro*. **b**. Representative histograms and adjoining quantifications showing cell surface expression of CD71 at distinct stages of human erythroid differentiation (day 7) upon vehicle (Veh) vs FF (5 μM) treatment. **c,** Histogram showing cell surface expression patterns of CD235a across distinct stages of human erythroid differentiation *in vitro*. **d**. Representative histograms and adjoining quantifications showing cell surface expression of CD235a at distinct stages of human erythroid differentiation (day 7) upon vehicle (Veh) vs FF (5 μM) treatment. Use of biexponential transformation resulted in negative MFI values for CD235a in EP1, EP2, and EP3,4. **e**, Quantifications showing cell surface expression of CD235a in reticulocytes upon vehicle (Veh) vs FF (5 μM) treatment. **f**, **g**, CD235a cell surface expression and distinct stages of erythroid differentiation (day 7) in *ADRB2*-deficient (ADRB2 KD) vs control HSPCs upon FF (5 μM) treatment. **h-j**, Erythropoiesis (CD235a), myelopoiesis (CD11b) and megakaryopoiesis (CD41/61) after treatment of $CD34^+$ BM cells isolated from MDS patients (n=40) with FF/vehicle treatment in liquid differentiation culture. Data represented as mean ± SEM. Two-tailed unpaired t test in **b, d, e.** One-way analysis of variance (ANOVA) with Dunnett's multiple comparisons test performed in **f**. Two-tailed non-parametric Wilcoxon matched-pairs signed rank test performed in **h-j**.

Extended Data Fig. 5. FF stimulates erythropoiesis and rescues anemia *in vivo*. a, Absolute hemoglobin (Hb) and hematocrit (HCT%) levels after 15 days of Phz administration in mice treated with daily IP of FF (0.3 mg/kg).

b, Proportions of RI, RII, RIII, RIV erythroid progenitors (EP) per 1^10^6 viable bone marrow (BM) cells of Veh vs FF-treated mice (n=9). **c**, White blood cells (WBCs) and platelets in peripheral blood (PB) analyzed at indicated time points in vehicle (Veh) vs FF-treated mice upon phenylhydrazine (Phz) administration (n=9). **d**, **e**, Granulocyte-macrophage progenitors (GMP) and megakaryocytic-erythroid progenitors (MEP) per 1^10^6 viable BM cells isolated from Phz-administered mice treated with Veh or FF 0.3 mg/kg (n=5). **f**, **g**, Spleen pictures and quantifications of splenic weights in Veh vs FF-treated mice at various time-points after Phz administration. **h**, Total erythroid progenitors (EPs) per 1^10^6 viable spleen cells of Veh vs FF 0.3 mg/kg-treated mice (n=5) at various time-points after Phz administration (No RBC lysis). **i**, **j**, Flow plots and quantifications showing proportions of RI, RII, RIII, RIV erythroid progenitors (EP) per 1^10^6 viable spleen cells of Veh vs FF-treated mice (n=5) after 15 days of Phz administration (No RBC lysis). **k**, Hemoglobin (Hb) and hematocrit (HCT%) in peripheral blood (PB) analyzed at indicated time points in vehicle (Veh) vs FF 0.3 mg/kg-treated mice with or without Phz administration (n=5).. **l-n**, Hb, WBCs and platelets in Veh vs FF-treated mice (daily drug administration via IP at varying doses of 0.1-0.3-0.5 mg/kg) at steady state. **o, p**, GMPs and MEPs per 1^10^6 viable BM cells isolated from Veh vs FF-treated mice at steady state (n=5). Data represented as mean ± SEM. Two-tailed unpaired t test in **a, b, d, e, f, g, h, j**. One-way analysis of variance (ANOVA) with Dunnett's multiple comparisons test performed in **l, o, p.** Two-way ANOVA (mixed model) with Dunnett's multiple comparison's test in **c, k, m, n**.

Extended Data Fig. 6. FF promotes erythropoiesis without causing organ toxicities *in vivo*. a, Hematocrit% (HCT%) and red blood cells (RBCs) of mice treated with a lethal dose of phz (120 mg/kg). **b, c**, Serum erythropoietin and hepcidin levels in mice treated with Veh or FF IP daily for 30 days. **d**, Serum ferritin, free iron and transferrin saturation levels in mice treated with Veh or FF (0.3 mg/kg) IP daily for 30 days. **e**, **f,** Systolic, diastolic blood pressure (BP) and heart rates of mice treated with Veh or FF IP daily for 30 days; bmp: beats per minute. **g**, Absolute hemoglobin (Hb) and hematocrit (HCT%) levels after 15 days of Phz administration in mice treated with FF (0.5 mg/kg) via oral gavage (OG). **h-j**, HCT and hemoglobin (Hb) levels in PB analyzed at

indicated time points in Veh vs FF (0.5 mg/kg)-treated mice via oral gavage (OG) at steady state (n=5). **k-m**, EPs, GMPs, and MEPs per 1^10^6 viable BM cells isolated from Veh vs FF (0.5 mg/kg)-treated mice via OG at steady state (n=5). **n**, Histology (H&E staining) of organs isolated from mice treated with Vehicle (Veh) or FF (0.5 mg/kg) daily IP for 30 days, showing no signs of toxicity. Data represented as mean ± SEM. Two-way ANOVA (mixed model) with Dunnett's multiple comparisons test in **h**. Student's unpaired t-test performed in **a-g, i-m**. Scale bar 200 μm in **n**.

Extended Data Fig. 7. FF rescues anemia in pre-clinical mouse models of MDS and CKD. a, Absolute hemoglobin (Hb) levels in 8-10 months old myelodysplastic syndrome (MDS) mice treated with Veh or FF (0.3 mg/kg 5x weekly IP) and littermate controls treated with Veh (Control+ Veh). **b**, Paw redness of MDS mice treated with Veh or FF and littermate controls treated with Veh (Control+ Veh). **c**, **d**, Splenic erythroid progenitors (EP) and WBCs of MDS mice treated with Veh vs FF (n=5) for 4 weeks. **e**, Blast percentages in the bone marrow (BM) and spleen of MDS mice treated with Veh vs FF (n=5) for 4 weeks. **f**, Blood urea nitrogen (BUN) and creatinine levels in the serum isolated from Cisplatin (Cis)-driven chronic kidney disease **(**CKD) mice treated with Veh or FF (0.3 mg/kg) and Cis-untreated controls (n=4-5). **g**, **h**, Erythropoietin and Hb levels in the peripheral blood of CKD mice treated with Veh or FF (0.3 mg/kg) and Cis-untreated controls. **i**, Hematocrit% (HCT%) in peripheral blood (PB) analyzed at indicated time points in Cis-driven CKD mice treated with Veh or FF (n=4/5). **j, k**, Granulocyte-macrophage progenitors (GMP) and megakaryocytic progenitors (MkP) per 1^10^6 viable BM cells isolated from Cis-driven CKD mice treated with Veh or FF (n=4/5). **l, m**, Absolute Hb and paw redness of Apc^{min} mice treated with Veh or FF and littermate controls treated with Veh (Control+ Veh). **n**, Kidney histology showing signs of CKD upon 5 months of aristolochic acid (AA) treatment (5 mg/kg once weekly IP). **o, p**, Serum erythropoietin, absolute Hb and HCT levels in AA-driven CKD mice treated with Veh or FF or Daprodustat (Dap) at 0.3 mg/kg 5x weekly via oral gavage (n=5). **q**, HCT% and Hb in PB analyzed at indicated time points in AA-driven CKD mice treated with Veh or FF or Daprodustat (Dap) at 0.3 mg/kg 5x weekly via oral gavage (n=5). Data represented as mean ± SEM. One-way analysis of variance (ANOVA) with Dunnett's multiple comparisons

test performed in **a-h, j-m, o, p**. Two-way ANOVA (mixed model) with Dunnett's multiple comparison's test in **i, q**. Scale bar 50 μm in **n**.

Extended Data Fig. 8. ADRB2 is expressed on the cell surface of human and murine erythroid progenitors. **a**, Absolute hemoglobin (Hb) levels in MDS mice treated with low dose of FF vs high doses of EPO or Reb for 3 weeks (n=4-5). **b**, **c**, % changes and absolute Hb levels in MDS mice comparing low dose of FF vs high doses of EPO or Reb for 4 weeks as single agents vs combination treatments (FF+Epo and FF+Reb) (n=4-5) (0= Basal, 2=2 weeks after treatment, 4= 4 weeks after treatment). **d**, **e**, Spleen images showing splenic size and adjoining quantifications showing splenic weights in MDS mice treated with low dose of FF, high doses of EPO or Reb, and combination treatments (FF+Epo and FF+Reb) for 4 weeks (n=4-5). **f**, **g**, Histograms and adjoining quantifications showing cell surface expression of ADRB2 at distinct stages of erythroid differentiation in primary human HSPCs (day 7) using 2 different antibodies against ADRB2, ADRB2-I: BS-0947R and ADRB2-II: AAR-016. **h**, Quantifications showing cell surface expression level of Adrb2 on murine hematopoietic stem cells (HSC), multipotent progenitors (MPP) and erythroid progenitors at different stages of differentiation (CFU-E, RI-E, RII-E, RIII-E, RIV-E) in the BM using Adrb2 antibody: AAR-016. **i**, Histograms showing cell surface expression level of Adrb2 on total murine erythroid progenitors in the spleen using Adrb2 antibody: BS-0947R. Data represented as mean ± SEM. One-way analysis of variance (ANOVA) with Dunnett's multiple comparisons test performed in **a, c, e**. Two-way ANOVA (mixed model) with Dunnett's multiple comparison's test in **b**.

Extended Data Fig. 9. *Adrb2* deficiency in the hematopoietic and erythroid compartments impairs revival from anemia under hemolytic stress. **a**, mRNA levels of *Adrb2* in the bone marrow cells of *Adrb2*-deficient ($Adrb2^{WT/fl}Vav^{cre}$; $Adrb2^{fl/fl}Vav^{cre}$) vs proficient littermate controls ($Adrb2^{WT/WT}Vav^{cre}$). **b**, Absolute hemoglobin (Hb) and hematocrit (HCT) levels in peripheral blood (PB) of $Adrb2^{WT/fl}Vav^{cre}$ vs littermate controls ($Adrb2^{WT/WT}Vav^{cre}$) at steady state. **c**, **d**, Platelets and white blood cells (WBCs) in Phz-treated $Adrb2^{WT/fl}Vav^{cre}$

and *Adrb2*$^{WT/WT}$*Vav*^{cre} mice. **e**, mRNA levels of *Adrb2* in erythroid progenitors (EP) of bone marrow isolated from *Adrb2*-deficient (*Adrb2*$^{WT/fl}$*EpoR*^{cre}*; Adrb2*$^{fl/fl}$*EpoR*^{cre}) vs proficient littermate controls (*Adrb2*$^{WT/WT}$*EpoR*^{cre}). **f**, Histogram showing cell surface expression of erythroid progenitors in *Adrb2*-deficient (*Adrb2*$^{WT/fl}$*EpoR*^{cre}*; Adrb2*$^{fl/fl}$*EpoR*^{cre}) vs proficient littermate control (*Adrb2*$^{WT/WT}$*EpoR*^{cre}) mice using Adrb2 antibody: BS-0947R. **g**, Absolute Hb and HCT% levels in PB of *Adrb2*-deficient (*Adrb2*$^{WT/fl}$*EpoR*^{cre}*; Adrb2*$^{fl/fl}$*EpoR*^{cre}) vs littermate controls (*Adrb2*$^{WT/WT}$*EpoR*^{cre}) at steady state. **h, i**, Platelets and WBCs in Phz-treated *Adrb2*$^{WT/fl}$*EpoR*^{cre}*, Adrb2*$^{fl/fl}$*EpoR*^{cre} and *Adrb2*^{WTWT}*EpoR*^{cre} mice. **j**, Clustering of bone marrow (BM) progenitors isolated from naïve mice treated with Vehicle (Veh) or FF (0.3 mg/kg IP 5X weekly for a month). **k**, UMAP projections of overlaid BM progenitors of Veh vs FF-treated mice after batch correction. Data represented as mean ± SEM. One-way analysis of variance (ANOVA) with Dunnett's multiple comparisons test performed in **a, e, g**. Two-way ANOVA (mixed model) with Dunnett's multiple comparison's test in **c, d, h, i.** Student's unpaired t-test performed in **b.**

Extended Data Fig. 10. Analysis of bone marrow progenitors upon FF treatment. a, Enrichment of significantly-altered genes associated with heme biosynthesis, mitochondrial biogenesis, cell proliferation and hypoxia-responsiveness in erythroid progenitors upon FF treatment (scRNA-seq analysis). **b**, Quantifications showing 9 stages of erythroid differentiation in primary human HSPCs in response to FF (5 μM), Clenbuterol (Clen: 5 μM) or vehicle (Veh- DMSO) treatments at day 7 of differentiation *in vitro*. **c**, Hematocrit (HCT) and hemoglobin (Hb) levels in naïve mice treated with Veh or FF 0.3 mg/kg IP 3x weekly. **d**, Heat map showing expression patterns of HIF-1α-related gene signatures from bulk RNA sequencing of erythroid progenitors sorted from naïve mice treated with Veh or FF 0.3 mg/kg IP 3x weekly for 4 weeks. **e**, Validation of mRNA expressions of HIF-1α-related gene signatures identified in **d** in primary human HSPCs treated with FF (*ACTB* normalized). **f**, **g**, Western blotting and adjoining quantifications in primary human HSPCs treated with vehicle (Veh) vs FF showing HIF-1α and HIF-2α expression, respectively; protein levels are β-Actin normalized. **h**, Western blotting and adjoining quantifications in primary human HSPCs treated with vehicle (Veh) vs FF showing hydroxylated HIF-1α (Proline 564) expression. **i**, Western blotting and adjoining quantifications in HIF-1α- proficient (Control)

and HIF-1α-deficient (KD using 2 different gRNAs: KD#1, KD#2) human HSPCs treated with vehicle (Veh) vs FF showing HIF-1α expression. **j**, **k**, mRNA and protein levels (via immunoblotting) showing knockdown efficiency of *EPAS1* (encoding HIF-2α) in primary human HSPCs via CRISPR-Cas9 genome editing using 2 different guide RNAs (KD#1, KD#2) (TIDE analysis indel frequencies 52.9% and 91.4% in KD#1 and KD#2 cells, respectively); mRNA levels are *ACTB* normalized and protein levels are β-Actin normalized. **l**, Cell surface expression of CD235a in control (Ctrl) vs *EPAS1*-deficient (KD#1, KD#2) primary human HSPCs upon treatment with vehicle (Veh) vs FF (2 μM). **m**, Flow plots showing erythroblasts at distinct stages of erythroid differentiation in control (Ctrl) vs *EPAS1*-deficient (KD#1, KD#2) primary human HSPCs upon treatment with vehicle (Veh) vs FF (5 μM). Data represented as mean ± SEM. Two-way ANOVA (mixed model) with Dunnett's multiple comparisons test performed in **c**. One-way analysis of variance (ANOVA) with Dunnett's multiple comparisons test performed in **b, j** and Tukey's multiple comparisons test in **l**. Student's unpaired t-test performed in **e-h.** For uncropped Western blot data, see Supplementary Figure 1.

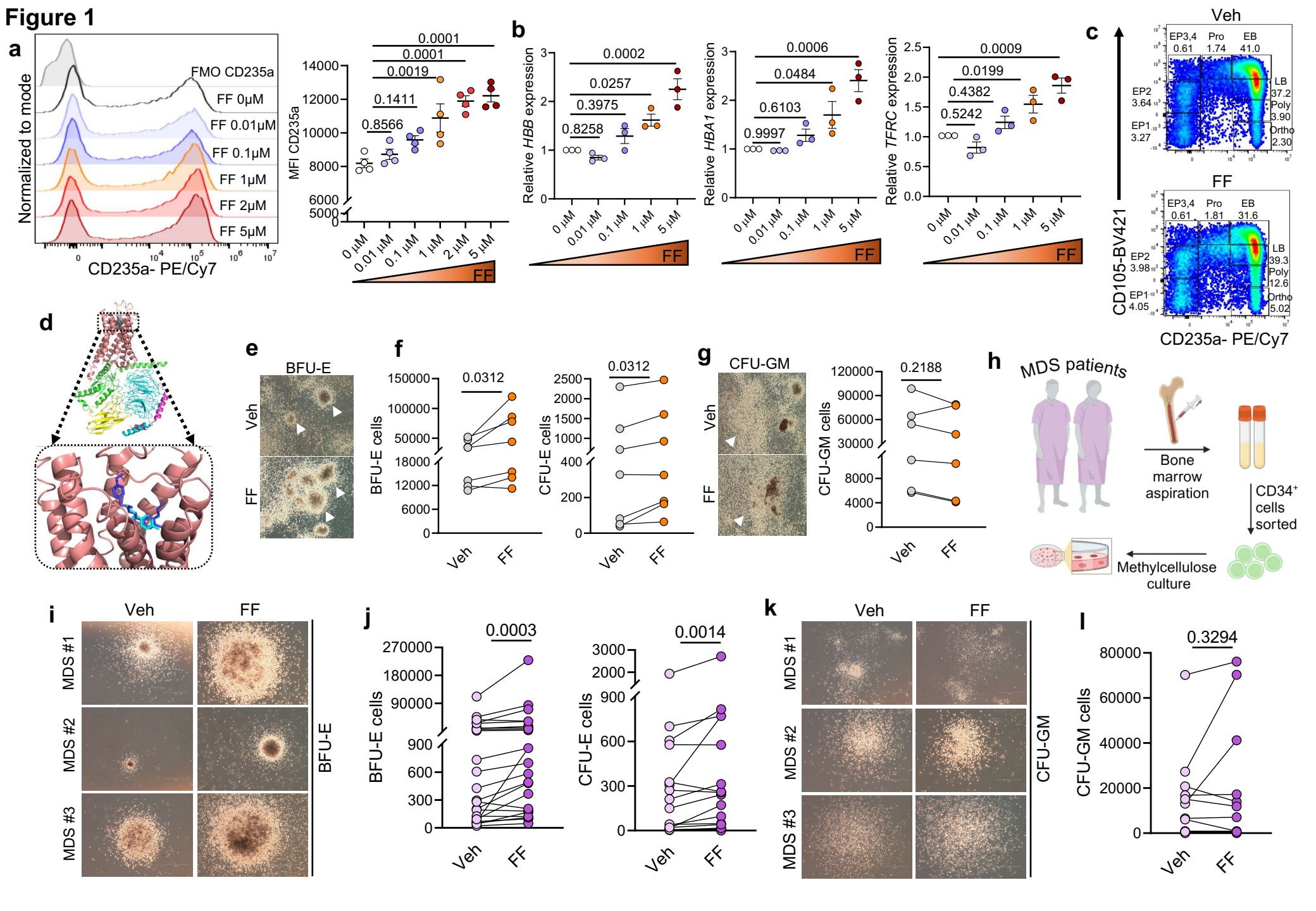
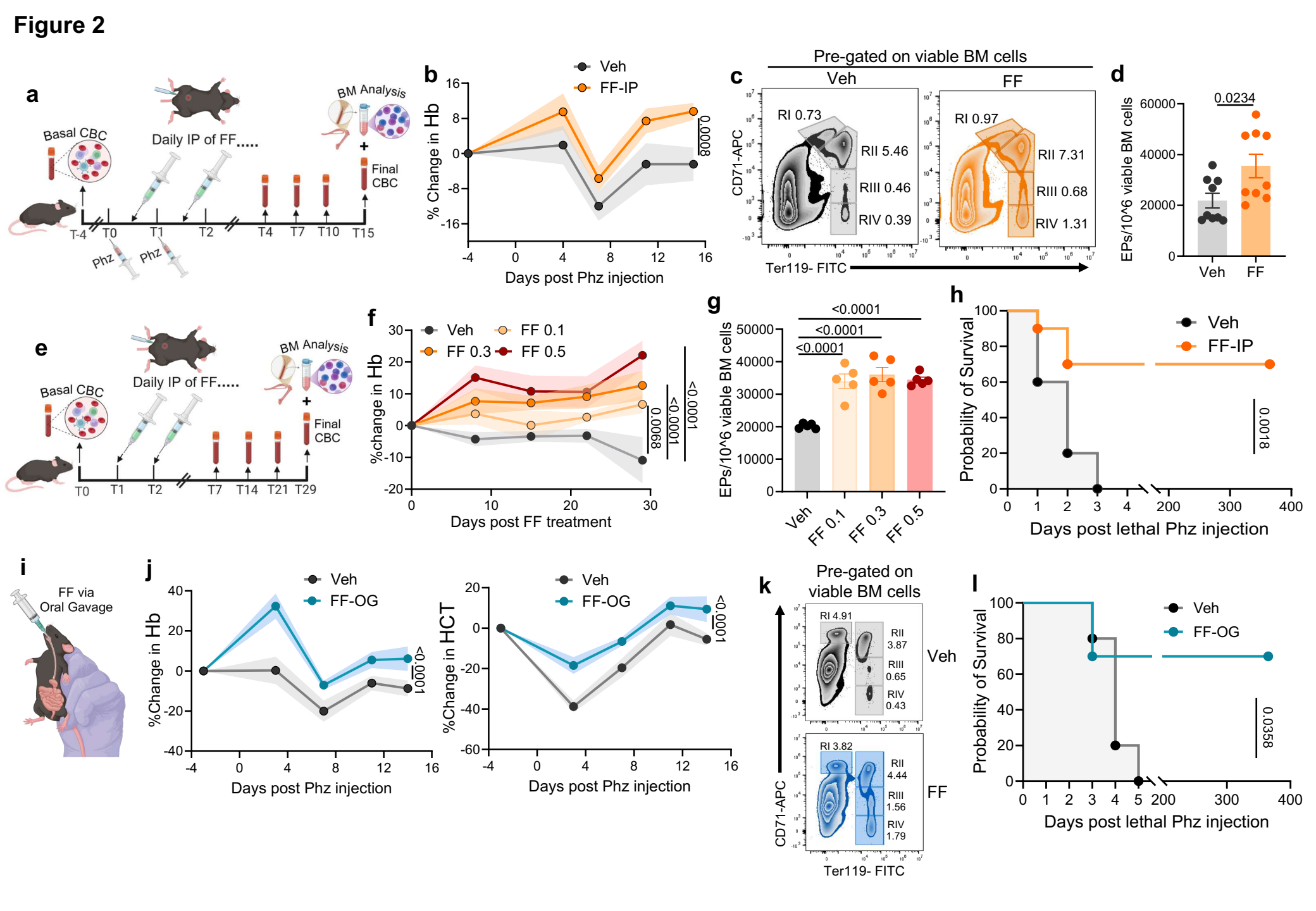

Figure 1
a
Normalized to mode
FMO CD235a
FF 0μM
FF 0.01μM
FF 0.1μM
FF 1μM
FF 2μM
FF 5μM
CD235a- PE/Cy7
MFI CD235a
0.0001
0.0001
0.0019
0.1411
0.8566
0 μM
0.01 μM
0.1 μM
1 μM
2 μM
5 μM
FF
b
Relative HBB expression
0.0002
0.0257
0.3975
0.8258
Relative HBA1 expression
0.0006
0.0484
0.6103
0.9997
Relative TFRC expression
0.0009
0.0199
0.4382
0.5242
c
Veh
FF
EP3,4
Pro
EB
0.61
1.74
41.0
EP2
3.64
EP1
3.27
LB
37.2
Poly
3.90
Ortho
2.30
0.61
1.81
31.6
3.98
4.05
39.3
12.6
5.02
CD105-BV421
CD235a- PE/Cy7
d
e
BFU-E
Veh
FF
f
BFU-E cells
0.0312
CFU-E cells
0.0312
g
CFU-GM
CFU-GM cells
0.2188
h
MDS patients
Bone marrow aspiration
CD34+ cells sorted
Methylcellulose culture
i
Veh
FF
MDS #1
MDS #2
MDS #3
BFU-E
j
BFU-E cells
0.0003
CFU-E cells
0.0014
k
CFU-GM
l
CFU-GM cells
0.3294

Figure 2


a
Basal CBC
Daily IP of FF.....
BM Analysis
Final CBC
T-4
T0
T1
T2
T4
T7
T10
T15
Phz
Phz
b
Veh
FF-IP
% Change in Hb
Days post Phz injection
0.0008
c
Pre-gated on viable BM cells
Veh
FF
RI 0.73
RII 5.46
RIII 0.46
RIV 0.39
RI 0.97
RII 7.31
RIII 0.68
RIV 1.31
CD71-APC
Ter119- FITC
d
0.0234
EPs/10^6 viable BM cells
Veh
FF
e
Basal CBC
Daily IP of FF.....
BM Analysis
Final CBC
T0
T1
T2
T7
T14
T21
T29
f
Veh
FF 0.1
FF 0.3
FF 0.5
%change in Hb
Days post FF treatment
0.0068
<0.0001
<0.0001
g
<0.0001
<0.0001
<0.0001
EPs/10^6 viable BM cells
Veh
FF 0.1
FF 0.3
FF 0.5
h
Veh
FF-IP
Probability of Survival
Days post lethal Phz injection
0.0018
i
FF via Oral Gavage
j
Veh
FF-OG
%Change in Hb
Days post Phz injection
<0.0001
Veh
FF-OG
%Change in HCT
Days post Phz injection
<0.0001
k
Pre-gated on viable BM cells
RI 4.91
RII 3.87
RIII 0.65
RIV 0.43
Veh
RI 3.82
RII 4.44
RIII 1.56
RIV 1.79
FF
CD71-APC
Ter119- FITC
l
Veh
FF-OG
Probability of Survival
Days post lethal Phz injection
0.0358

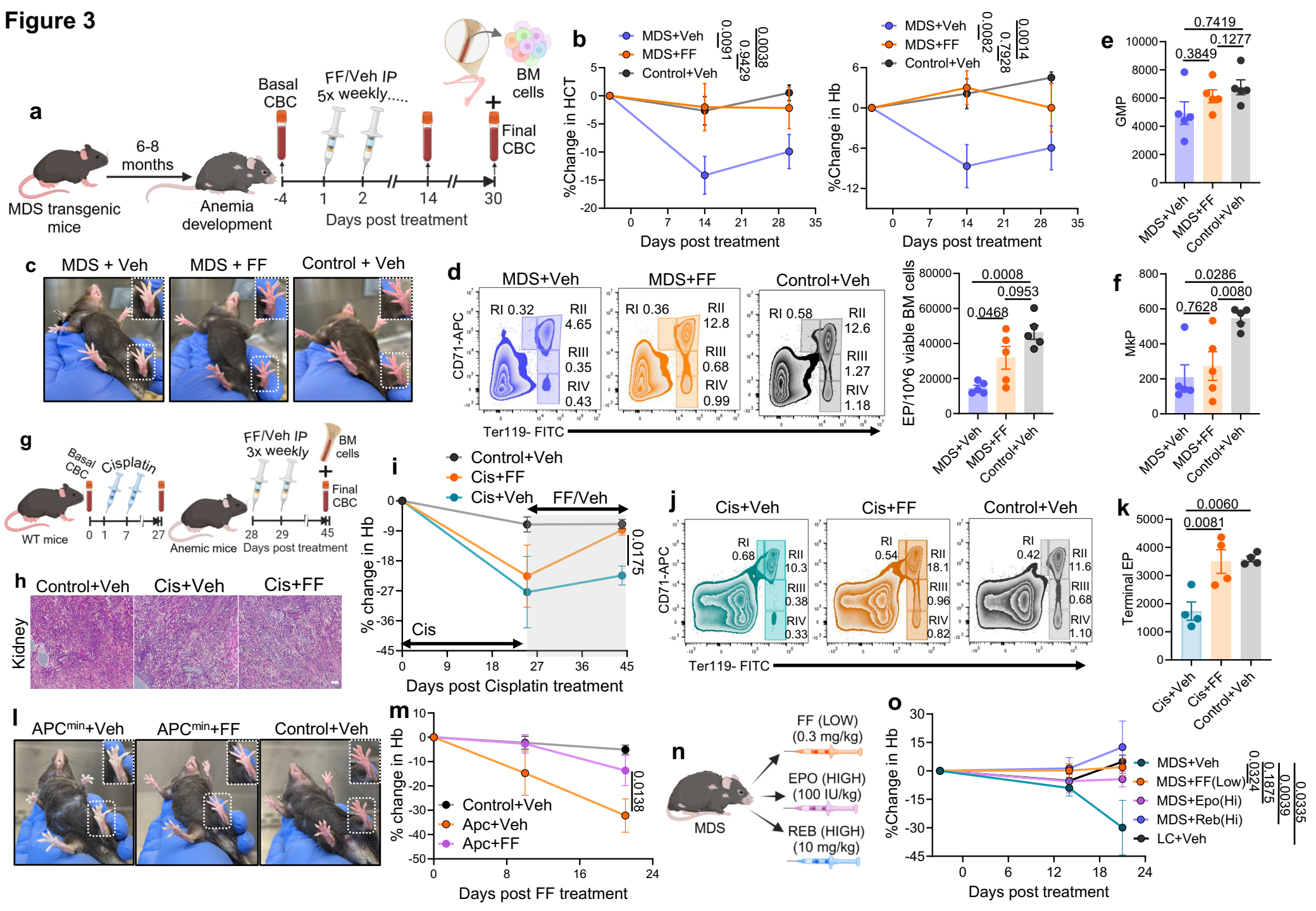

Figure 3
a
6-8 months
MDS transgenic mice
Anemia development
Basal CBC
FF/Veh IP 5x weekly.....
BM cells
Final CBC
-4
1
2
14
30
Days post treatment
b
MDS+Veh
MDS+FF
Control+Veh
0.0091
0.0038
0.9429
%Change in HCT
Days post treatment
0.0082
0.7928
0.0014
%Change in Hb
e
0.7419
0.1277
0.3849
GMP
c
MDS + Veh
MDS + FF
Control + Veh
d
MDS+Veh
MDS+FF
Control+Veh
RI 0.32
RII 4.65
RIII 0.35
RIV 0.43
RI 0.36
RII 12.8
RIII 0.68
RIV 0.99
RI 0.58
RII 12.6
RIII 1.27
RIV 1.18
CD71-APC
Ter119- FITC
0.0008
0.0953
0.0468
EP/10^6 viable BM cells
f
0.0286
0.0080
0.7628
MkP
g
Basal CBC
Cisplatin
FF/Veh IP 3x weekly
BM cells
Final CBC
WT mice
Anemic mice
0
1
7
27
28
29
45
Days post treatment
i
Control+Veh
Cis+FF
Cis+Veh
FF/Veh
Cis
0.0175
% change in Hb
Days post Cisplatin treatment
j
Cis+Veh
Cis+FF
Control+Veh
RI 0.68
RII 10.3
RIII 0.38
RIV 0.33
RI 0.54
RII 18.1
RIII 0.96
RIV 0.82
RI 0.42
RII 11.6
RIII 0.68
RIV 1.10
CD71-APC
Ter119- FITC
k
0.0060
0.0081
Terminal EP
h
Control+Veh
Cis+Veh
Cis+FF
Kidney
l
APC^min+Veh
APC^min+FF
Control+Veh
m
Control+Veh
Apc+Veh
Apc+FF
0.0138
% change in Hb
Days post FF treatment
n
MDS
FF (LOW) (0.3 mg/kg)
EPO (HIGH) (100 IU/kg)
REB (HIGH) (10 mg/kg)
o
MDS+Veh
MDS+FF(Low)
MDS+Epo(Hi)
MDS+Reb(Hi)
LC+Veh
0.0324
0.1875
0.0039
0.0335
%Change in Hb
Days post treatment

Figure 4

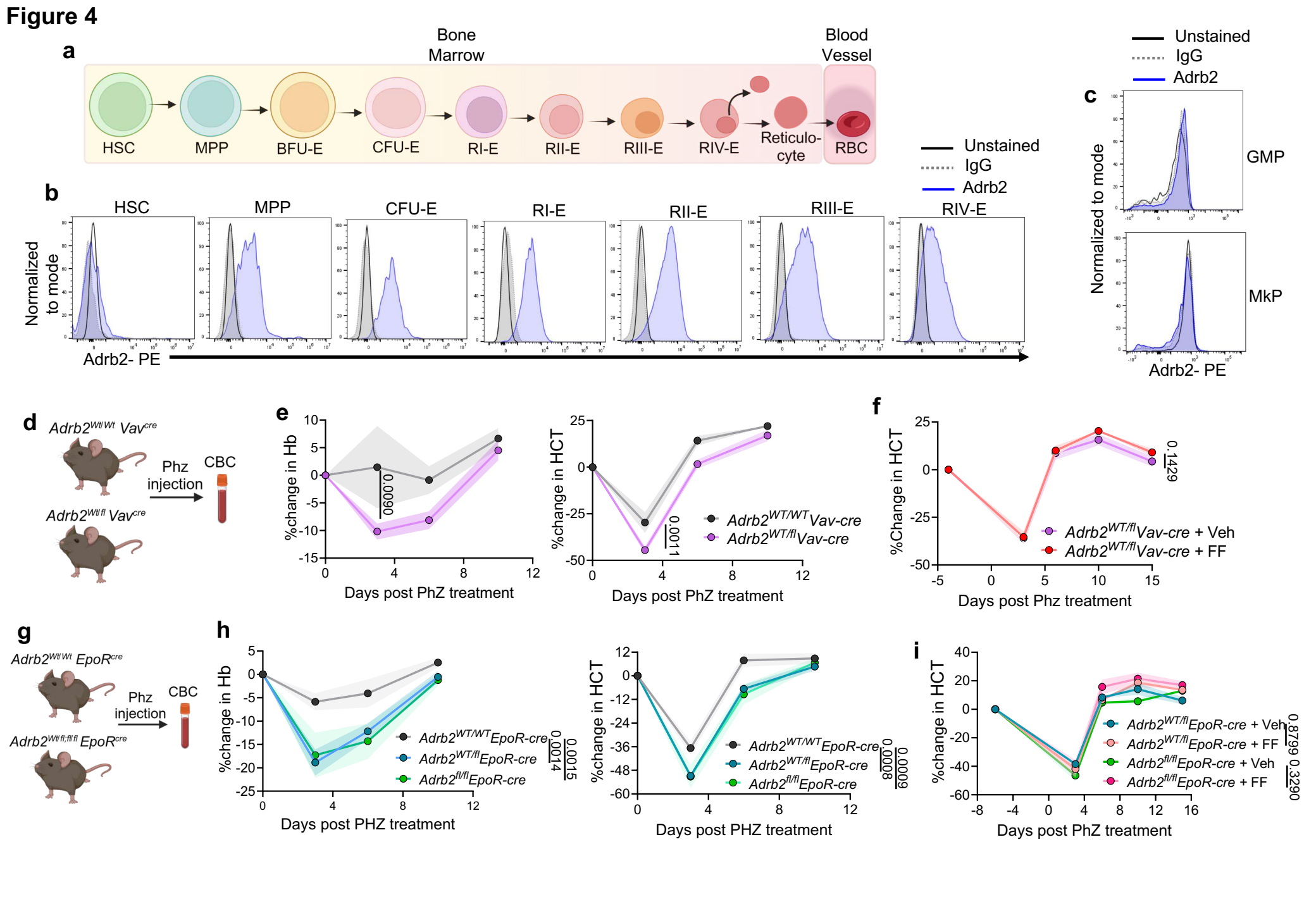

a
Bone Marrow
Blood Vessel
HSC
MPP
BFU-E
CFU-E
RI-E
RII-E
RIII-E
RIV-E
Reticulo-cyte
RBC
Unstained
IgG
Adrb2
b
HSC
MPP
CFU-E
RI-E
RII-E
RIII-E
RIV-E
Normalized to mode
Adrb2- PE
c
GMP
MkP
Normalized to mode
Adrb2- PE
d
Adrb2Wt/Wt Vavcre
Adrb2Wt/fl Vavcre
Phz injection
CBC
e
%change in Hb
Days post PhZ treatment
0.0090
%change in HCT
0.0011
Adrb2WT/WTVav-cre
Adrb2WT/flVav-cre
f
%Change in HCT
0.1429
Adrb2WT/flVav-cre + Veh
Adrb2WT/flVav-cre + FF
Days post Phz treatment
g
Adrb2Wt/Wt EpoRcre
Adrb2Wt/fl;fl/fl EpoRcre
Phz injection
CBC
h
%change in Hb
Adrb2WT/WTEpoR-cre
Adrb2WT/flEpoR-cre
Adrb2fl/flEpoR-cre
0.0014
0.0015
Days post PHZ treatment
%change in HCT
0.0008
0.0009
i
%change in HCT
Adrb2WT/flEpoR-cre + Veh
Adrb2WT/flEpoR-cre + FF
Adrb2fl/flEpoR-cre + Veh
Adrb2fl/flEpoR-cre + FF
0.8799
0.3290
Days post PhZ treatment

Figure 5

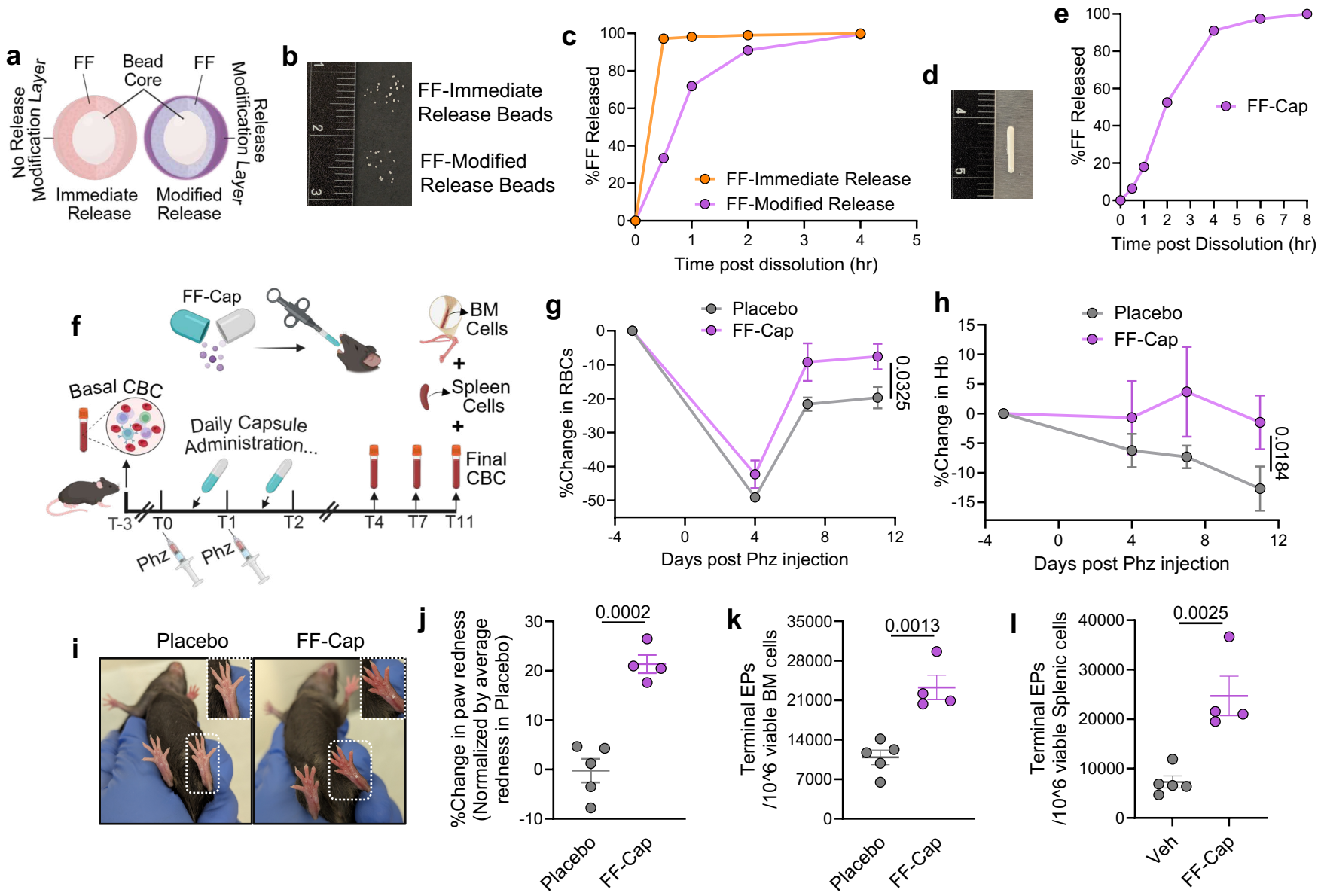
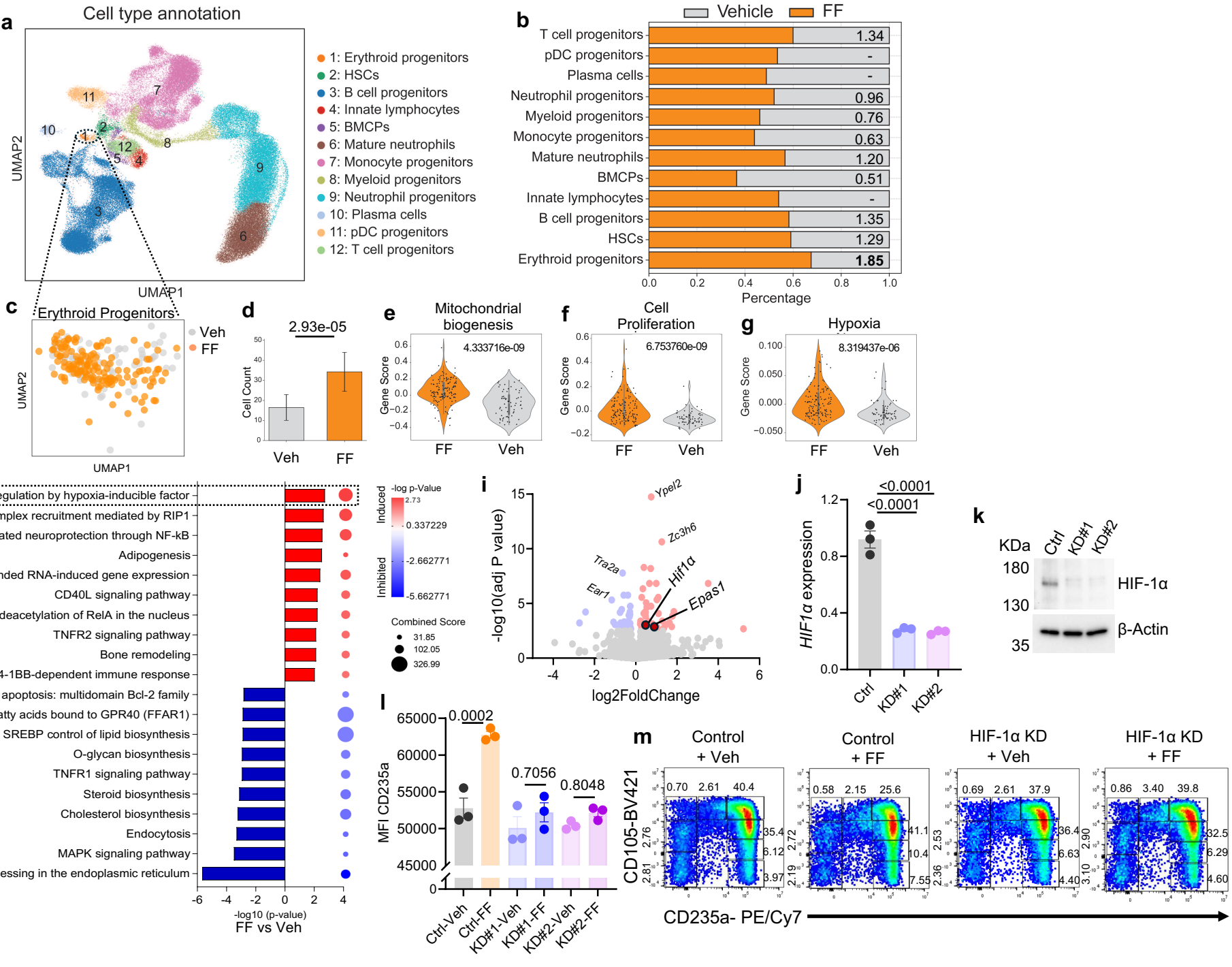
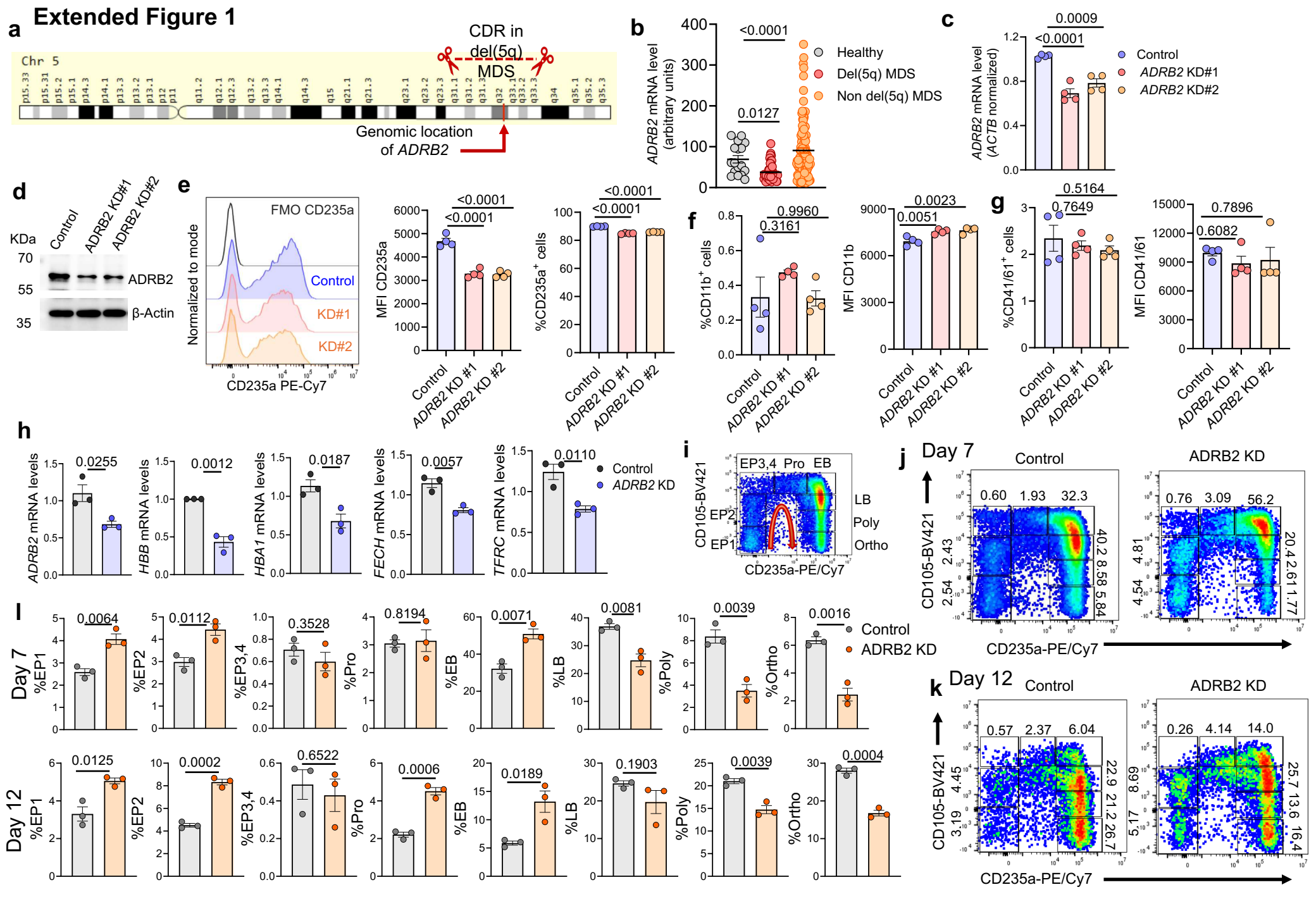

a
FF
Bead Core
FF
No Release Modification Layer
Release Modification Layer
Immediate Release
Modified Release
b
FF-Immediate Release Beads
FF-Modified Release Beads
c
%FF Released
Time post dissolution (hr)
FF-Immediate Release
FF-Modified Release
d
e
%FF Released
Time post Dissolution (hr)
FF-Cap
f
FF-Cap
BM Cells
Spleen Cells
Final CBC
Basal CBC
Daily Capsule Administration...
T-3
T0
T1
T2
T4
T7
T11
Phz
Phz
g
Placebo
FF-Cap
%Change in RBCs
Days post Phz injection
0.0325
h
Placebo
FF-Cap
%Change in Hb
Days post Phz injection
0.0184
i
Placebo
FF-Cap
j
%Change in paw redness (Normalized by average redness in Placebo)
0.0002
Placebo
FF-Cap
k
Terminal EPs /10^6 viable BM cells
0.0013
Placebo
FF-Cap
l
Terminal EPs /10^6 viable Splenic cells
0.0025
Veh
FF-Cap

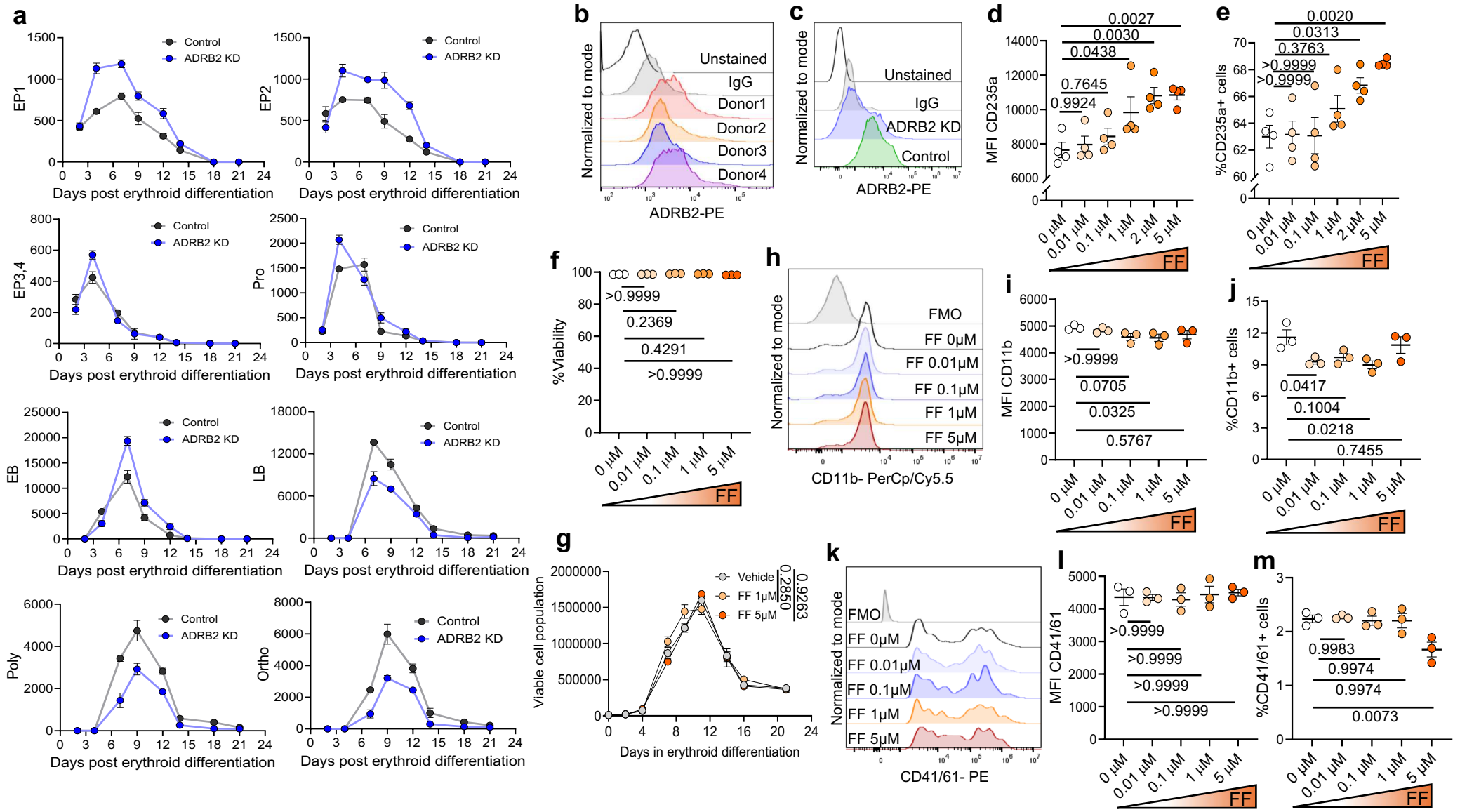
Figure 6


a
Cell type annotation
UMAP2
UMAP1
1: Erythroid progenitors
2: HSCs
3: B cell progenitors
4: Innate lymphocytes
5: BMCPs
6: Mature neutrophils
7: Monocyte progenitors
8: Myeloid progenitors
9: Neutrophil progenitors
10: Plasma cells
11: pDC progenitors
12: T cell progenitors
b
Vehicle
FF
T cell progenitors 1.34
pDC progenitors -
Plasma cells -
Neutrophil progenitors 0.96
Myeloid progenitors 0.76
Monocyte progenitors 0.63
Mature neutrophils 1.20
BMCPs 0.51
Innate lymphocytes -
B cell progenitors 1.35
HSCs 1.29
Erythroid progenitors 1.85
Percentage
c
Erythroid Progenitors
Veh
FF
d
2.93e-05
Cell Count
e
Mitochondrial biogenesis
4.333716e-09
Gene Score
f
Cell Proliferation
6.753760e-09
g
Hypoxia
8.319437e-06
h
Gene expression regulation by hypoxia-inducible factor
IKK complex recruitment mediated by RIP1
Erythropoietin-mediated neuroprotection through NF-kB
Adipogenesis
Double stranded RNA-induced gene expression
CD40L signaling pathway
Acetylation and deacetylation of RelA in the nucleus
TNFR2 signaling pathway
Bone remodeling
4-1BB-dependent immune response
Mitochondrial pathway of apoptosis: multidomain Bcl-2 family
Insulin secretion regulation by fatty acids bound to GPR40 (FFAR1)
SREBP control of lipid biosynthesis
O-glycan biosynthesis
TNFR1 signaling pathway
Steroid biosynthesis
Cholesterol biosynthesis
Endocytosis
MAPK signaling pathway
Protein processing in the endoplasmic reticulum
-log10 (p-value)
FF vs Veh
-log p-Value
Induced
Inhibited
Combined Score
i
Ypel2
Zc3h6
Tra2a
Hif1α
Ear1
Epas1
-log10(adj P value)
log2FoldChange
j
<0.0001
<0.0001
HIF1α expression
Ctrl
KD#1
KD#2
k
KDa
Ctrl
KD#1
KD#2
180
130
35
HIF-1α
β-Actin
l
0.0002
0.7056
0.8048
MFI CD235a
Ctrl-Veh
Ctrl-FF
KD#1-Veh
KD#1-FF
KD#2-Veh
KD#2-FF
m
Control + Veh
Control + FF
HIF-1α KD + Veh
HIF-1α KD + FF
CD105-BV421
CD235a- PE/Cy7

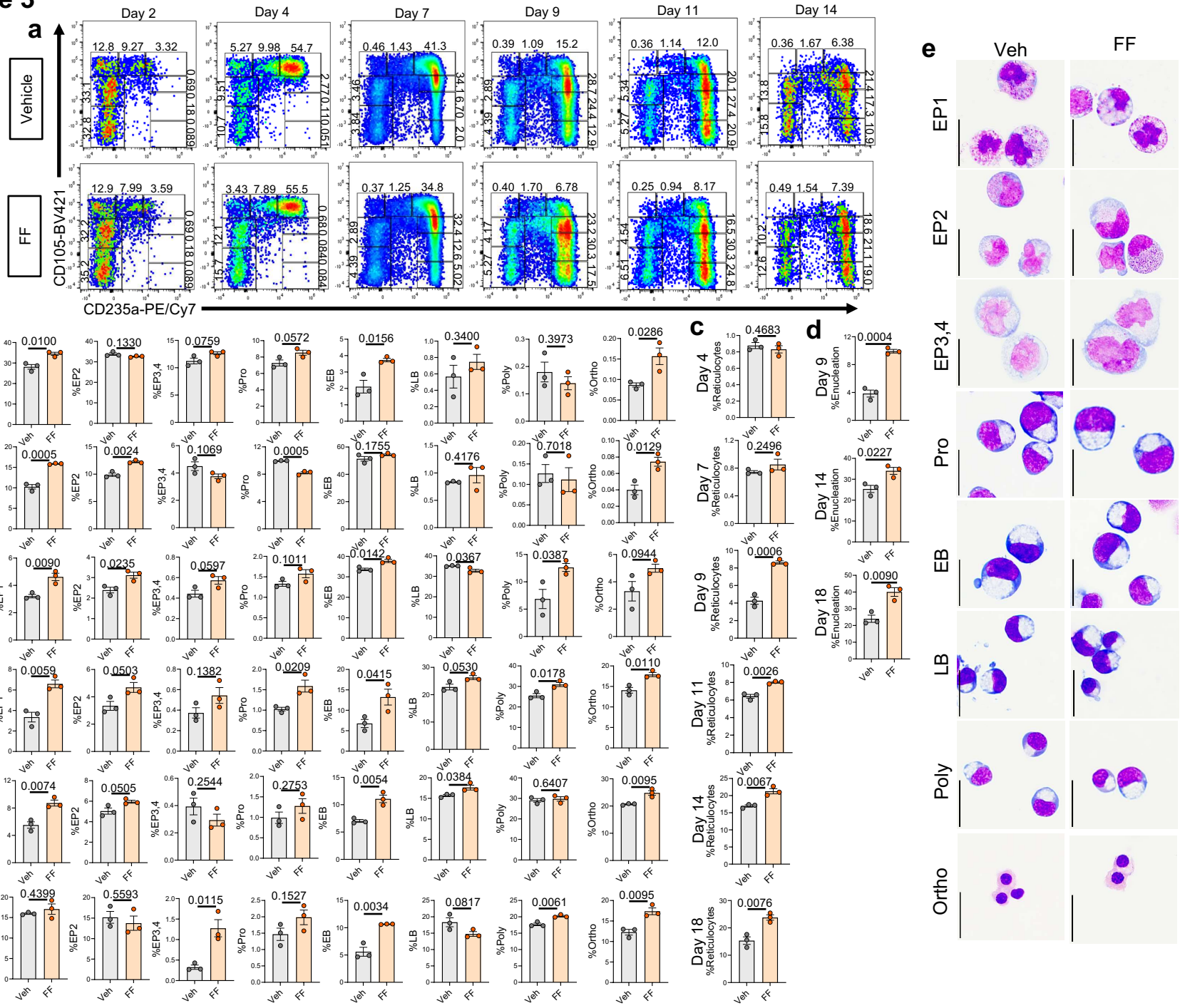
Extended Figure 1



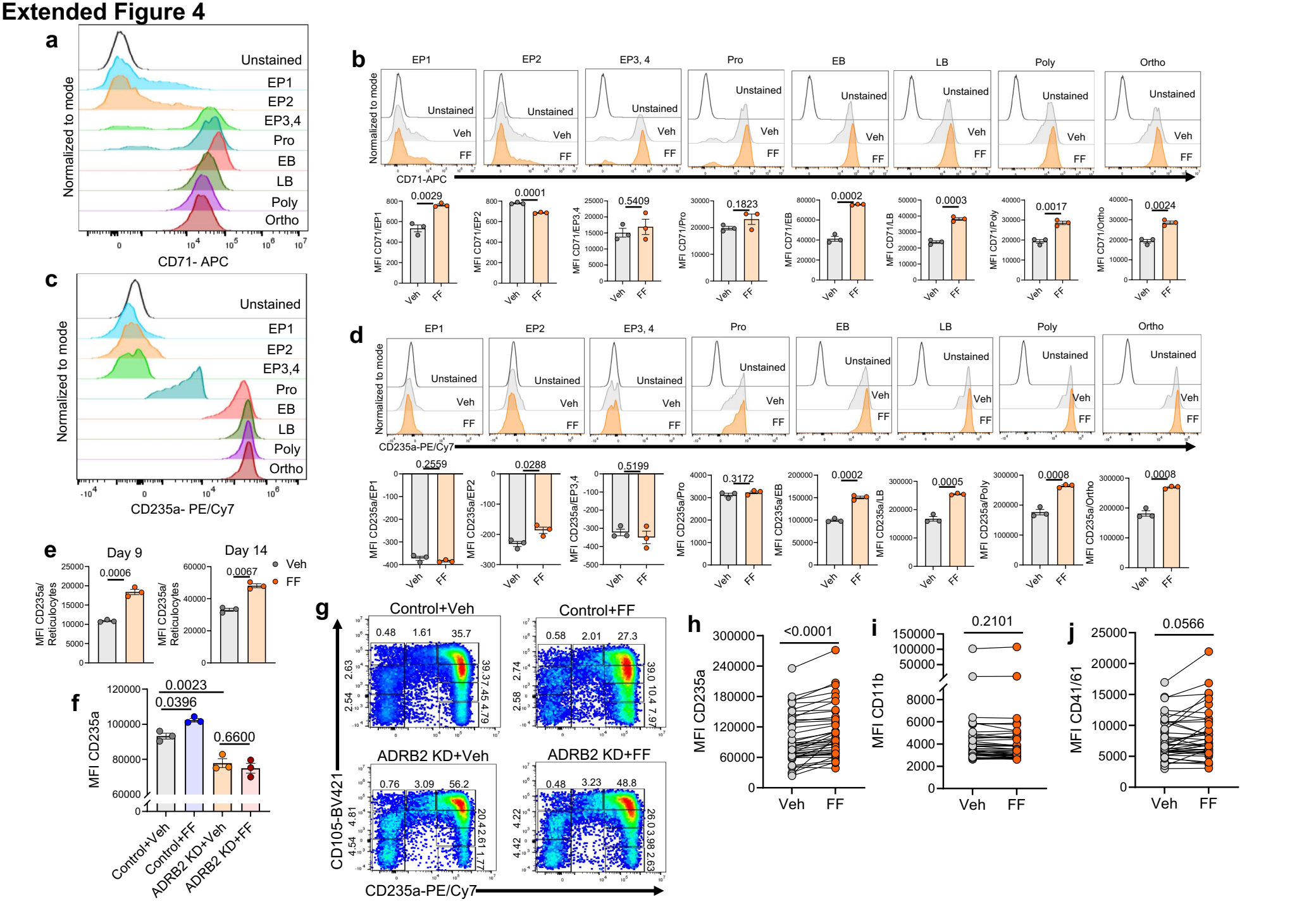
Extended Figure 2



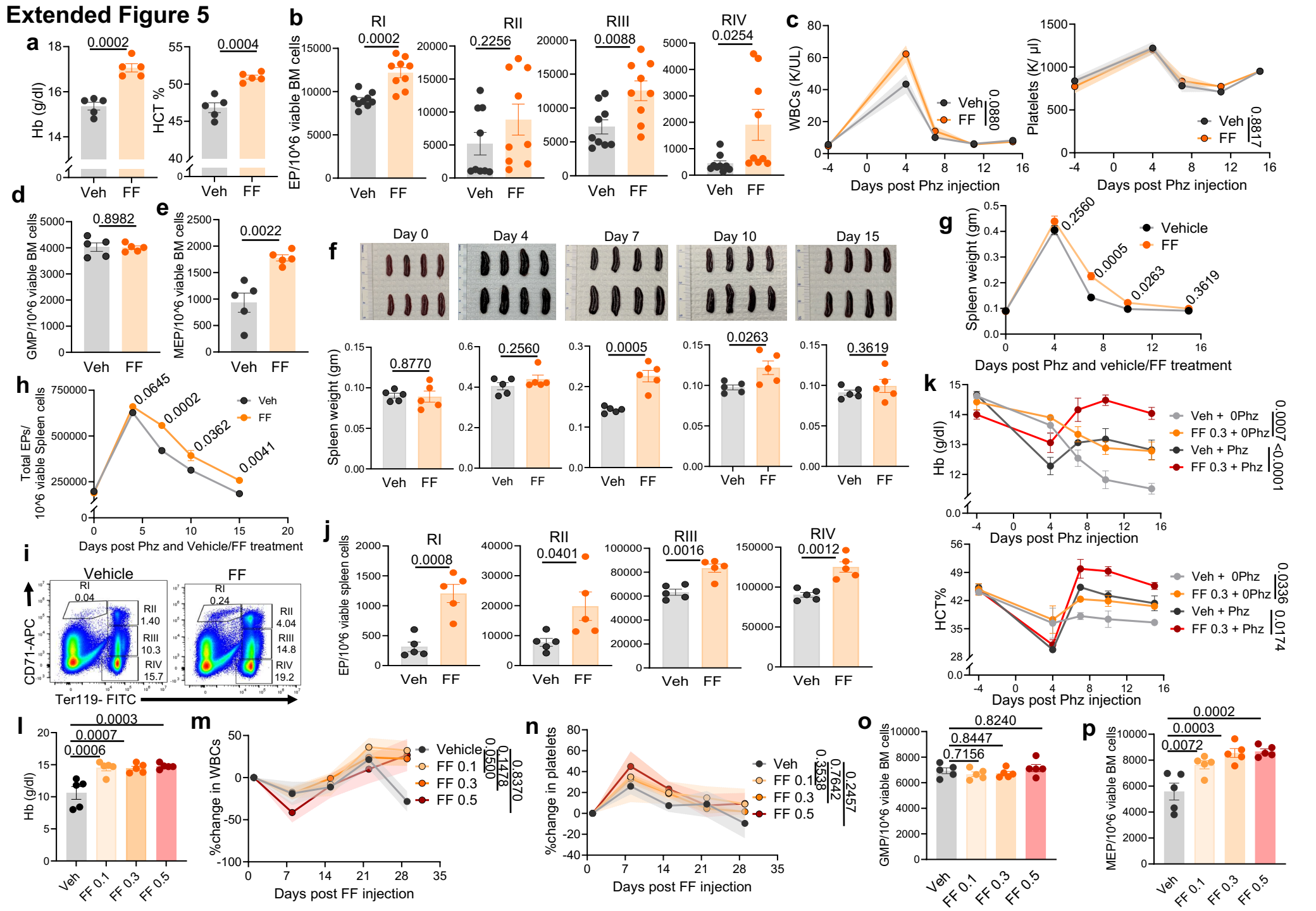
Extended Figure 3



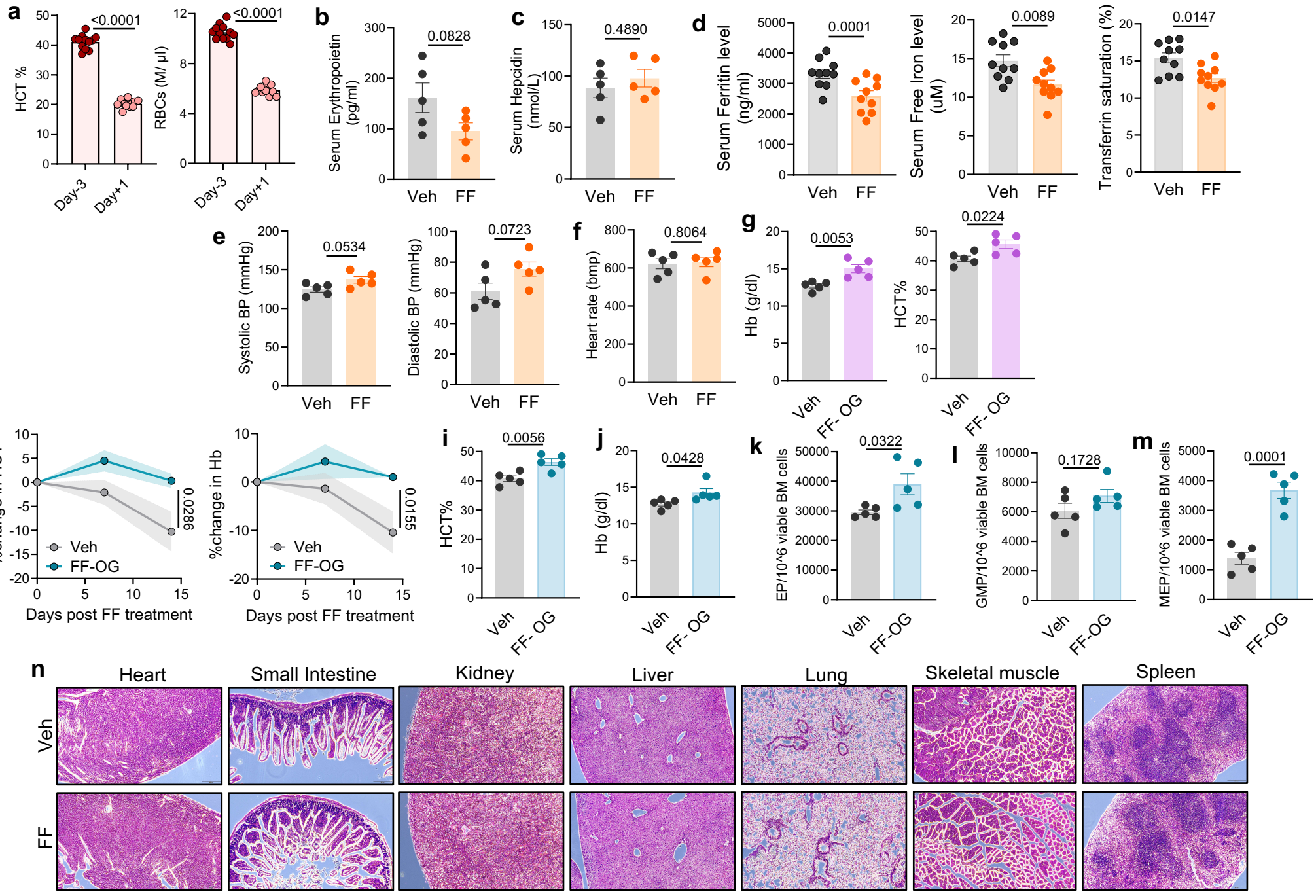
Extended Figure 4



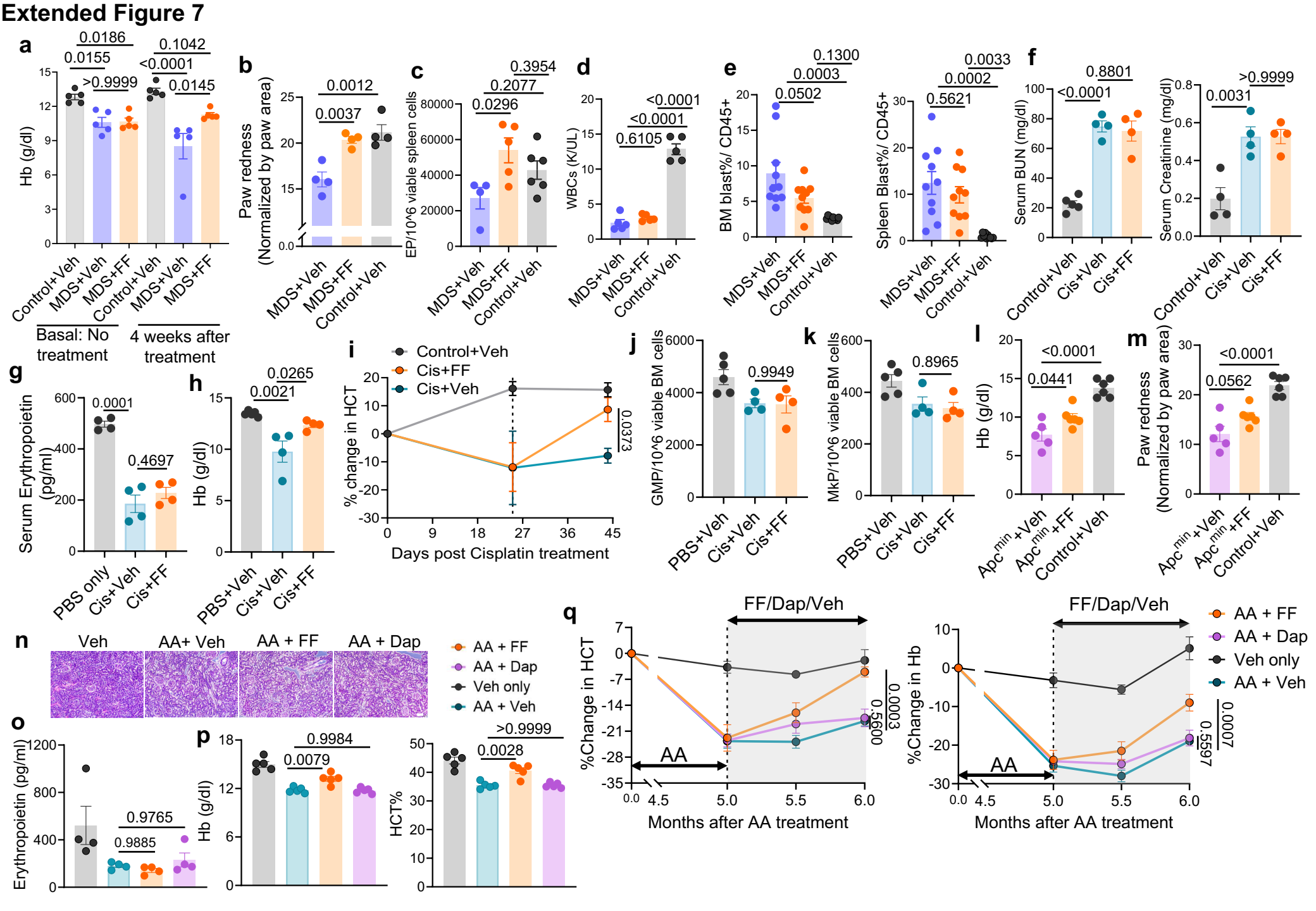
Extended Figure 5



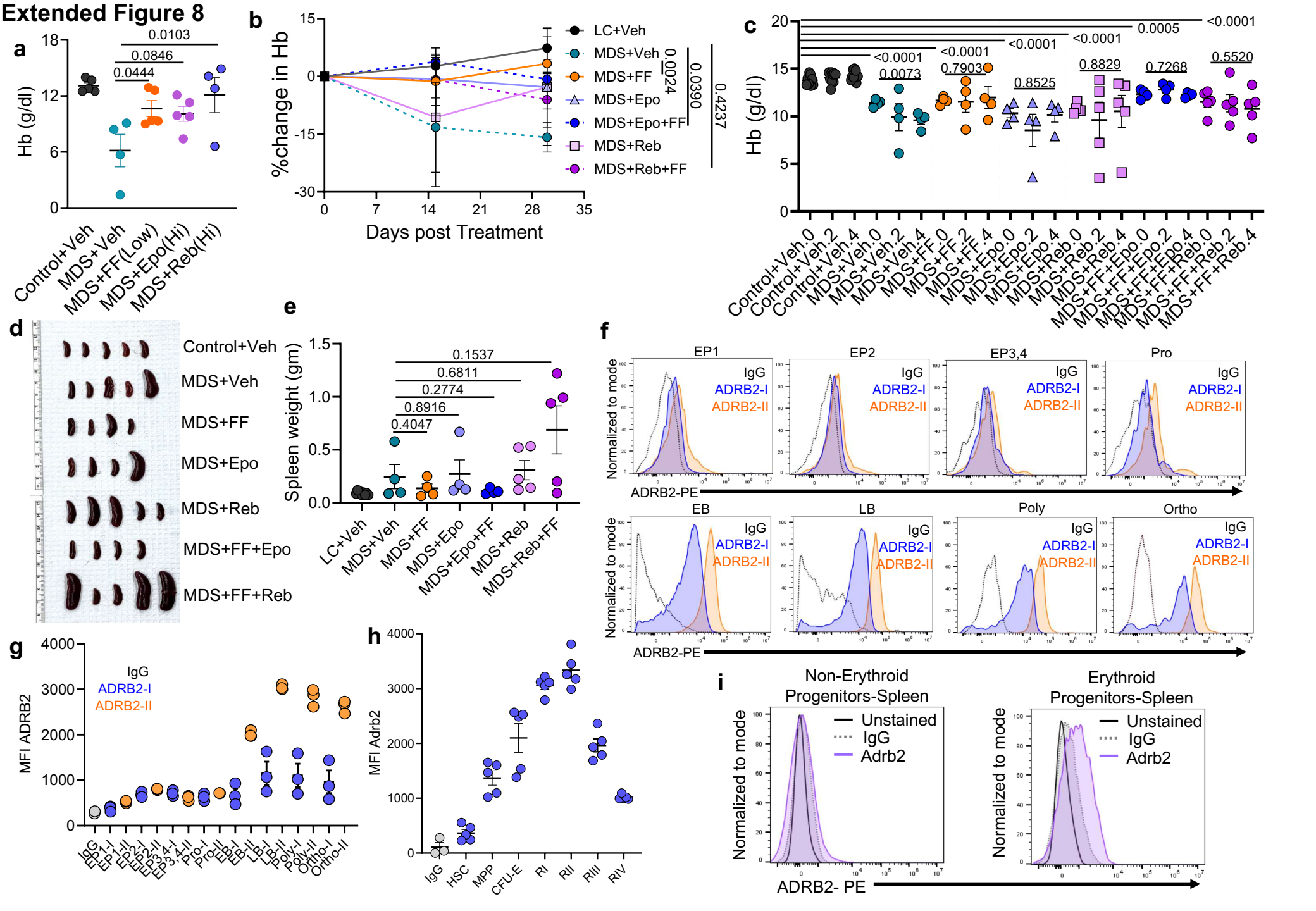
Extended Figure 6



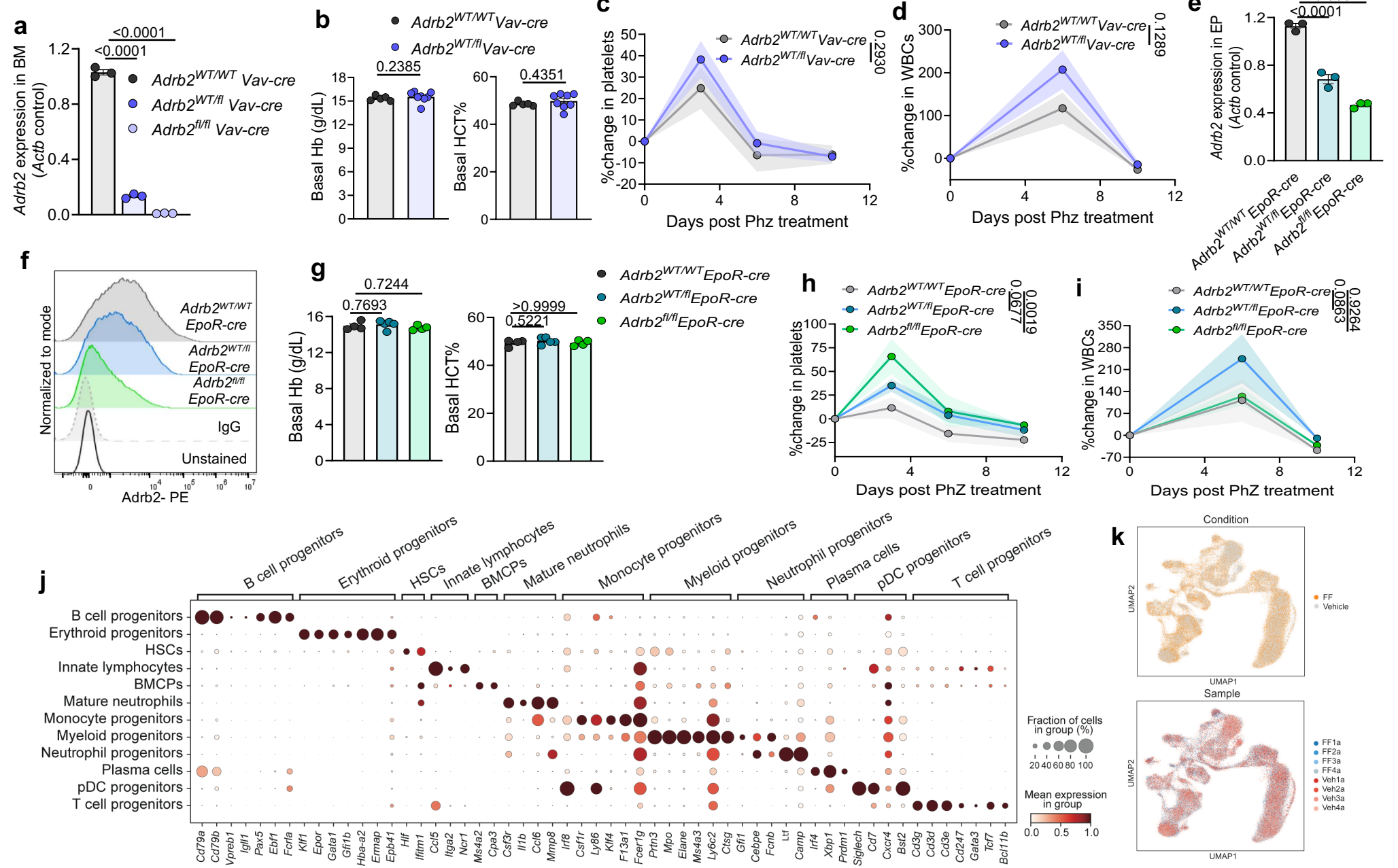
Extended Figure 7



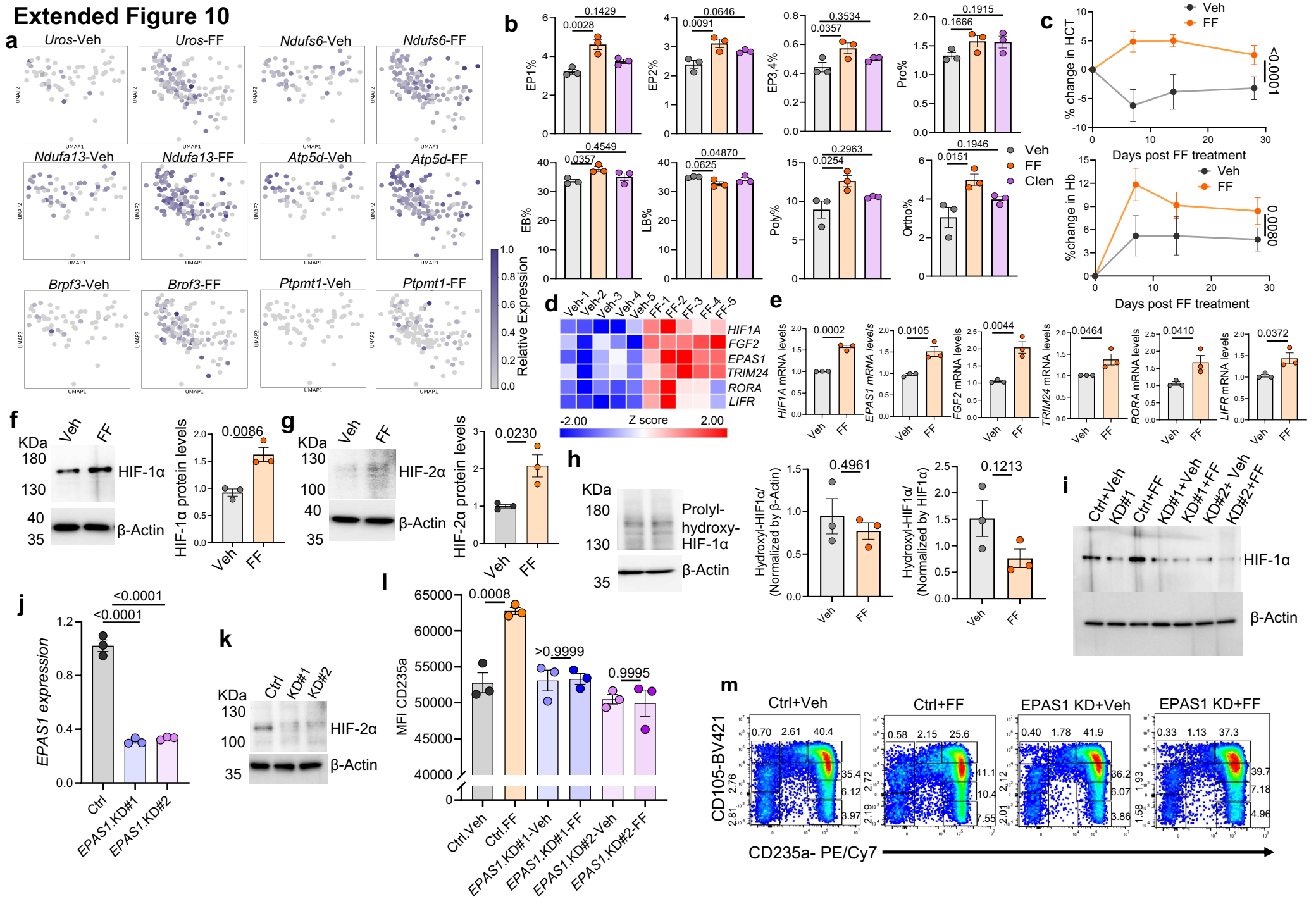
Extended Figure 8



Extended Figure 9

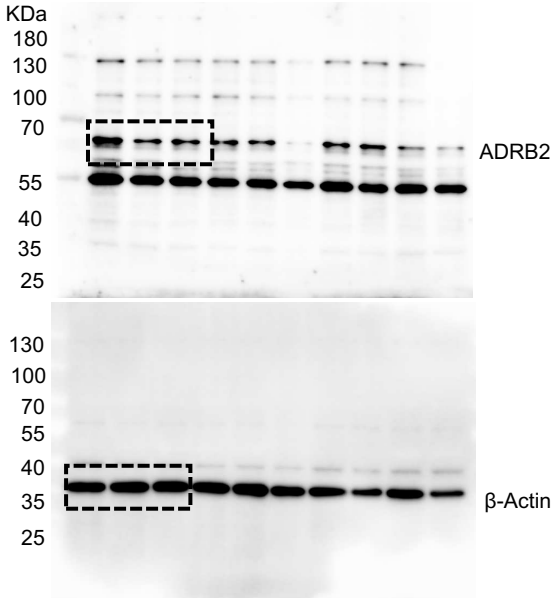


Extended Figure 10

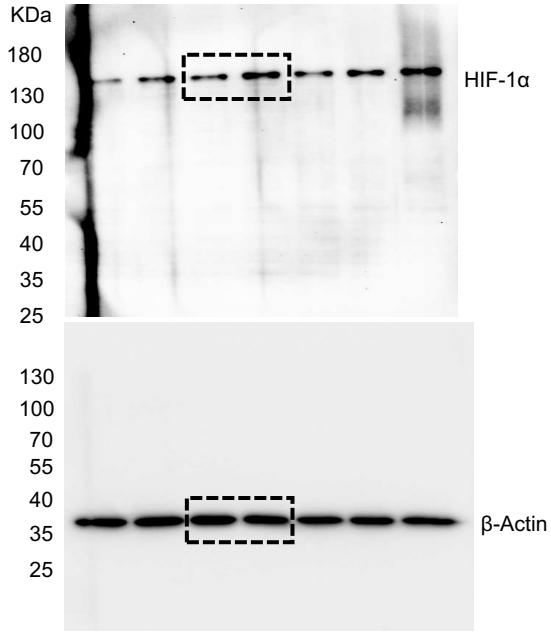


Uncropped blots

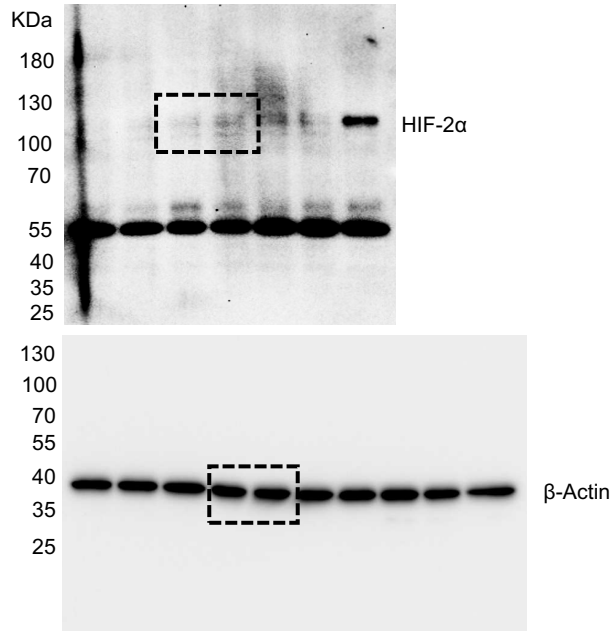
Extended Figure 1d



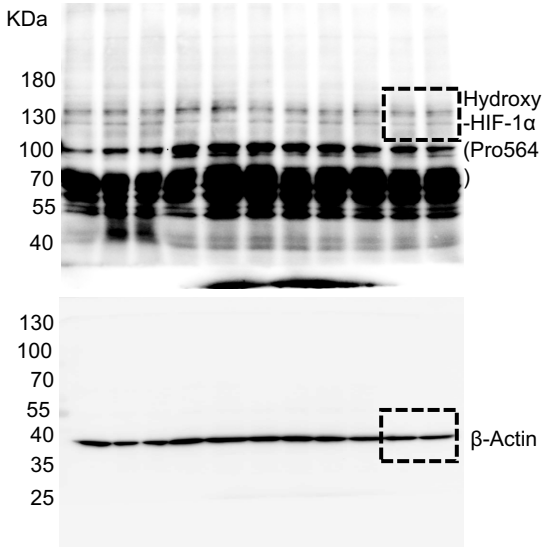
Extended Figure 10f



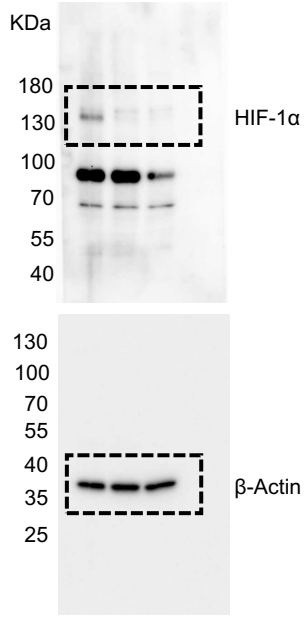
Extended Figure 10g



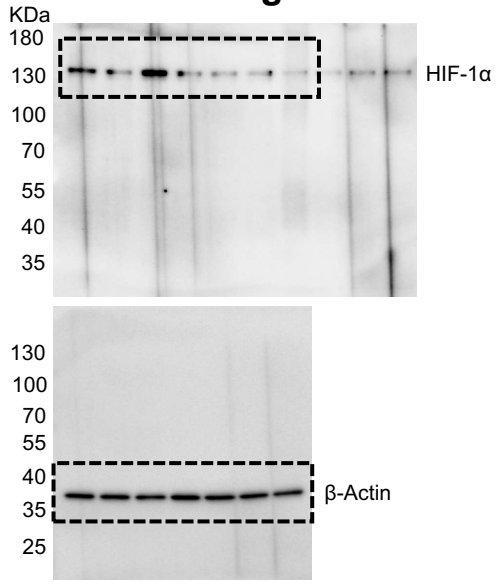
Extended Figure 10h



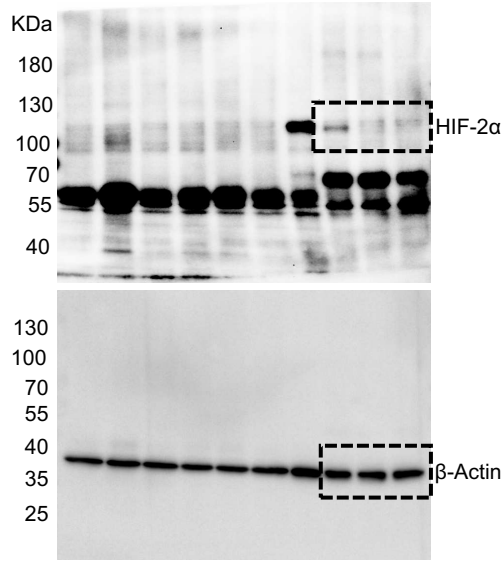
Main Figure 6k



Extended Figure 10i



Extended Figure 10k



Supplementary Files

This is a list of supplementary files associated with this preprint. Click to download.

- SupplementaryFigure1.pdf
- ExtendedDataFigure2.tif
- ExtendedDataFigure7.tif
- SupplementaryTable1.xlsx
- ExtendedDataFigure9.tif
- ExtendedDataFigure10.tif
- ExtendedDataFigure5.tif
- ExtendedDataFigure3.tif
- ExtendedDataFigure4.tif
- ExtendedDataFigure1.tif
- ExtendedDataFigure6.tif
- ExtendedDataFigure8.tif
- Supplementaryvideo1.mp4